Electroreduction of nitrate and carbon dioxide on copper electrodes: a mechanistic study

Perez Gallent, E.

ELECTROREDUCTION OF NITRATE AND CARBON DIOXIDE ON COPPER ELECTRODES

A mechanistic study

Proefschrift

ter verkrijging van

de graad van Doctor aan de Universiteit Leiden,

op gezag van Rector Magnificus Prof. Mr. C. J. J. M. Stolker

volgens besluit van het College voor Promoties

te verdedigen op donderdag 1 februari 2018

klokke 11:15 uur

door

Elena Pérez Gallent

geboren te Valencia, Spanje in 1988

Promotiecommissie

Promotor : Prof. Dr. M. T. M. Koper

Co-promotor : Dr. F. Calle-Vallejo

Overige leden : Prof. Dr. H. S. Overkleeft (Universiteit Leiden)

Prof. Dr. E. Bouwman (Universiteit Leiden)

Prof. Dr. Ir. B.M. Weckhuysen (Universiteit Utrecht)

Dr. W.A. Smith (Technische Universiteit Delft)

Dr. B.S. Yeo (National University of Singapore)

ISBN 978-94-6299-842-1

Printed by Ridderprint BV

Cover designed by Elena Pérez Gallent and Marta Ramirez Angulo

Life is and will ever remain an equation incapable of solution, but it contains certain known factors. **Nikola Tesla**

Contents

Chapter 1

Introduction

1.1 The Birth of Electrochemistry

Despite the broad knowledge of electricity gained during the 17th and the 18th century by scientists like William Gilbert, Stephen Gray, Charles Francois, Jean-Antoine Nollet, William Watson and Charles-Augustin Coulomb, among others, it was not until the late 18th century that Luigi Galvani pronounced the birth of electrochemistry by creating a bridge between muscular contractions of a frog's leg and electricity. In 1791 Galvani established that animals hold a vital force, namely "animal electricity", which activates muscles when placed between two metals. Alessandro Volta postulated that the real source of stimulation was the contact of dissimilar metals connected by a moist conductor (a frog's leg). Volta persistently studied this phenomenon in order to explain his "contact" theory of electricity, and in 1800 he announced his invention of the first electrical battery, the voltaic pile. Years later, Humphry Davy established that the voltaic pile produces electricity depending on the event of chemical reactions, and not just on the contact of dissimilar metals as Volta proposed. Davy's successor, Michael Faraday, studied the effects in electrochemical decomposition, which was discovered by Paets van Troostwijk and Deiman by splitting water into hydrogen and oxygen by electrolysis. Faraday concluded that the passage of electricity through a conducting liquid medium causes the molecules to dissociate and the amount of product decomposed was directly proportional to the amount of electricity passing through the solution. These laws are still fundamental to industrial electrolytic production of chemicals. This story illustrates how even an immature, undeveloped or imperfect scientific idea can assist in the development of a cultivated and world-wide accepted scientific theory. Every minor stage in research triggers the commence of an open discussion that with effort, time and lots of re-thinking and understanding will result in a putative theory.

1.2 Electrocatalysis

A catalyst is defined as a substance that intervenes in a chemical reaction modifying the reaction rate without being consumed or chemically changed. Electrocatalysts are specific forms of catalysts where the rate of an electrochemical reaction occurring on an electrode surface is enhanced. Electrocatalysts are classified in two categories: homogeneous, in which catalyst and reactants have the same phase, and heterogeneous, where the reaction takes place at the interface between the catalyst (the electrode) and the reactant phase. In electrocatalysis, the reactions involve electric charges flowing between the electrodes and the ionic conductor, the electrolyte. Thus, electrochemistry handles the interaction between electrical energy and chemical change.

Every electrochemical cell reaction consists of two half reactions, one occurring at the anode where a certain substance will donate electrons and become oxidized, and one occurring at the cathode where a certain substance will accept electrons and become reduced. This thesis is focused on reduction reactions of nitrate and carbon dioxide taking place at a cathode made of a solid metal electrode, mainly copper.

The performance of the catalyst for a certain reaction depends on a vast number of parameters, such as electrode material, oxidation state of the material, electrode morphology, surface roughness, differences in adsorption sites, pH and the nature of the species in solution, etc. A good strategy to develop an active and efficient new catalyst is by first determining how all these parameters affect the reaction and its mechanism. In that vein, the scope of this thesis is to investigate the mechanism of nitrate and CO_2 reduction and how different parameters have an impact on the catalytic performance of copper.

1.3 The potential of electrochemistry in industrial processes

The use of electrochemical techniques for the synthesis of valuable products provides several advantages over chemical synthesis. An important advantage that makes electrochemistry attractive for industry is the ease of scalability, which allows large-scale chemical production. A classic example of ton-scale production is the chloralkali process[2], where aqueous sodium chloride, normally brine obtained directly from natural salt deposits, is electrolyzed to form chlorine gas and sodium hydroxide. The chloralkali process is the largest of the electrolytic industry. The preparation of chlorine electrochemically in industrial scale was first achieved in 1892. In 1987 it was responsible for about 10% of the total world production, and in 2000, 95 % of the world's chlorine production was obtained by the chloralakli process[3]. Another example of large-scale synthesis is the Hall-Héroult process, where Al_2O_3 is electrolyzed to produced elemental aluminium[4]. The Hall-Héroult process is the largest in terms of energy usage in industrial processes[5]. In addition, organic chemicals such as adiponitrile, an intermediate to nylon, or ethylene glycol, used as antifreeze or in PET bottles, are also produced electrochemically in large scale. 200 million kg of Adiponitrile are produced per year by electrohydrodimerization of acrylonitrile[6], and about 10 billion kg of ethylene glycol are produced per year by catalytic oxidation of ethylene oxide followed by hydrolysis[5].

One of the most important contemporary benefits of electrochemistry in industrial processes is an environmentally friendly and clean process by employing renewable electricity. Electrochemical processes use electric current as energy source, averting the use of stoichiometric amounts of oxidants or reductants, dramatically lowering the amount of by-products formed and thus the pollutant levels. A precise control of oxidation or reduction levels can be achieved by the adjustment of the electrode potential. The electrochemical synthesis of compounds offers a precise control of the product yield through the applied current or

potential, virtually leading to higher energy efficiencies compared to thermal-based processes, and to more pure products than those synthesized by chemical routes. The electrochemical synthesis of DZ-2384, a diazoamide-based preclinical candidate for oncology, marked an improvement in terms of selectivity and environmental footprint. This substance is now prepared by an intramolecular electrochemical oxidative coupling[7], while previously it was synthesized with the use of oxidants such as $PhI(OAc)_2$. The reagent-based process led to significant by-product formation which limited the yield of DZ-2384 and complicated its purification[7-9].

The use of less extreme process conditions such as lower temperature and pressure potentially leads to less degradation of the starting material or products, making electrochemical methods industrially interesting. In addition, a lower number of steps might be involved in the process, for instance, by combining in one reactor the electrochemical synthesis and the product separation. In the chloralkali process, the formation of chlorine gas occurs in the anodic compartment of the reactor, whereas sodium hydroxide is formed in the cathodic compartment; therefore, the separation process is direct.

However, the existence of physical restrictions such as mass transport limitations and more importantly economically unprofitable processes, makes electrochemical processes less beneficial. For large-scale production, electrochemical processes are costly. The traditional chemical preparation, even being less selective, is usually economically more beneficial[5].

Electrochemical routes are not always economically feasible if the selectivity for the desired product is low or inadequate. In aqueous systems where the competitive reaction is based upon oxygen or hydrogen formation, the process becomes especially unfeasible in economic terms, due to the ease of H_2 or O_2 production compared to the formation of the desired product. In electrochemical processes, high-energy consumption is usually required.

However, direct conversion with the use of renewable energies offers a cheap source of energy which may partially help overcome this problem. In addition, the use of abundant and thereby less expensive starting materials such as CO_2 and nitrate also helps in counteracting the expenses and readjusting the balance to beneficial values.

Despite the advantages previously mentioned, it is important to remark the existence of several drawbacks which limit the industrial application of electrochemical processes. Important factors that make processes economically unfeasible are the short lifetime and/or the high cost of some electrode materials. Ideally, the electrode material should be cheap and stable in the electrolysis medium. In addition, some electrochemical reactions have low current efficiency under some conditions and/or high activity towards side reactions limiting the production yield of the desired product. It is important to mention the vast amount of factors that affect electrochemical conversion and, therefore, determine the electrolysis performance[10] such as the electrolyte nature, concentration, pH or conductivity and the nature and structure of the catalyst, among many others. Other factors such as the potential or current distribution, the mass-transport regime and the electrochemical cell design are also of paramount importance[11]. The geometry of the electrodes, the inter-electrode distance, the cell dimensions and the operation mode of the reactor, among others, are decisive parameters that affect the electrochemical performance of the process[10].

In the interest of eventually obtaining an efficient and economically feasible process for the industry, a detailed mechanistic study of the reaction must be addressed, to understand which factors play a role in the efficient and selective formation of the desired product. An attractive process would be the conversion of a cheap and abundant substance to a more valuable product. In this thesis three different reactions and their mechanisms are the object of study: the electrocatalytic reduction of nitrates to hydroxylamine, and the electrocatalytic reduction of carbon dioxide for two different purposes,

namely the formation of hydrocarbons and the formation of cyclic carbonates.

1.4 Electrocatalytic reduction of nitrate

The reduction of nitrate has attracted interest due to its environmental significance[12] in view of the contamination of groundwater,[13-14] and because it causes serious health problems[15] such as liver disease, cancer and blue baby syndrome. Nitrate contamination is a result of industrial waste, nuclear industries and agricultural runoff such as livestock feces and the use of fertilizers, which currently induce severe alterations in the nitrogen cycle[16]. This biogeochemical cycle is a complex network of biological and abiotic processes through which nitrogen circulates through the organic and physical world. A very simplified scheme of the nitrogen cycle is displayed in Fig.1.1. The atmosphere is the main reserve of nitrogen, however, the majority of the living beings cannot use atmospheric nitrogen to generate amino acids and other nitrogen-based compounds. Therefore, atmospheric nitrogen must be converted to ammonia which can be used by organisms through a process called nitrogen fixation. The formed ammonia is oxidized by bacteria to first form nitrites that will be further oxidized to nitrates (nitrification). The absorption of nitrate by plants incorporates the nitrogen in proteins, nucleic acids and chlorophyll, which will be further converted to nitrogen-based animal compounds when assimilated by animals. The nitrogen cycle is closed by the denitrification process, where bacteria reduce nitrates to N_2, which is freed back into the atmosphere.

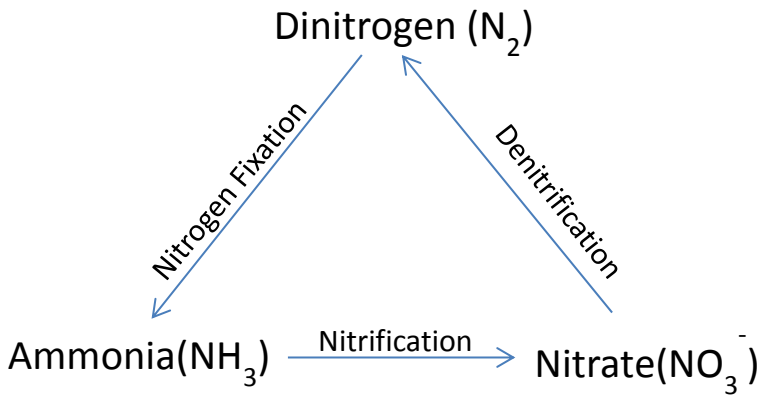

Figure 1.1: Simplification of the nitrogen cycle. Adapted from ref. [1]

The main cause of the destabilization of the nitrogen cycle is the usage of fertilizers, which contain large amounts of nitrates, causing environmental issues like the contamination of groundwater. Governmental regulations limit the maximum concentration of nitrate in drinking water to 10 mg/L [17]. However, the overpass of this limit in certain regions[18] leads to a need for nitrate removal from water. As the natural process of denitrification is unable to handle the excess of nitrite-derived substances, several methods to remove NO_3^- ions from contaminated water have been developed. Physicochemical methods like electrodialysis[19], ion exchange resins[20] or reverse osmosis[21] only provide a separation method but do not convert nitrate. Biological methods[22] are slow and difficult to control and cannot be used for high nitrate concentrations to avoid poisoning the bacteria. These methods are hardly acceptable for large-scale applications due to the low reaction rate, continuous monitoring and/or large amounts of by-products. Electrochemical reduction of nitrate presents an alternative and promising solution, because it is selective, environmentally friendly and cost-effective[23]. Nitrate can be used as starting material to produce useful chemicals such as ammonia, hydroxylamine, hydrazine or azide. The intricacy of the electrochemical reduction of nitrogen-containing compounds is related to the existence of numerous stable species with

oxidations states from -3 to +5. The electrochemical reactions and their equilibrium potentials for the formation of the different reduction products are listed below[24]:

$NO_3^- + 2H^+ + 2e^- \rightarrow NO_2^- + H_2O$ E° = 0.835 V vs. NHE (1.1)

$NO_3^- + 4H^+ + 3e^- \rightarrow NO(g) + 2H_2O$ E° = 0.958 V vs. NHE (1.2)

$2NO_3^- + 10H^+ + 8e^- \rightarrow N_2O + 5H_2O$ E° = 1.116 V vs. NHE (1.3)

$2NO_3^- + 12H^+ + 10e^- \rightarrow N_2(g) + 6H_2O$ E° = 1.246 V vs. NHE (1.4)

$NO_3^- + 8H^+ + 6e^- \rightarrow NH_3OH^+ + 2H_2O$ E° = 0.727 V vs. NHE (1.5)

$NO_3^- + 10H^+ + 8e^- \rightarrow NH_4^+ + 3H_2O$ E° = 0.875 V vs. NHE (1.6)

The obtained product varies depending on the cathode material, the electrolyte used and the potential applied[25-29]. Platinum has been the most studied catalyst for nitrate reduction. The reaction is pH dependent, being active in acidic media with the consequent formation of ammonium, but inactive at higher pH[26]. In addition, nitrate reduction on platinum in acidic media is surface structure dependent due to the structure-sensitive adsorption of hydrogen and anions[30-31]. Other metals such as rhodium show high activity for nitrate reduction over a wide pH range[32-33], forming ammonium in acidic medium and nitrite in alkaline media[34]. Some coinage metals like Cu, Ag and Au have also been studied in acidic media[35]: among these metals, copper showed the highest activity for nitrate reduction, with ammonia as the main product[29]. The high activity observed for nitrate reduction on copper in alkaline media[36-37] makes it an interesting system due to the less probable formation of products like toxic nitrogen oxides compared to reduction in acidic media[38]. In this thesis, we investigated the mechanism of nitrate reduction on copper electrodes in acidic and alkaline media by cyclic voltammetry, Fourier Transform Infrared Spectroscopy, Ionic Chromatography and Rotating Disc Electrodes. Copper single crystals were used to unravel the structure sensitivity of the reaction (Chapter 2).

1.5 Electrocatalytic reduction of CO_2

The accelerated increase of the population in the last century has resulted in a massive growth of energy consumption. 85 % of the world's energy demand is supplied by fossil fuels, the consumption of which creates an increase of greenhouse gases (GHG) in the atmosphere[39]. An increase of atmospheric levels of GHG creates environmental issues such as climate change. Although GHG such as methane and chlorofluorocarbons have much higher greenhouse effect per mass of gas, carbon dioxide is the largest contributor to global warming due to the substantial amounts present in the atmosphere[40]. Several strategies can be used to decrease the atmospheric CO_2 levels. First of all, one can reduce the world's energy consumption by means of more energy-efficient processes. Reduction in the carbon intensity of energy usage can be achieved by switching to renewable energies such as wind, solar or geothermal. Another option would be the capture and sequestration of CO_2[41]. However, this is a rather expensive option, and only provides a mid-term solution. A good strategy to make CO_2 capture more interesting would be to convert it to valuable chemicals and fuels by electroreduction[42]. The use of CO_2 as a C1 feedstock for the formation of more valuable chemicals offers the use of an easy, available and renewable carbon source, which is non-toxic and abundant. However, CO_2 is the most oxidized state of carbon, being thermodynamically and kinetically stable, such that it requires a large energy input to convert it into other molecules. The energy necessary for the electrochemical conversion can be obtained by renewable energies, making the combination of renewable energies with the electrochemical reduction of CO_2 a promising path towards a sustainable energy future with net neutral CO_2 emissions.

A significant amount of molecules can be formed from electroreduction of CO_2 especially on copper electrodes. In this thesis, we focus our attention on the formation of hydrocarbons such as methane, ethylene and ethanol and on the formation of bigger molecules such as cyclic

carbonates. Ethylene is a widely used industrial building block, and ethanol is a valuable fuel. Therefore, the reduction towards these desired products is potentially interesting, due to their higher energy density compared to single carbon products. The formation of cyclic carbonates offers wide applications in the chemical industry, as these are used as fuel additives, in plastics, as green solvents and as electrolytes for Li ion batteries.

1.5.1 Electroreduction of CO_2 to hydrocarbons

The electrochemical reduction of carbon dioxide has gained extraordinary interest in the past decades as a means of energy storage.

The simplest products obtained are those for which only 2 e- transfers are involved in the reaction path, such as carbon monoxide and formic acid. However, the formation of hydrocarbons would be the most significant target of CO_2 utilization due to their high energy density and the benefit of direct use without changing the present infrastructures based on fossil fuels.

The electrochemical reactions and their equilibrium potential for the formation of different products of carbon dioxide reduction are listed below:

$CO_2 + 2H^+ + 2e^- \rightarrow CO + H_2O$ $E° = -0.10$ V vs. RHE (1.7)

$CO_2 + 2H^+ + 2e^- \rightarrow HCO_2H$ $E° = -0.20$ V vs. RHE (1.8)

$CO_2 + 4H^+ + 4e^- \rightarrow H_2CO + H_2O$ $E° = -0.07$ V vs. RHE (1.9)

$CO_2 + 6H^+ + 6e^- \rightarrow CH_3OH + H_2O$ $E° = 0.02$V vs. RHE (1.10)

$CO_2 + 8H^+ + 8e^- \rightarrow CH_4 + 2H_2O$ $E° = 0.17$ V vs. RHE (1.10)

$2CO_2 + 12H^+ + 12e^- \rightarrow CH_3CH_2OH + 3H_2O$ $E° = 0.09$ V vs. RHE (1.12)

$2CO_2 + 12H^+ + 12e^- \rightarrow C_2H_4 + 4H_2O$ $E° = 0.08$ V vs. RHE (1.13)

The product distribution resulting from the electrochemical reduction of CO_2 depends on the metal used as electrode. A screening of several transition metals used for carbon dioxide was performed and a classification regarding the product formed was suggested[43]. The product selectivity is mainly determined by how CO_2 is reduced initially at the electrode surface. In the first group belong metals such as In, Sn, Hg and Pb that selectively form formic acid. These metals have high hydrogen overvoltage and low CO adsorption strength, therefore the intermediates are weakly adsorbed on the surface making those metals unable to catalyze the breaking of the C-O bond in CO_2 and thus facilitating the formation of formic acid. The second group of metals, where Ag and Au belong, produces mainly CO. CO is formed on these metals, especially on Au, at less negative potentials than formic acid. Hansen et al[44] developed a model to describe trends in catalytic activity for CO_2 reduction in terms of the adsorption energies of the reaction intermediates. Considering that CO is formed through the adsorbed intermediates *COOH and *CO, Au is able to stabilize *COOH without over-stabilizing CO. This explains the formation of CO on Au at lower potentials than formic acid formation suggesting a different mechanism for the formation of CO. The third group consists of metals such as Ni, Fe, Pt and Ti, which evolve hydrogen at low potentials. On these metals CO_2 is reduced to CO, but it is strongly adsorbed on the surface, poisoning the metal and blocking possible further reactions. Therefore, the main product formed is hydrogen from the competitive hydrogen evolution reaction. Metals with a moderate CO adsorption energy are able to further reduce CO to hydrocarbons. Elements such Mo and Ru have been reported to convert CO_2 to methanol and methane but with low efficiencies[45-46]. However, copper is a unique metal able to form hydrocarbons, mainly methane and ethylene with high efficiencies[47]. Formation of oxygenated species such as ethanol and propanol has also been observed, although normally in smaller amounts[48-49]. Jaramillo et al. recently observed the formation of 16 different products: besides the main products such methane, ethylene, formate, CO, ethanol and propanol, other minor products such as allyl alcohol, methanol,

glycoaldehyde, acetaldehyde, ethylene glycol, propionaldehyde, acetone, acetate and hydroxyacetone were also observed with lower efficiency[50]. The extraordinary ability of copper to form hydrocarbons has motivated a substantial effort to understand its special activity for the carbon dioxide reduction reaction. Numerous experimental and theoretical studies have proposed mechanisms for the reduction of CO_2 on copper[48, 50-56]. However, a detailed mechanism for this reaction is still under debate[49, 51-52, 57-58]. Ethylene and methane formation follow two different pathways[59] having carbon monoxide as the key intermediate in the formation of both products[60-62]. The formation of methane has been found to be pH dependent[61, 63], which implies that the rate-determining step must involve the transfer of a proton and an electron. Hori suggested a path for the formation of methane via adsorbed COH[61]. In contrast, the formation of ethylene is pH independent,[61, 63] which implies that the rate-determining step does not involve a proton transfer. However, the formation of ethylene does depend on the potential, so that an electron transfer must be involved. A C-C coupling of two adsorbed CO molecules through a reductive dimerization step has been proposed as a rate-determining step[51, 57]. In chapter 4 of this thesis the formation of this CO dimer will be discussed in detail.

Several factors such as the electrode morphology[47, 64], the pH of the electrolyte[63], the identity of the cations and anions[56, 65], the size and shape of nanoparticles[66], the oxidation state of the copper electrode[67] , among others, have been extensively studied to gain insight into the extraordinary reactivity of copper to form hydrocarbons from carbon dioxide.

In this thesis, we focus our attention on the study of several steps during the reduction of CO_2 such as the reduction of CO (chapters 4 and 5) and the reduction of acetaldehyde (chapter 3) in order to gain insight into the mechanism of the reaction. In addition we investigated how different factors such as the structure of the electrode, the potential applied or/and the effect of the cations influence the mechanism of these reactions. The study was performed with a combination of

techniques such as cyclic voltammetry, High Performance Liquid Chromatography, Online Electrochemical Mass Spectrometry, Fourier Transform Infrared Spectroscopy and Density Functional Theory calculations.

1.5.2 Electroreduction of CO_2 to cyclic carbonates

Cyclic carbonates are profitable synthetic targets starting from CO_2 due to the added value of these organic molecules compared to CO_2. In addition, the fixation of CO_2 into organic molecules offers an environmentally friendly alternative to storage solutions[68]. The formation of cyclic carbonates has been an area of interest due to the versatility of these compounds. Cyclic carbonates can be used as electrolytes for Li ion batteries, fuel additives, as aprotic polar solvents, as green reagents and as useful intermediates for manufacturing polycarbonates[69-70]. Polycarbonates are the most widely used engineering plastics, currently synthesized through the phosgene process. The use of a highly toxic substance like phosgene, which is regulated by the international treaty concerning chemical weapons [71], makes the synthesis of polycarbonates environmentally unacceptable. Substituting phosgene with CO_2 will radically diminish environmental issues due to not only the elimination of toxic by-products but also due to the capture and conversion of CO_2.

In view of the commercial importance of cyclic carbonates and their broad applications in industry, the catalytic synthesis of these compounds has been extensively studied. Several homogeneous catalysts based on metal complexes[72-74] have been proposed for the conversion of CO_2 and epoxides to cyclic carbonates. However, most of the currently used catalysts for this process demand high operational temperatures and/or high carbon dioxide pressures[75-77]. The use of electrochemistry allows for the synthesis of cyclic carbonates under mild conditions with high efficiencies[78-79]. Copper, among other metals tested for this process such as Ni, Ag or graphite, has been found to be

one of the most efficient metals for the conversion of carbon dioxide and epoxides to cyclic carbonates[79-81]. Copper and copper nanoparticles have been employed as cathode for the synthesis of cyclic carbonates, achieving high conversion and selectivity [78, 80].

Despite all the studies concerning this process, the mechanism of the reaction is still under debate. While numerous studies argue that the key step for the synthesis of cyclic carbonates is the activation of the epoxide via the ring opening[72, 74, 82-83], other studies consider the activation of carbon dioxide through the formation of the radical anion $CO_2^{\cdot-}$ to be the key step for the synthesis of organic carbonates[81, 84].

In this thesis, we employed Fourier Transform Infrared Spectroscopy (FTIR) and High Performance Liquid Chromatography (HPLC) to gain insight into the mechanism of cyclic carbonates synthesis and establish that adequately activated CO_2 is able to carboxylate organic molecules, such as epoxides, to form cyclic carbonates.

1.6 Copper, an extraordinary catalyst

Copper has been used since 8000 BC due to the luxury of direct use in metallic form without its extraction from an ore. Copper is abundant on Earth, with 10^{14} tons existing in the first kilometer of the Earth's crust. The abundance of copper and its ease of mining make it a rather inexpensive metal. The price of copper has been unstable during history[85], although in the last 10 years it has been more stable with values around US$3/kg. The price of copper is more than 10000 times lower than other metals like Pt or Au. The abundant and cheap nature of copper, has generated interest into its use as a catalyst in electrochemical processes. Metallic copper, copper-based and oxide-derived copper catalysts are able to efficiently catalyze numerous reactions[29, 47, 57, 67-68, 86]. In this thesis, we will focus our attention on the reduction of nitrates, the reduction of carbon dioxide and the

conversion of carbon dioxide and propylene oxide to propylene carbonate on metallic copper electrodes.

The morphology of the catalyst is crucial to understand the mechanism of the reaction carried out on the copper surface. For that reason, copper single crystals were employed.

Copper is a face-centered cubic (fcc) metal with copper atoms located at each of the corners of the unit cell and at the center of all the cubic faces. Bulk copper has a coordination number of 12 since 12 of their atoms are shared with other unit cells. The fcc unit cell consists of a net total of four atoms, eight eighths from corner atoms and six halves from the face atoms. In order to identify the different planes and directions in a crystal structure, Miller indices are used which consist of three values of h, k and l as directional parameters. The most studied surfaces are those for which the plane is perpendicular to the principal axis, called basal planes. For an fcc structure the basal planes are (100), (111) and (110). In addition, other surfaces with larger Miller indices, namely stepped surfaces, can also be studied. Ideal stepped surfaces consist of terraces

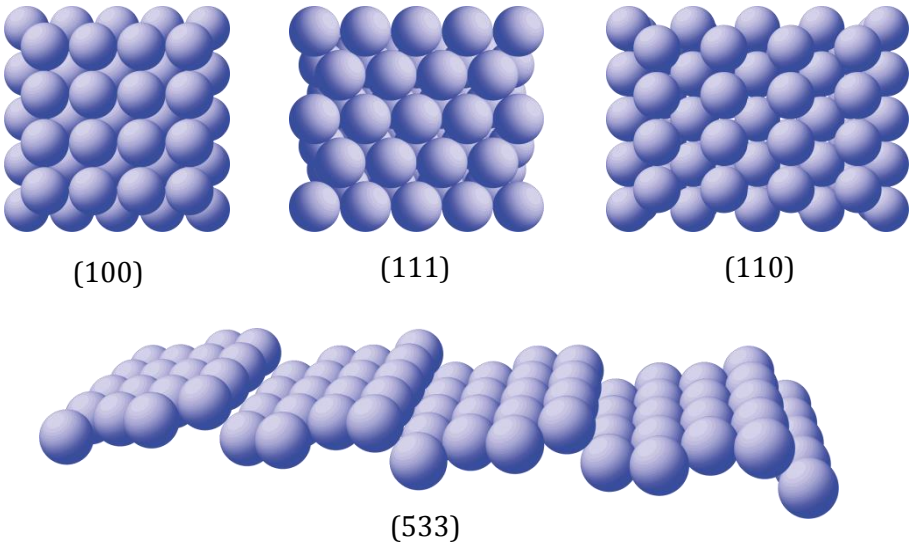

Figure 1.2: Representation of different surface structures of an fcc crystal, taken from surface explorer.(http://surfexp.fhi-berlin.mpg.de)

with a low index atomic arrangement, separated by monoatomic steps. A representation of such surfaces is displayed in Figure 1.2. The use of single crystals in electrochemistry helps in understanding how different adsorption sites influence the stability of intermediates in a certain reaction, catalyzing more efficiently the conversion of different species.

1.7 Scope and outline of this thesis

The general focus of the research offered in this thesis is the electro-conversion of environmentally harmful chemicals, such as nitrates and carbon dioxide, into more valuable and less polluting compounds. In particular, the study is focused in the understanding of the mechanistic aspects of these reactions carried out on copper electrodes.

In chapter 2, we study the electrochemical reduction of nitrates on copper single-crystal electrodes in acidic and basic media to evaluate the reaction mechanism and the products obtained in the different media and on the different surfaces employed. Using electrochemical techniques coupled to analytical techniques we observe differences in product distribution depending on the pH of the electrolyte. Whereas in acidic media the reduction of nitrate leads to NO and ammonia, in basic media the product observed is hydroxylamine. Furthermore, the reaction is structure sensitive in basic media: Cu(100) is most active for the formation of hydroxylamine. Conversely, in acidic media the reaction is independent of the catalyst's structure.

In chapter 3 we study the electroreduction of acetaldehyde to ethanol, a reaction which is supposed to take place at a late stage in the reduction of carbon dioxide. Combining experimental techniques with density functional theory we outline the structure sensitivity of the reaction. Experiments show that more open facets have lower overpotentials for the formation of ethanol. DFT calculations predict that the formation of ethanol proceeds via a weakly bounded $CH_3CH_2O^*$ intermediate which binds more favourably on open surfaces, explaining the earlier

formation of ethanol on those facets. In addition, DFT calculations show higher thermodynamic limitations for ethanol compared to ethylene. Making use of the structure selectivity observed for ethanol formation, the selectivity towards ethanol formation can be enhanced.

In chapter 4 we study the early stages of CO reduction by Fourier Transform Infrared Spectroscopy and Density Functional Theory. We show experimentally that Cu(100) electrodes in LiOH solutions host a C-containing adsorbate at low overpotentials, which we propose to be a hydrogenated CO dimer (OCCOH). The formation of the hydrogenated dimer is a structure-sensitive process, which does not occur on Cu(111) surfaces, confirming the theoretical hypothesis that the dimerization is favoured on square-symmetry sites.

In chapter 5 we show how the combined effect of alkaline cations, catalyst structure and applied potential can steer the selectivity of CO reduction towards ethylene or methane. First, we find that the nature of the cation affects the product selectivity, depending on the potential applied. Whereas larger cations enhance the selectivity to ethylene at potentials more positive than -0.45 V vs RHE, the selectivity towards methane is enhanced by larger cations at more negative potentials. The fact that ethylene formation declines at potentials for which methane formation increases, suggests that the pathway towards ethylene is blocked by the enhancement of the pathway that leads to methane. Secondly, we observe that cation effects are structure dependent, as the onset potential for ethylene formation depends on the electrode structure and cation size, whereas the onset potential for methane formation does not. The formation of the intermediate suggested in chapter 4 (OCCOH) was found to be dependent on the nature of the cation, so that the hydrogenated dimer can be detected with FTIR in presence of Li^+, Na^+ and K^+, but not in presence of Rb^+ or Cs^+. DFT calculations explain that the potential necessary to form *OCCOH from *CO in presence of Cs^+ is more negative compared to Li^+ or Na^+. Lastly, we point out the role of the cations as catalytic promoters by stabilizing intermediates through favourable electrostatic interactions.

In chapter 6 we investigate the conversion of CO_2 to organic molecules, specifically the reaction between CO_2 and propylene oxide to form propylene carbonate. Employing cyclic voltammetry, Fourier Transform Infrared Spectroscopy and High Performance Liquid Chromatography we study the mechanism of the reaction. We rule out different reduced forms of CO_2, such as CO and (bi)carbonate as possible carboxylation agents. Moreover, we rule out the electrochemical activation of propylene oxide via ring opening as the initial step for this reaction. We propose an electrochemical reaction initiated by the activation of CO_2 to $CO_2^{\cdot-}$ which then attacks propylene oxide to form propylene carbonate.

Chapter 2

Electroreduction of nitrate on copper single crystals in acidic and alkaline media

Nitrate reduction on Cu (100) and Cu (111) surfaces in alkaline and acidic solutions was studied by electrochemical methods (cyclic voltammetry, rotating disc electrode) coupled with online and in situ characterization techniques (mass spectrometry, ion chromatography and Fourier transformed infra-red spectroscopy) to evaluate the reaction mechanism and products on the different surfaces. Electrochemical results show that reduction of nitrate in alkaline media on Cu is structure sensitive. The onset potential on Cu (100) is +0.1 V vs. RHE, ca. 50 mV earlier than on Cu (111). The onset potentials for nitrate reduction on Cu (100) and Cu (111) in acidic media are rather similar. Analytical techniques show a diverse product distribution for both surfaces and for both electrolytes. Whereas in acidic media both Cu electrodes show the formation of NO and ammonia, in alkaline media Cu reduces nitrate to nitrite and further to hydroxylamine. In alkaline media, Cu (100) is a more active surface for the formation of hydroxylamine than Cu (111).

This chapter has been published as: E Pérez-Gallent, MC Figueiredo, I Katsounaros, MTM Koper, Electrochimica Acta, 2017, 227, 77-84

2.1 Introduction

Human activities like the combustion of fossil fuels, the nuclear industry, the production of nitrogen fertilizers and the cultivation of nitrogen-fixing plants are inducing severe alterations in the global nitrogen cycle [16]. The rate of many human-caused global changes has increased severely in last decades, but none so rapidly as industrial production of N fertilizers, which has grown exponentially since the 1940s. The increase of the availability of N also increases biomass production and accumulation significantly[87] . Consequently, changes in nitrogen cycle can also lead to changes in the global carbon cycle, generating an increase of carbon dioxide in the atmosphere [88]. The slow natural process of denitrification is unable to deal with the surplus of nitrate-derived compounds leading to a deteriorating effect on our ecological system and human health.

Electrochemistry could play an important role in the development of new denitrification technologies due to its environmental compatibility, versatility, energy efficiency, selectivity and low associated costs, as well as the non-requirement of reduction agent[23, 35]. However, there is a need for an appropriate electrocatalyst that can provide an optimized process with high selectivity to harmless products like N_2 or valuable products such as ammonia or hydroxylamine. The electrochemical reduction of nitrate has been studied on several transition and coinage metal electrodes in acidic media[35]. Copper has been shown to be the most active coinage metal for this reaction having ammonia as main product[36-37]. A high electrochemical activity for nitrate reduction has also been observed on copper electrodes in alkaline solutions[38]. Nitrate reduction in alkaline media is of interest due to the less probable solution-phase formation of products like toxic nitrogen oxides[89] , as compared to reduction in acidic media, and because of the concern of removing nitrate from alkaline nuclear waste. In this context, the use of single-crystal copper surfaces offers the unique opportunity to evaluate

the effect of the surface atomic structure on the reaction rate, the preferred reaction paths and the resulting product distribution.[90]

In this chapter, we study the influence of the surface structure of Cu electrodes on the nitrate reduction in alkaline and acidic media. We use electrochemical techniques (cyclic voltammetry, rotating disc electrode) coupled with online and in situ characterization techniques (mass spectrometry, ion chromatography and Fourier transformed infra-red spectroscopy) to evaluate the reaction mechanism and products on the different surfaces and their dependence on the available atomic sites.

2.2 Experimental

Prior to each electrochemical experiment, the glassware used was stored overnight in a solution of $KMnO_4$ that was rinsed with a mixture of ultra clean water (Millipore MilliQ, resistivity > 18.2 MΩ), 20 mL/L of hydrogen peroxide and 1 mL/L of concentrated sulfuric acid. The glassware was further cleaned by boiling 4 times in Millipore MilliQ water. A coiled platinum wire was used as a counter electrode and a reversible hydrogen electrode (RHE) in the same electrolyte was used as the reference electrode. All potentials in this chapter are referred to RHE.

The copper electrodes used were 99.99% copper disks with a diameter of 6mm, purchased from Mateck and aligned to < 0.5° accuracy. Prior to every experiment, the electrodes were electropolished in a 10:5:2 mixture of H_3PO_4:H_2O:H_2SO_4 at +3 V vs. Cu for 30 s, followed by a stabilization step at 0 V for 30 s. After thorough rinsing with ultrapure water, the surface of the crystal was characterized by cyclic voltammetry at a scan rate of 50 mV/s in NaOH 0.1 M solution[91]. Cyclic voltammograms were recorded by an Ivium A06075 potentiostat.

Electrolytes were made from ultra-pure water (Millipore MilliQ, resistivity > 18.2 MΩ) and high purity reagents (Sigma Aldrich

TraceSelect). Before every experiment, Argon (Linde, 6.0) was bubbled through the electrolyte for 15 min in order to remove air from the solution, and during the experiments the argon was kept flowing above the solution.

In order to control mass transfer rates, Cyclic Voltammetry (CV) under hydrodynamic conditions was performed with a home-made hanging-meniscus rotating disc electrode (HMRDE) configuration, compatible with single-crystal electrodes. The rotation was controlled with a modulated speed rotator (PINE, MSR). Experiments were carried out at a rotation rate of 400 rpm.

Online Electrochemical Mass Spectroscopy (OLEMS)[92] was used to detect the gaseous products formed during the reaction. The reaction products at the electrode surface were collected by a hydrophobic Teflon tip situated very close to the surface of the electrode (about 10 μm). The tip is a 0.5 mm diameter porous Teflon cylinder with an average pore size of 10-14 μm in a Kel-F holder, connected to a mass spectrometer by a PEEK capillary. Before every experiment, the tip was submerged in a solution of 0.2 M $K_2Cr_2O_7$ in 2 M H_2SO_4 and rinsed extensively with MilliQ water. A Balzers Quadrupole mass spectrometer with a secondary electron multiplier (SEM) voltage of 2400 V was used for the detection of every mass. The different mass signals were followed while changing the electrode potential from +0.25 V to -1 V vs. RHE and back at a scan rate of 1 mV/s.

Online Ion Chromatography (IC) was utilized to detect ionic products dissolved in the electrolyte[93]. The reaction products were collected with an automatic sample collector (FRC-10A, Shimadzu) by an open tip situated very close (about 10 μm) to the electrode. The potential of the electrode was changed from 0.35 V to -0.6 V and back at a scan rate of 1 mV/s. Every sample contains 60 μL and they were collected with a rate of 60 μL/min, meaning that every sample contains the average products of a change in potential of 60 mV. After voltammetry, all the samples collected were analyzed with IC (Shimadzu, Prominence) equipped with a conductivity detector (CDD-10A vp, Shimadzu). For the detection of

the anion (NO_2^-), sodium nitrite (Merck, 99.99%) was utilized to prepare standard solutions, from which the retention time was determined and the concentration was calibrated. An NI-424 (Shodex) anionic column was used at a constant temperature of 40 °C with an eluent flow rate of 1 mL/min. The eluent consists of 2.8 mM BIS-TRIS (Fluka, BioXtra, >99%), 2 mM phenylboronic acid (Fluka, purum, >97%), 8mM 4-hydroxybenzoic acid (Sigma-Aldrich, 99%), and 0.005 mM trans-1,2-diaminocyclohexane-N,N,N',N'-tetra acetic acid (Sigma- Aldrich, ACS reagent, >99%).

In all the above techniques, the electrode was in hanging meniscus configuration, meaning that only the face of the crystal with the desired structure was in contact with the electrolyte.

FTIR measurements were performed with a Bruker Vertex 80 V Infrared spectrophotometer[94]. The electrochemical cell was assembled on top of a 60° CaF_2 prism, and the electrode was situated against this prism to form a thin layer. The measurements were performed under external reflection. FTIR spectra were obtained from an average of 100 scans with a resolution of 8 cm^{-1} at the selected potentials. Every spectrum was obtained by applying single potential steps compared to the reference potential (+0.35 V vs. RHE). The spectra are shown as ($R-R_0/R_0$) where R is the reflectance at the sample potential and R_0 is the reflectance at the reference potential. Thereby the ratio $\Delta R/R_0$ gives positive bands for the formation of species at the sample potential, and negatives bands correspond to the loss of species at the sample potential. P-polarized light was used to probe species both near the electrode surface and in solution.

2.3 Results and Discussion

2.3.1 Nitrate reduction in alkaline media

2.3.1.1 Cyclic voltammetry (CV) and hanging-meniscus rotating disc electrode (HMRDE) measurements.

Fig 2.1a shows the cyclic voltammograms for Cu (111) (blue curve) and Cu (100) (green curve) in 0.1 M NaOH solution (dashed lines) and in 0.1M NaOH with 2 mM of $NaNO_3$ (full lines). In the blank voltammetry, for both surfaces we observe a featureless voltammogram between +0.3 V and -0.5 V vs. RHE. When more negative potentials are applied, both surfaces evolve hydrogen, with Cu (111) being more active for HER with an onset potential of -0.4 V compared to -0.5 V for Cu (100). With nitrate in solution, reduction currents are observed for both surfaces at much lower potentials than HER. Cu (111) shows two reduction peaks, the first one starts at +0.15 V reaching a maximum current density of ca. -0.4 mA/cm^2 at +0.1 V. The second peak has an onset potential of -0.15 V reaching a maximum current density of ca. -3 mA/cm^2 at -0.5 V. On the other hand, Cu (100) shows one peak starting at +0.1 V reaching a maximum current density of ca. -4.3 mA/cm^2 at -0.3 V. According to the literature[24, 32, 37, 95] the first reduction product of nitrate reduction is nitrite. The small reduction peak starting at +0.15 V on the Cu (111) electrode is probably associated with this first reduction step:

$$NO_3^- + H_2O + 2e^- \rightarrow NO_2^- + 2OH^- \quad (2.1)$$

as is evidenced by the absence of this peak when the reactant is $NaNO_2$ (see Fig. 2.1b). The voltammogram obtained with Cu (100) only shows one wave with an onset potential of +0.1 V, associated with the formation of nitrite and further reduced products as suggested by the CVs for nitrite reduction shown in Fig 2.1b. Cu (100) shows a diffusion-limited plateau with a maximum current density of ca. -4.3 mA/cm^2 at around -0.3 V, this limiting current being dependent on rotation rate. A

Levich plot of the rotation-rate dependence of the current plateau is not perfectly linear; from the slope we estimate that the number of electrons involved in the process is between 5 and 7 (with 6 corresponding to the formation of hydroxylamine). On the other hand, the CV obtained for Cu (111) is only partially diffusion limited and does not reach a plateau current. Although on Cu (111) the reduction of nitrate has a lower onset potential, the reaction appears to become blocked by intermediates of the hydrogen evolution reaction, which has a more positive onset potential on Cu (111) than on Cu (100), and as a result the nitrate reduction is not able to reach full diffusion limitation on Cu (111).

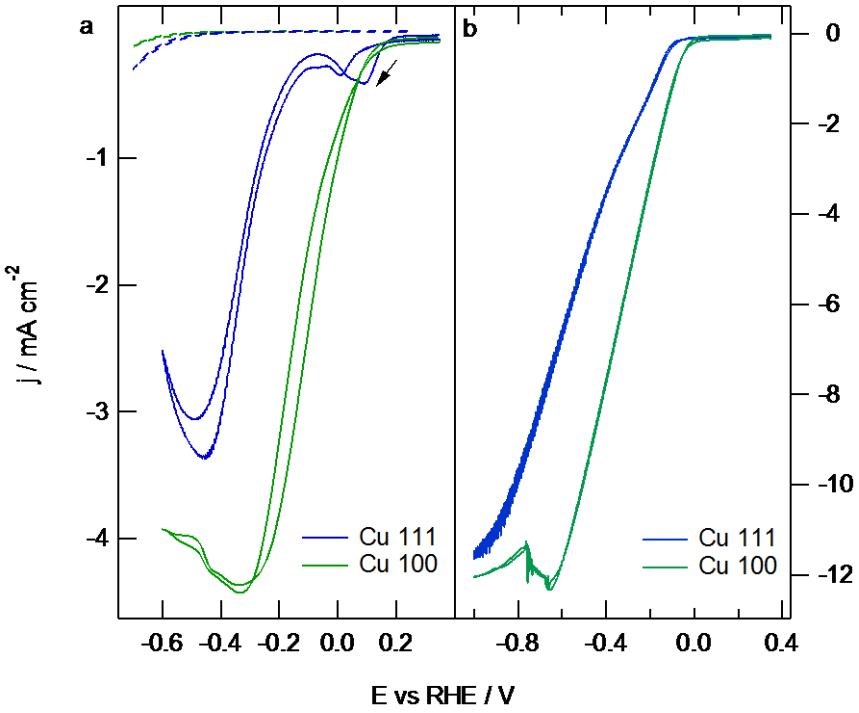

Figure 2.1: Cyclic voltammetry recorded at Cu (111) and Cu (100) electrodes in 0.1M NaOH in the absence (dashed lines) and presence (solid lines) of a) 2 mM $NaNO_3$ and b) 10 mM $NaNO_2$ Experimental conditions: scan rate 50 mV/s; rotation rate 400rpm.

We note that in the presence of nitrate there is a strong poisoning effect on Cu (111) as illustrated in figure 2.2, showing cyclic voltammograms of the nitrate reduction reaction as a function of the cycle number for Cu (100) (Fig.2.2a) and Cu (111) (Fig.2.2b) electrodes in a 0.1 M NaOH solution containing 2 mM $NaNO_3$. The reduction peak observed at +0.15 V in the first cycle of nitrate reduction on Cu (111) is absent in the following cycles, suggesting that the reaction on Cu (111) is inhibited already after the first cycle. Both electrodes show deactivation with cycling in the potential window shown in Fig.2.2, but the deactivation of the Cu (111) electrode is much more pronounced than for Cu (100). If the negative vertex of the potential window is limited to -0.4 V (see Fig.2.3a), Cu (100) does not show deactivation, suggesting that the deactivation is associated with the formation of adsorbed hydrogen. On the contrary, Cu (111) still shows deactivation also if the potential scan is limited to -0.4V (see Fig.2.3b), in agreement with the lower onset potential for hydrogen evolution and hydrogen adsorption on Cu (111). This inhibition and deactivation by adsorbed hydrogen is also known for nitrate reduction on Pt[24, 96]. Similarly to nitrate reduction on Pt the negative differential resistance that is the result of the inhibition by adsorbed hydrogen can give rise to spontaneous (current) oscillations[97] during nitrate reduction, as illustrated in Fig.2.2a for Cu (100). These oscillations are caused by the interplay between the negative differential resistance and the ohmic resistance of the electrolyte solution[98]. The possibility of poisoning of the electrode by intermediate N-containing species was also considered. However, we consider it less likely considering that self-poisoning typically does not lead to a negative differential resistance, but rather to a lower overall current. The observed negative differential resistance is characteristic for poisoning by a parallel side reaction, in this case hydrogen adsorption.

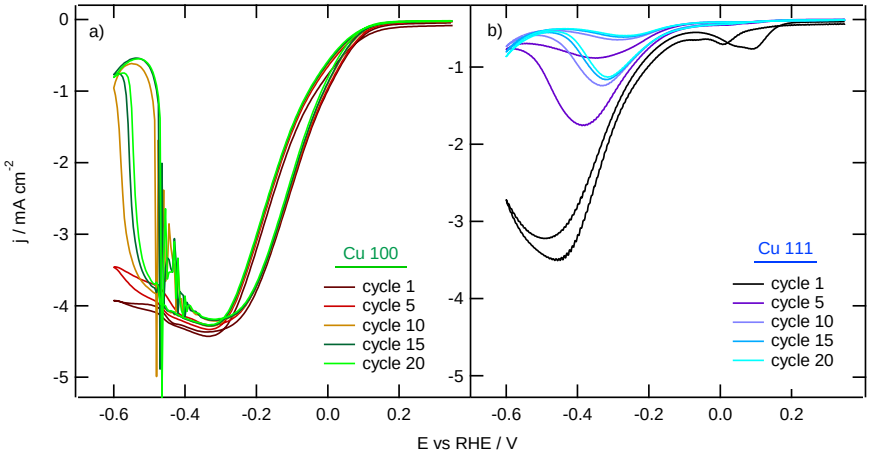

Figure 2.2: Cyclic voltammetry recorded at a) Cu (100) and b) Cu (111) electrodes in 0.1 M NaOH in the presence of 2 mM NaNO3 as a function of the cycle number. First cycle starts at 0.35 V vs. RHE. Experimental conditions: scan rate 50 mV/s; rotation rate 400rpm

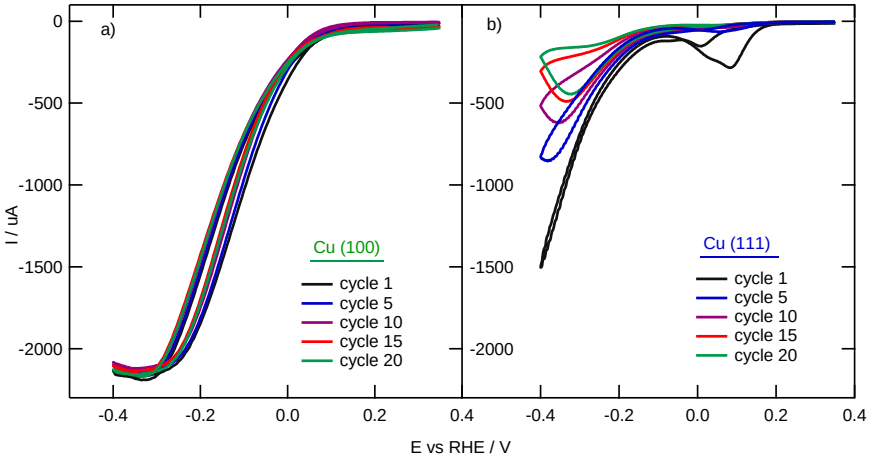

Figure 2.3: Cyclic voltammetry recorded at a) Cu (100) and b) Cu (111) electrodes in 0.1 M NaOH in the presence of 2 mM $NaNO_3$ in the potential window between +0.35 and -0.4 V vs. RHE as a function of the cycle number. Experimental conditions: scan rate 50 mV/s; rotation rate 400rpm.

2.3.1.2 Ion Chromatography and OLEMS data

Fig.2.4 illustrates the formation of nitrite detected by Ion Chromatography as a function of the cycle number for Cu (100) (Fig. 4a) and Cu (111) (Fig. 4b) in a 0.1 M NaOH solution containing 2 mM $NaNO_3$. The onset potential for the formation of nitrite matches the onset potential seen in voltammetry (see Fig.2.1), i.e. +0.15 V for Cu (111) and +0.1 V for Cu (100). The profile of the formation of nitrite on Cu (100) shows a maximum at -0.1 V, and decreases at more negative potentials, indicating the further reduction of nitrite. On the other hand, the formation of nitrite on Cu (111) shows a less accentuated profile, with a plateau, suggesting that further reduction is slow. Moreover, consistent with the deactivation of Cu (111) shown in Fig.2.2, Cu (111) does not form any nitrite in the second cycle of the voltammetry, whereas Cu (100) shows only a small decay in the amount of nitrite formed compared with the amount formed in the first cycle. Note, however, that the employed scan rate in Figure 2.4 is significantly lower than in Figures 2.2 and 2.3.

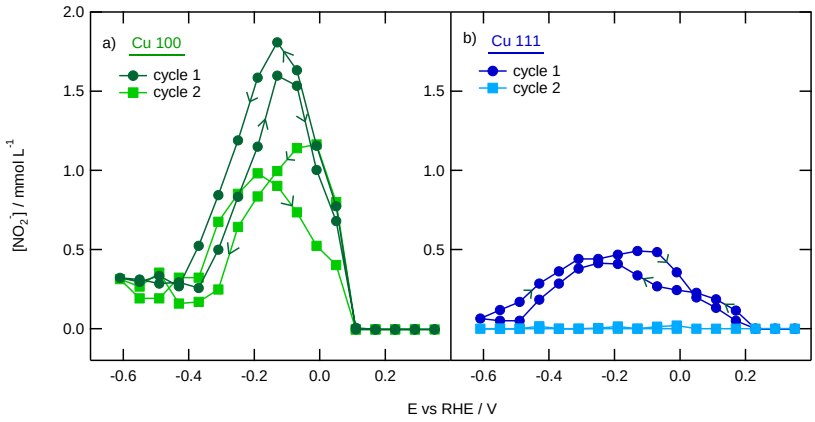

Figure 2.4: Formation of NO_2^- detected with online ion chromatography from a) Cu (100) electrode and b) Cu (111) electrode in a 0.1 M NaOH solution containing 10 mM $NaNO_3$. Scan rate = 1 mV/s

The possible formation of gaseous products such as N_2O, NO or N_2 during the reduction of nitrate, was followed by OLEMS. As Fig. 2.5 shows, neither Cu (111) nor Cu (100) form any gaseous products other than hydrogen, which is associated with the reduction of water from the electrolyte.

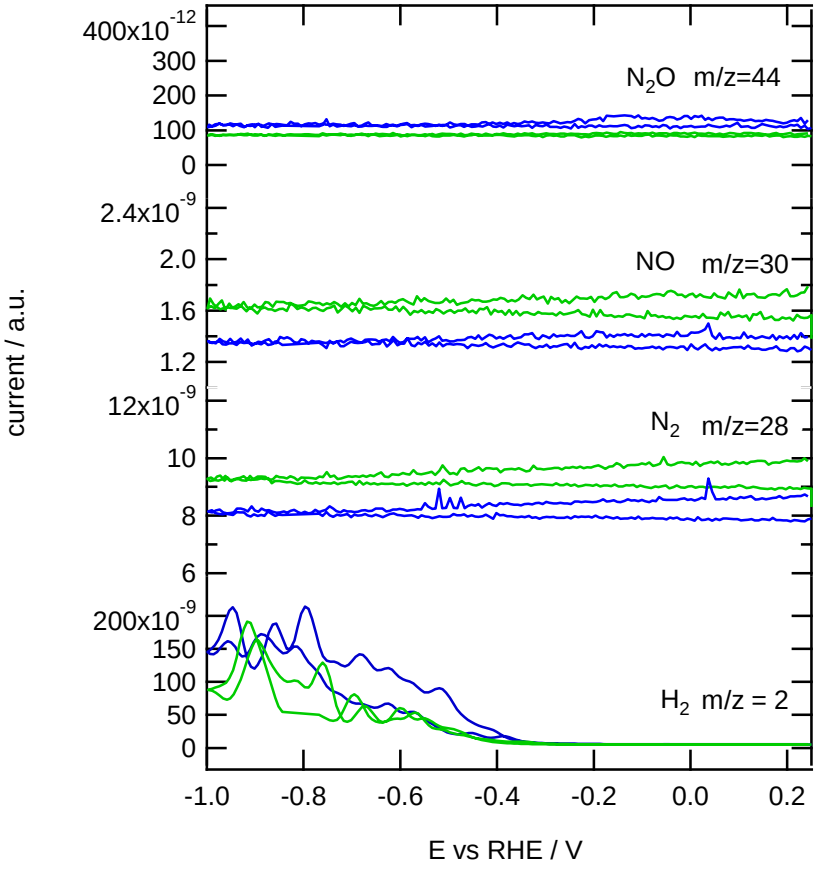

Figure 2.5: Mass fragments associated with various products measured with OLEMS for the reduction of 10 mM $NaNO_3$ in 0.1 M NaOH solution in Cu (100) (green curves) and Cu (111) (blue curves) electrodes. Scan rate = 1mV/s

2.3.1.3 FTIR spectroscopy

Reaction intermediates or possible adsorbates on the electrodes were followed by FTIR in order to obtain a better insight about the intermediates and the mechanism of the reaction. Fig.2.6 displays the potential dependent absorbance spectra with respect to the reference potential (0.35 V). In agreement with the onset potentials for nitrate reduction observed in the CVs (fig.2.1) and IC (fig.2.4), the absorbance spectra also show that the onset potential for the reduction of nitrate is 0.15 V on Cu (111) and +0.1 V on Cu (100), as observed by a negative band at 1370 cm^{-1} associated with the consumption of nitrate[94]. Simultaneously to nitrate consumption the formation of nitrite can be seen by the positive band at 1231 cm^{-1}, which appears at similar potentials to those observed by IC (Fig.2.4). Interestingly, the band observed at 1191 cm^{-1} during the reduction of nitrate on Cu (100) indicates the production of hydroxylamine (NH_2OH)[99] at potentials more negative than 0 V (see Fig.2.6 left panel). By contrast, the spectra recorded with Cu (111) do not show the band at 1191 cm^{-1}. However, cathodic currents are observed in the reduction of $NaNO_2$ on Cu (111), suggesting that nitrite can still be reduced. Fig. 2.1b shows similar limiting currents for both surfaces, suggesting that the reduced product has the same nature, but is formed with a slower rate on Cu (111). Therefore, we suggest that, even though clear hydroxylamine bands are not present in the FTIR spectra on Cu (111), the most likely product is still NH_2OH. The absence of the bands related to hydroxylamine in the working potential range suggests that hydroxylamine is formed with a too low concentration at potentials less negative than -0.35V. Also, it is important to highlight the absence of adsorbed NO on both copper surfaces, even when the FTIR spectra were recorded in NaOH solution using D_2O (See Appendix I Fig. AI.1.). The negative band observed at 1623 cm^{-1} is due to the O-H bending of water.

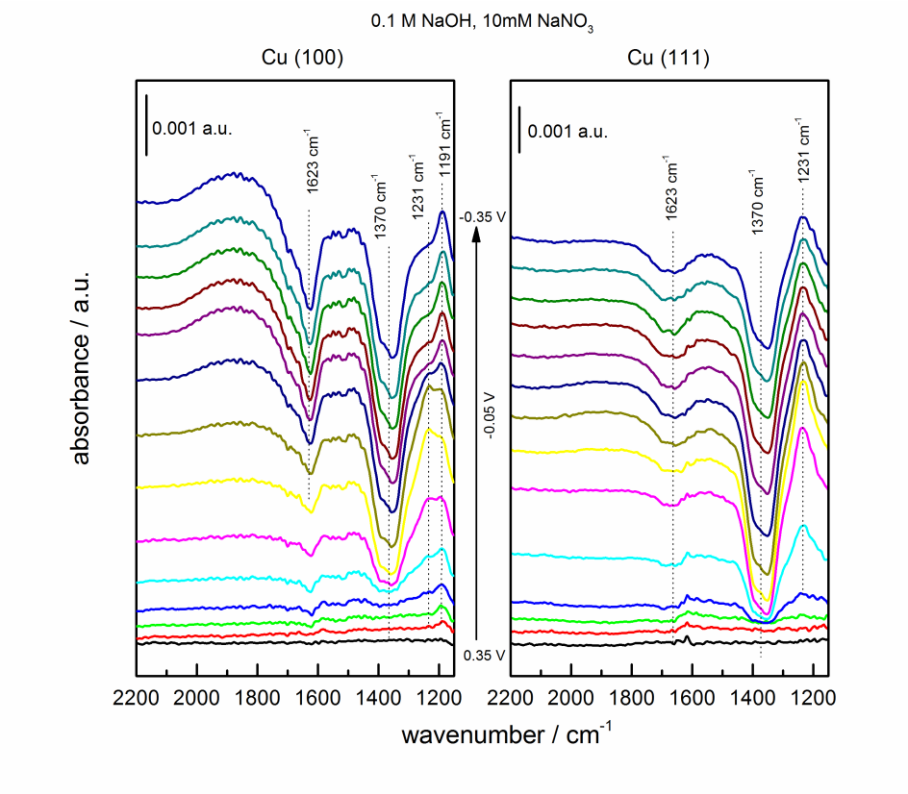

Figure 2.6: Potential dependent absorbance spectra for the reduction of 10 mM $NaNO_3$ on Cu (100) (left panel) and on Cu (111) (right panel) electrode in 0.1 M NaOH solution. Reference spectrum recorded at 0.35 V vs. RHE. Potential step is 0.05V.

The reduction of nitrite (NO_2^-) was also studied by FTIR on both copper surfaces (see Fig. 2.7). As the CVs in Fig.2.1b show, the reduction of nitrite on Cu (100) starts ca. +0.1 V earlier than on Cu (111). Similar to nitrate reduction, also for nitrite reduction the Cu (111) electrode shows a more pronounced inhibition by hydrogen than Cu (100). FTIR spectra were taken in 0.1 M NaOH solutions containing 10 mM of $NaNO_2$ (see figure 2.7). Spectra obtained with Cu (100) show a negative band at 1235 cm^{-1} corresponding with the consumption of nitrite[100] and a positive band at 1191 cm^{-1} assigned to the formation of

hydroxylamine[99]. When Cu (111) is used, the spectra only show a clear negative band at 1235 cm^{-1} corresponding to the consumption of nitrite suggesting that nitrite is indeed reduced further. A small band can be observed at 1190 cm^{-1} suggesting formation of hydroxylamine in accordance with the cathodic currents observed in the reduction of $NaNO_2$ on Cu (111).

Detection of hydroxylamine with another analytical technique such as IC was not technically feasible due to the chemically decomposition of hydroxylamine in alkaline media in the presence of oxygen as described by Hughes et al. [101].

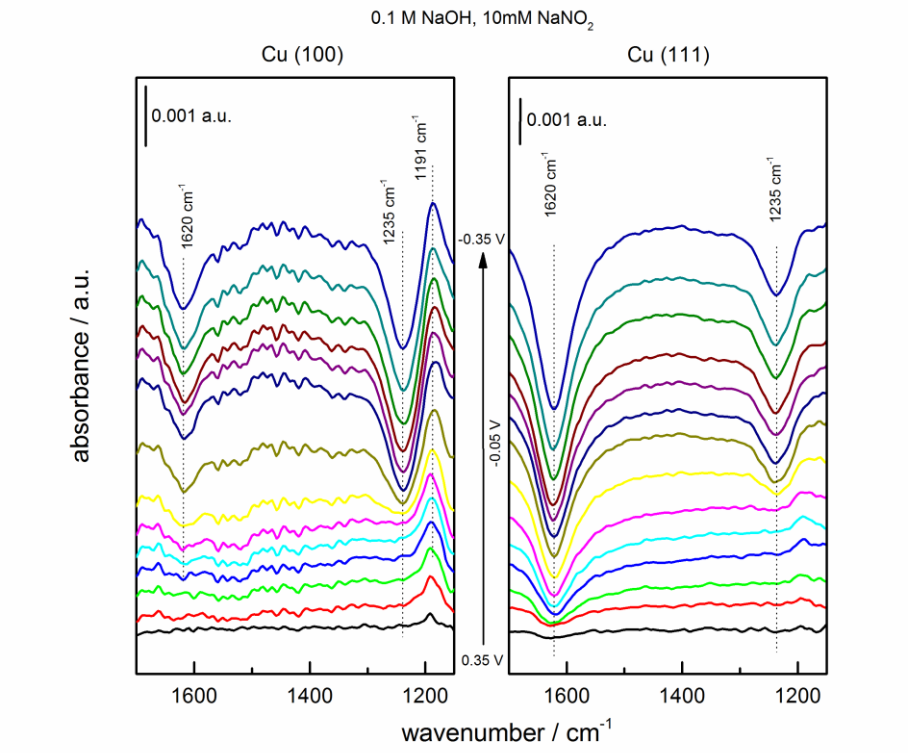

Figure 2.7: Potential dependent absorbance spectra for the reduction of 10 mM $NaNO_2$ on Cu (100) (left panel) and on Cu (111) (right panel) electrode in 0.1 M NaOH solution. Reference spectrum recorded at +0.35 V vs. RHE. Potential step is 0.05V.

2.3.2 Nitrate reduction in acidic media

In order to investigate the pH dependence of nitrate reduction, [32, 38, 90]cyclic voltammetry, OLEMS and FTIR measurements were performed in 0.1 M $HClO_4$ solution on both Cu (111) and Cu (100).

2.3.2.1 CV and RDE data

Fig.2.8 displays the cyclic voltammograms recorded for Cu (111) and Cu (100) in a 0.1 M $HClO_4$ solution. There is a significant dependence of the profile of the CV on the surface orientation of the copper electrode. In the absence of nitrate, Cu (111) is the more active surface for HER, as in alkaline media, starting at -0.4 V on Cu (111) and at -0.5 V on Cu (100). In the presence of nitrate, the onset potential for nitrate reduction in acidic media seems to be rather similar, around +0.2 V vs. RHE, for both copper surfaces. On both electrodes the cathodic current reaches a diffusion limited plateau at around -0.1 V. At Cu (111) the current drops drastically to a value close to zero at -0.3 V to eventually increase again at -0.4 V due to the hydrogen evolution reaction. The voltammogram for Cu (100) appears to show two waves with an inflection feature at around 0 V. The cathodic current reaches a plateau at around -0.2 V with the same current density as the plateau obtained on Cu (111), ca. -4.5 mA/cm^2. CVs recorded on Cu (100) show diffusion limited currents that depend on the rotation rate, following the Levich equation. From the slope of the Levich plot, the number of electrons involved in the process was calculated to be close to 5. From the reduction of NO_3^-, a $5e^-$ transfer process would suggest formation of N_2. However, OLEMS measurements showed the absence of nitrogen formation, with the only volatile product being NO, as shown in Fig.2.9. Cu (111) reaches the same diffusion-limited current at -0.2 V, but becomes poisoned at ca. -0.3 V, probably due to the blockage of the surface by adsorbed hydrogen.

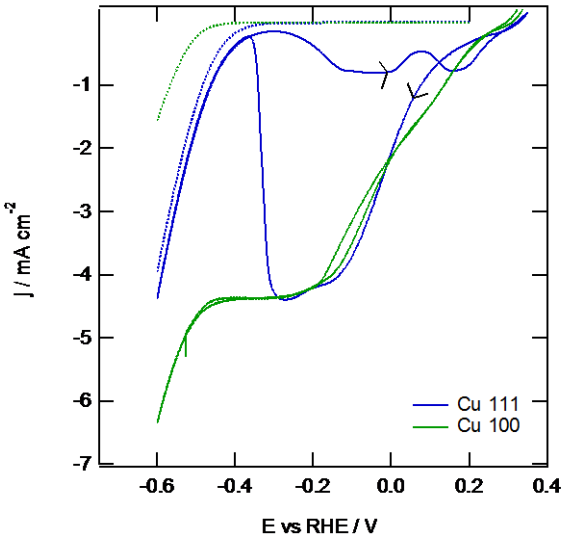

Figure 2.8: Cyclic voltammetry recorded at Cu (111) (blue curve) and Cu (100) electrodes (green curve) in 0.1M $HClO_4$ in the absence (dashed line) and presence (solid line) of $NaNO_3$. Experimental conditions: scan rate 50 mV/s; rotation rate 400rpm; [$NaNO_3$] = 2 mM

Cyclic voltammograms recorded on Cu (111) and on Cu (100) in a 0.1 M $HClO_4$ solution containing 2mM $NaNO_3$, as a function of the cycle number, are plotted in Fig. 2.10. The evolution of the CVs differs between the two surfaces. On Cu (111) (right panel) the features a, b and c give rise to a more negative currents with increasing number of cycles, and the decay in current observed at -0.3 V in the first cycle is shifted to more positive potentials in subsequent scans. On Cu (100), there is no strong effect of repeated cycling and no deactivation. In line with the greater extent of deactivation of Cu (111) in alkaline media, in acidic media Cu (111) also shows a much stronger deactivation than Cu (100) for the reduction of NO_3^-. However, the CV on Cu (111) shows no deactivation if the negative potential limit is kept above -0.2 V (see Fig.2.11), suggesting that the cause of the deactivation is adsorbed hydrogen. As mentioned above, the deactivation of Pt electrode during nitrate reduction has also been suggested to be related to the formation of H_{ads}.[24]

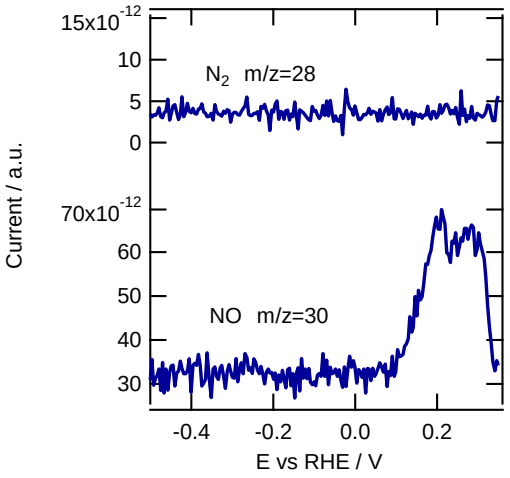

Figure 2.9: Mass fragments associated with various products measured with OLEMS for the reduction of 10 mM $NaNO_3$ in 0.1 M $HClO_4$ solution on a Cu (100) electrode. Scan rate = 1mV/s

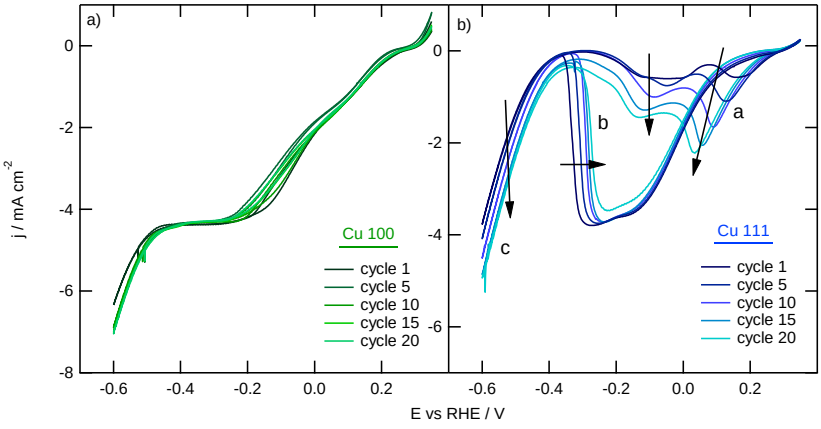

Figure 2.10: Cyclic voltammetry recorded at a) Cu (100) and b) Cu (111) electrodes in 0.1 M HClO4 in the presence of 2 mM $NaNO_3$ as a function of the number of cycles. Experimental conditions: scan rate 50 mV/s; rotation rate 400rpm.

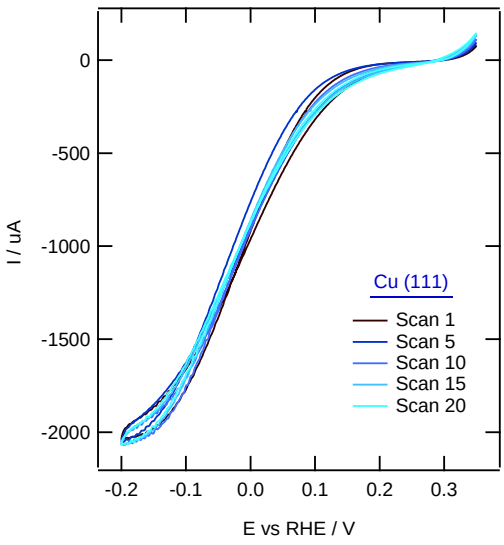

Figure 2.11: Cyclic voltammetry recorded at a Cu (111) electrode in 0.1 M HClO4 in the presence of 2 mM $NaNO_3$ as a function of the number of cycles. Experimental conditions: scan rate 50 mV/s; rotation rate 400rpm.

2.3.2.2 FTIR spectroscopy

With the aim to elucidate possible adsorbates or intermediates of the reaction, FTIR measurements were carried out on both copper electrodes in 0.1 M $HClO_4$ solution. Fig.2.12 shows the potential dependent absorbance spectra with respect to the reference potential of +0.35 V. The FTIR spectra indicate that the onset potential for nitrate reduction in acidic media is +0.15 V for Cu (100) and +0.1 V for Cu (111) as shown by the negative bands at 1270 cm^{-1} associated with the consumption of nitrate[94]. These values of the onset potential are in agreement with the values observed with cyclic voltammetry (see Fig.2.8). Interestingly, the band corresponding to nitrite is not present in the spectra, probably because of the fast conversion of nitrite into NO in acidic media, and subsequent reduction of NO to ammonium[24, 89]. N-O stretching bands corresponding to adsorbed NO are present in the

spectra of both electrodes. On Cu (111), the band appears at 1627 cm^{-1} [102] and on Cu (100) the band appears at 1617 cm^{-1} [103]. The onset potential for the formation of NO is difficult to estimate, since the small NO band is hidden in a fluctuation of the baseline of the spectra due to changes in the thin layer. Both copper surfaces show a positive band at 1460 cm^{-1} corresponding to NH_4^+.[94] Ammonium formation starts around +0.1 V vs. RHE for both copper orientations. These observations are consistent with the results by Bae et al.[90, 95] , who reported the formation of NO and ammonium for the reduction of nitrate on copper.

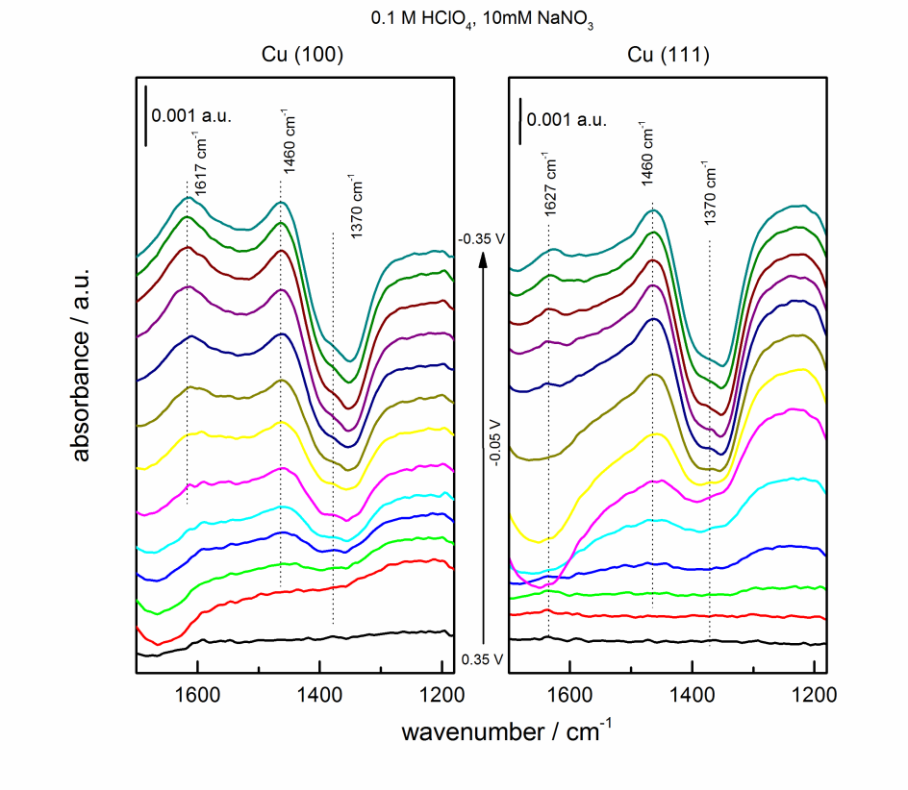

Figure 2.12: Potential dependent absorbance spectra for the reduction of 10 mM $NaNO_3$ on Cu (100) (left panel) and on Cu (111) (right panel) electrode in 0.1 M HClO4 solution. Reference spectrum recorded at 0.35 V vs. RHE.

2.3 General discussion

From the above results, we conclude that there are both structural and pH effects for nitrate reduction on copper single-crystal electrodes. We summarize the relevant reaction steps and observed products and intermediates in Fig.2.13.

In alkaline media, Cu (111) reduces NO_3^- to NO_2^- at lower overpotentials than on Cu (100). However, Cu (100) reduces NO_2^- further to NH_2OH with a considerably higher rate than Cu (111), reaching almost perfect diffusion limitation. Nitrite is observed as an intermediate of the reaction on both surfaces, but no other volatile or surface-adsorbed intermediates have been identified. Both Cu (100) and Cu (111) suffer from inhibition and deactivation by the concurrent hydrogen adsorption reaction. We attribute the deactivation to adsorbed hydrogen since it is not observed if the potential remains at values at which the HER does not occur. Cu (111) is more sensitive to this inhibition/deactivation than Cu (100) because the hydrogen evolution reaction is more active on Cu (111) and Cu (100), both in acidic and alkaline media. The higher activity of Cu (111) for HER as compared to Cu (100) is in agreement with recent theoretical predictions by Santos et al[104].

In acidic media, Cu (100) reduces NO_3^- to HNO_2 at slightly lower potential than Cu (111). In acid media HNO_2 forms NO in solution[89] leading to NO_{ads} on both Cu surfaces, which in turn is reduced to ammonium at roughly the same potential. The reduction of nitrate on Cu (100) is diffusion limited as in alkaline media, but the reduction does not seem to correspond to a single product. Irreversible deactivation is observed on Cu (111) in acidic media, due to the concomitant HER and the related formation of adsorbed hydrogen.

These results demonstrate that the most suitable copper surface for nitrate reduction is the Cu (100) surface, in terms of its activity, its ability to reduce nitrate to an interesting product (hydroxylamine) in alkaline media, and for its smaller tendency to deactivate due to its

lower HER activity compared to Cu (111). Remarkably, the final product of nitrate reduction appears to be pH sensitive: ammonia in acidic media, hydroxylamine in alkaline media.

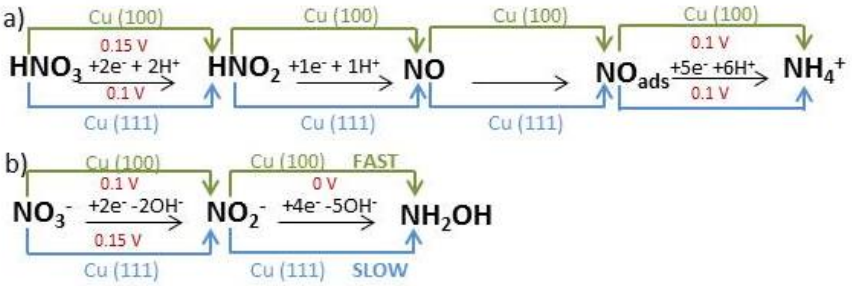

Figure 2.13: Proposed mechanism for nitrate reduction on copper single crystals in a) acidic media and b) alkaline media.

2.4 Conclusions

Electrocatalytic reduction of nitrate on Cu single crystals has been investigated by electrochemical methods coupled with in situ and online analytical techniques, showing that the reduction of nitrate on copper single crystals is sensitive to both surface structure and pH. In alkaline media, Cu (111) reduces nitrate to nitrite at slightly lower potentials than Cu (100), but Cu (100) performs much better in reducing nitrite further to hydroxylamine. In acidic media, there are some differences in the CV profiles, but both copper electrodes give the same intermediates and products: NO, NO_{ads} and NH_4^+. In addition, deactivation of Cu (111) during the reduction of nitrate or nitrite has a larger effect than on Cu (100), in both alkaline and acidic electrolytes studied. The nature of the deactivation is presumably due to the formation of H_{ads} and the difference between the extent of deactivation of the two surfaces can be

related to the higher hydrogen evolution activity of the Cu (111) electrode. Therefore, nitrate reduction on copper is a pH dependent reaction, forming NO and NH_4^+ when an acidic electrolyte is used, and NO_2^- and NH_2OH when the electrolyte is alkaline

Chapter 3

Structure-sensitive electroreduction of acetaldehyde to ethanol on copper and its mechanistic implications for CO and CO_2 reduction

Ethanol is a highly desirable product of the electrochemical reduction of CO and/or CO2 on copper. Although ethanol and ethylene share common intermediates at the early stages of CO/CO2 reduction to C2 species on copper, the pathways bifurcate and most copper surfaces favor the formation of ethylene. We present here a combined experimental-computational study of the electroreduction of acetaldehyde to ethanol on Cu(111), Cu(100) and Cu(322). The experiments show structure-sensitive onset potentials for acetaldehyde reduction such that lower overpotentials are observed for more open facets (η322 < η 100 < η 111). Our DFT calculations show that the electrochemical reduction of acetaldehyde proceeds via a CH3CH2O* intermediate on the three electrodes at high *H coverage, and that the stability of this weakly bound intermediate determines the onset potential. Our results suggest that during the late stages of CO/CO2 reduction to C2 species on copper, ethanol formation has higher energetic barriers than ethylene formation, and hence the selectivity is inclined towards the latter. Importantly, our results suggest that the barriers for ethanol formation can be lowered by making use of its structure sensitivity.

This chapter has been published as: I Ledezma-Yanez, E Pérez-Gallent, MTM Koper, F Calle-Vallejo, Catalysis Today, 2016, 262, 90-94

3.1 Introduction

It is well known that CO and CO_2 can be reduced electrochemically to useful products. The seminal works of Hori and co-workers pointed out that copper is a unique catalyst for electrochemical CO_2 reduction [105-106], as it is able to produce methane, ethylene and ethanol in different proportions depending on the electrode potential and morphology. However, substantial overpotentials and low Faradaic efficiencies prevent the widespread use of electrolyzers based on copper electrocatalysts. Currently, the challenges are, first of all, to achieve a thorough understanding of the intricate multielectron reaction mechanism, and secondly, to design efficient and selective catalysts based on such understanding.

The major C_2 product on copper is ethylene, while there is a marginal production of ethanol and traces of acetaldehyde [105-106]. There are several indications that these three products share the same reaction pathway up to a given key intermediate, the ease of protonation of which ultimately determines the selectivity [107-108]. Given that in the context of a solar-fuel-based economy ethanol is a highly desirable product, it is important to understand the mechanistic features of its formation, as the C_2 selectivity is usually inclined towards ethylene instead of ethanol. However, Kanan and co-workers have shown recently that the selectivity of copper-based electrocatalysts for CO reduction can be steered to favor ethanol over ethylene [48], although the atomic-scale justification for such a change is still unclear.

According to previous work from our group [107-109], acetaldehyde reduction corresponds to the late stages of the reaction pathway of ethanol production from CO/CO_2. Thus, the study of acetaldehyde reduction reaction can shed light on the features of copper electrodes that may favor ethanol production, as well as provide design principles to devise new catalysts that are selective towards ethanol.

In this chapter, we present a combined experimental/theoretical study of acetaldehyde reduction, taking into account pH effects and structure sensitivity. Our findings provide new insights on the reaction mechanism through which ethanol is produced on copper-based catalysts and help explain why ethylene is the major C_2 product of the reduction of CO/CO_2.

3.2 Experimental

Prior to the experiments, all the glassware was cleaned by boiling in a sulfonitric solution, which is a mixture of concentrated sulfuric acid and nitric acid in a 3:1 ratio. After the acid bath, the glassware was rinsed and boiled five times with ultra-clean water (Milipore® MiliQ; resistivity >18.2 MΩ).

The electrochemical measurements were carried out using an METROHM μAUTOLABIII - Compact Design potentiostat connected to the three-electrode cell. The working electrodes (WE) were bead-type copper single crystals, with a polishing orientation < 0.5 degrees. These electrodes were electropolished before each experiment, using 66% H_3PO_4 (Suprapur Merck) at 2.3 V vs a Cu counter electrode for 2 s, and in open circuit potential (OCP) for 30 s. After cleaning and rinsing with water, the electrode surfaces were characterized by performing four cycles between -0.25 and 0.35 V_{RHE}, at 50 mV s^{-1} in 0.1 M NaOH (Sigma–Aldrich TraceSelect), following the procedure described previously by Schouten et al on Cu single-crystal characterization [110], see Appendix II, Figure AII.1. The results show that the electrodes possessed their distinctive features before the electroreduction experiments. However, we do not discard H- or OH-induced surface reconstruction under reaction conditions.

The counter electrode (CE) consisted of a gold wire, while the reference electrode (RE) was a reversible hydrogen electrode (RHE). All potentials in this work are reported against the RHE, unless otherwise stated.

The experiments were carried out in a solution containing 0.1 M $HClO_4$ (Suprapur Merck) for pH1, and 0.001 M $HClO_4$ + 0.099 M $KClO_4$ (Sigma-Aldrich TraceSelect) for pH 3. These values of pH are used to guarantee the stability of acetaldehyde, which is prone to decomposition in alkaline conditions. All solutions were prepared with ultra-clean water. Argon (Linde, 6.0) was used as purge gas.

The detection of ethanol from the reduction of 0.1 M acetaldehyde (puriss. p.a., anhydrous, ≥99.5% (GC) FLUKA) was monitored by means of online High Performance Liquid Chromatography (HPLC) [111] in a three-electrode cell containing solutions with pH 1 and 3, prepared as previously described. The soluble reduction products were detected by collecting from the solution in the cell using a Teflon tip (0.38 mm in diameter) by means of a fraction collector (FRC-10A, Shimadzu) during the voltammetric scan at a scan rate of 1 mV s^{-1}. The tip was positioned in parallel configuration, approximately 10 μm from the middle of the electrode surface. The fractions collected were deposited in a 96-well microtiter plate. The flow rate of sample collection was adjusted to 60 μL min^{-1} with a Shimadzu pump (LC-20AT). Each of the samples collected were 60 μL. The well was placed in the autosampler, and 30 μL of sample was injected in the high-performance liquid chromatography (HPLC) column. The column used was an Aminex HPX 87-H, Biorad. The temperature of the column was maintained at 85 °C in an oven (CTO-20 A).

3.3 Computational details

The DFT calculations and thermodynamic modeling in this study have been performed using the same methodologies used in our previous work [107]. Here we provide a brief description of the methods used: all adsorption energies were calculated by means of DFT calculations using the VASP code [112] with the PBE exchange-correlation functional [113] and the projector augmented wave (PAW) method [114]. The (111), (100) and

(322) surfaces of copper were modeled with 4-layer-thick slabs. Cu(111) and Cu(100) used 3×2 supercells, while Cu(322) is 5(111)×(100) with a 3-atom wide step edge. The vertical separation between periodically repeated images was more than 16 Å and, additionally, dipole corrections were applied. The structures were optimized allowing the adsorbates and the two topmost layers to relax in all directions, while fixing the 2 bottom layers at the optimized bulk positions, where the lattice constant is 3.64 Å. The relaxations were carried out with a plane-wave cut-off of 400 eV, using the conjugate-gradient scheme until the maximum force on any atom was below 0.05 eV $Å^{-1}$. The Brillouin zones of the (100) and (111) surfaces were sampled with 6×8×1 Monkhorst-Pack meshes [115], while a 4×3×1 mesh was used for the (322) surface. The Fermi level of the surfaces was smeared using the Methfessel-Paxton method [116] with an electronic temperature of 0.2 eV, and all energies were extrapolated to T = 0 K. Acetaldehyde (CH_3CHO) and ethanol (CH_3CH_2OH) were calculated in boxes of 15 Å ×15 Å × 15 Å, with an electronic temperature of 0.001 eV, the gamma point only, and Gaussian smearing. The free energies are estimated from DFT-calculated energies in the following way:

$$G = E_{DFT} + ZPE - TS \quad (3.1)$$

The zero-point energies (ZPE) of the adsorbates (see Table 3.1) and molecules (1.468 and 2.118 eV for CH_3CHO and CH_3CH_2OH) were calculated from vibrational frequency analysis using the harmonic oscillator approximation. Vibrational contributions to the entropy were considered only for adsorbed species and can be found in Table 3.1, while total entropies for molecules were taken from standard thermodynamic tables at 298.15 K and 1 bar [117], so that the gas-phase *TS* corrections for ethanol and acetaldehyde are 0.870 and 0.815 eV, respectively. However, ethanol and acetaldehyde are liquid at the conditions of the experiments carried out here. Although it is normally difficult to estimate the liquid-phase free energies of substances within standard DFT, there is a simple thermodynamic workaround [107, 118-119]. Essentially, the substance is simulated in the gas phase and the

difference between the free energies of formation of its liquid and gas phases is added to the gas-phase entropy. Such differences are 0.072 eV for ethanol and -0.056 eV for acetaldehyde, so that the final TS corrections are 0.942 and 0.759 eV, respectively. The high-coverage (HC) situations on the (111), (100) and (322) surfaces contained 5, 5, and 4 *H coadsorbates around CH_3CH_2O*/CH_3*CHOH.

Table 3.1. *ZPE* and TS_{vib} contributions at 298.15 K to the free energies of adsorbates on the (111) and (100) facets of copper. NH: No coardsorbed hydrogen. HC: High coverage of hydrogen.

Adsorbate	ZPE_{111}	ZPE_{100}	ZPE_{322}	$TS_{vib,111}$	$TS_{vib,100}$	$TS_{vib,322}$
*CH_3CH_2O (NH)	1.837	1.822	1.833	0.304	0.310	0.302
*CH_3CHOH (NH)	1.809	1.794	1.821	0.316	0.277	0.213
*CH_3CH_2O (HC)	2.860	2.487	2.463	0.295	0.394	0.261
*CH_3CHOH (HC)	2.820	2.438	2.432	0.320	0.409	0.371

We have added a solvation correction of -0.38 eV to CH_3*CHOH due to the presence of the OH group, making use of the approximations described elsewhere [107, 120]. Finally, we have used the computational hydrogen (CHE) approach to simulate concerted proton-electron transfers[121]. In this approach, the energetics of H_2(g) rather than that of (H^++e^-) is used as electrochemical reference due to the following relationship in equilibrium: $\mu\left(H^+ + e^-\right) = \frac{1}{2}\mu\left(H_2\right)$.

3.4 Results and discussion

The linear sweep voltammetry (LSV) of the three copper single-crystals shows reduction currents at negative potentials which are mainly due to hydrogen evolution, see Appendix II, Figure AII.2. To probe the reduction of acetaldehyde to ethanol, we need to use online HPLC, since LSV does not show the separated features for acetaldehyde reduction. Figure 3.1 shows the HPLC results for the electrochemical reduction of results in more negative onset potentials, as the coordination number is 7 for the step edge on acetaldehyde on three different copper electrodes and at different pH values. We observe that the onset potential for the formation of ethanol follows the trend Cu(322) > Cu(100) > Cu(111) for both values of pH (see also Figure 3.4). This means that increase in surface coordination the (322) electrode (note that (322) electrodes are also denoted 5(111)×(100), as they have 5-atom wide (111) terraces separated by (100) steps), and the coordination numbers are 8 and 9 on the (100) and (111) terraces, respectively. For instance, at pH 1, the onsets are located at -0.30 ± 0.03 V_{RHE}, -0.54 ± 0.03 V_{RHE} and -0.78 ± 0.03 V_{RHE}, for the three facets.

Note that the equilibrium potential for this reaction is located at 0.24 V_{RHE} at pH 0, and also that it is generally observed that adsorbates bind more strongly to undercoordinated facets [122-125]. These two observations suggest that the adsorbed intermediates of the reduction of acetaldehyde are less stable than acetaldehyde itself under equilibrium conditions. Thus, the applied potential is used to make their adsorption thermodynamically and kinetically favorable. Therefore, the onset of ethanol greatly depends on the stabilization of such intermediates on the electrode surface. In order to gain further insight into the reaction mechanism, we have performed DFT calculations on Cu(111), Cu(100) and Cu(322) in the way described in the Computational Details section. The two possible adsorbed intermediates resulting from the transfer of a proton-electron pair to acetaldehyde are CH_3CH_2O* and CH_3*CHOH. The proposed reduction mechanism in Figure

3.2 includes the reactant and the product, namely acetaldehyde and ethanol, and the most stable adsorbed intermediate, which is CH_3CH_2O*. The adsorption energies in the pathway that goes through the other possible intermediate, CH_3*CHOH, are provided in Figure 3.3. As CH_3CH_2O* is more stable than CH_3CHOH on all facets regardless of the presence or absence of co-adsorbed H*, in the following we focus only on the results for CH_3CH_2O* in Figure 3.2.

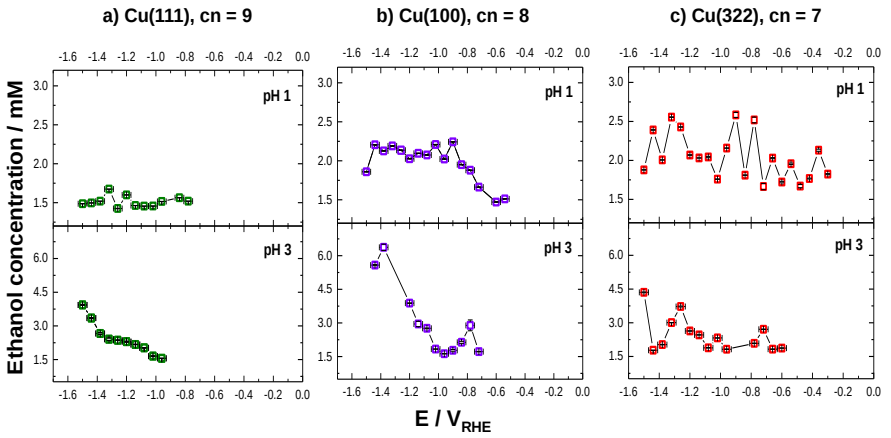

Figure 3.1: Concentration of ethanol produced as a function of potential for the electroreduction of 0.1 M acetaldehyde on three different copper surfaces: a) Cu(111), b) Cu(100), c) Cu(322). The solutions used are: 0.1 M $HClO_4$ (pH 1), and 0.001 M $HClO_4$ + 0. 099 M $KClO_4$ (pH 3). Argon atmosphere. Lines connecting the data points are given as a guide to the eye. An earlier onset of the reaction is associated to surfaces with lower coordination numbers.

The calculations in Figure 3.2.a, which contain only adsorbed CH_3CH_2O* on the slabs, indicate that already at 0 V and in the absence of *H the reduction of acetaldehyde is thermodynamically favorable on the three facets under study. However, this is not what we observe experimentally. In experiments, acetaldehyde reduction takes place in a high-coverage regime of *H, which is included in Figure 3.2.b. Therefore, a high-coverage situation is a more realistic approximation to the experimental environment in which the intermediates of acetaldehyde

reduction ($CH_3CH_2O^*$) compete with those of hydrogen evolution (*H) for active sites at copper surfaces.

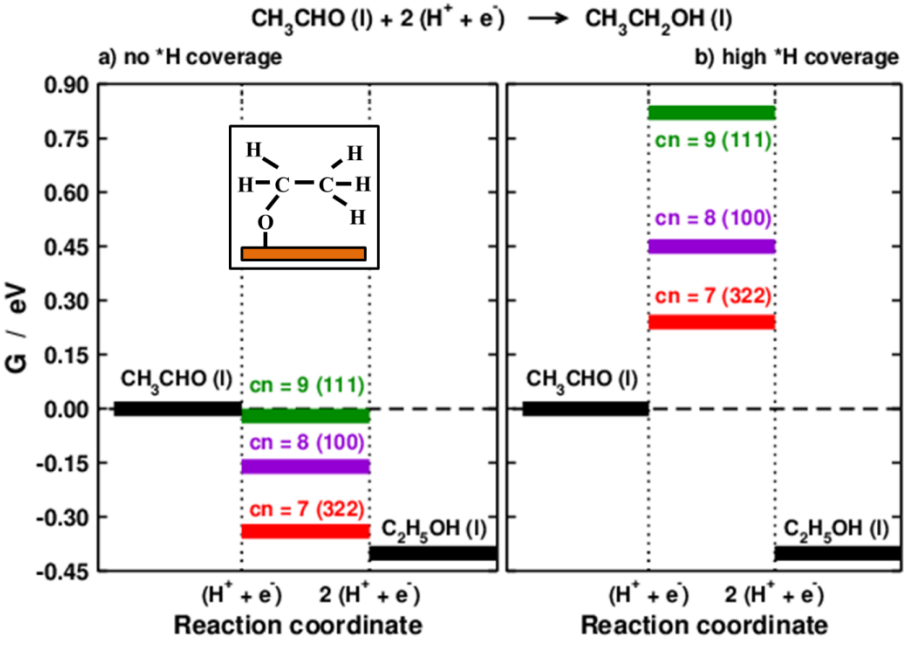

Figure 3.2: Electrochemical reduction of acetaldehyde (CH3CHO) to ethanol (C2H5OH) on various facets of copper at 0 V: Cu(111) (green, cn = 9), Cu(100) (violet, cn = 8) and Cu(322) (red, cn =7). The pathways proceed via CH3CH2O* (see the inset). a) With no *H coverage. b) With high *H coverage.

The observed effect of hydrogen coadsorption on all facets is a weakening of the metal-adsorbate interactions, which ultimately results in predicted onset potentials which are far from the equilibrium potential: -0.28 V for Cu(322), -0.45 V for Cu(100) and -0.82 V for Cu(111), in very reasonable agreement with experiment. Note in passing that Peterson and co-workers have studied the opposite effect, namely the effect of *CO coverage on hydrogen evolution and found that it systematically weakens the adsorption energies of *H on various metals [126]. Therefore, the coadsorption of *H and *CO weakens the adsorption energies of both species.

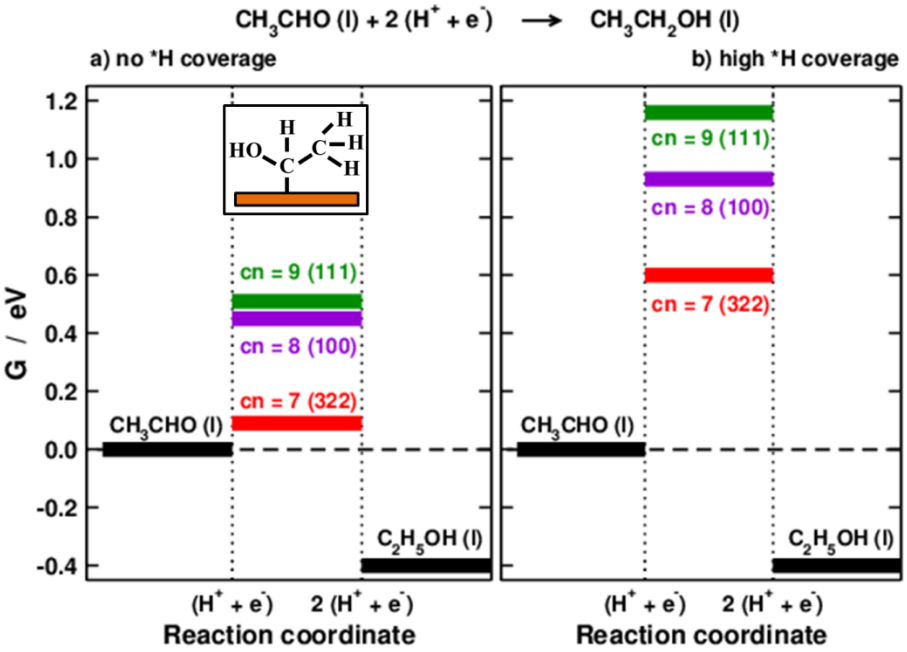

Figure 3.3: Electrochemical reduction of acetaldehyde (CH_3CHO) to ethanol (C_2H_5OH) on various facets of copper at 0 V: Cu(111) (green, cn = 9), Cu(100) (violet, cn = 8) and Cu(322) (red, cn =7). The pathways proceed via CH_3*CHOH (see the inset). a) With no *H coverage. b) With high *H coverage.

According to Figure 3.2.b and in line with the experimental observations in Figure 3.1, the adsorption energies of CH_3CH_2O* at 0 V are higher than the energetic levels of acetaldehyde and ethanol on all facets. This means that the first proton-electron transfer is uphill in energy, while the second one is downhill. Thus, the predicted onset potentials on all facets in Figure 3.2.b correspond to the energy difference between acetaldehyde and the adsorbed intermediates.

As observed in the experiments in Figure 3.1, copper facets with lower coordination numbers exhibit less negative onset potentials, which can be intuitively understood as follows: in general, it is observed that adsorbates are more strongly bound to undercoordinated sites [122-125],

which implies that the step edge on the (322) facet, where the coordination number is 7, will display more negative adsorption energies for CH_3CH_2O* compared to the (100) and (111) facets, where the coordination numbers are 8 and 9, respectively. Since these endothermic adsorption energies are more positive than the level of acetaldehyde (see Figure 3.2), stronger adsorption energies imply earlier onset potentials. In summary, our high-coverage DFT calculations confirm the structure-sensitive reduction of acetaldehyde to ethanol observed experimentally, and show that the mechanism proceeds on the three facets via CH_3CH_2O*, which becomes more stable as the coordination of the adsorption sites is decreased. The calculations also show the importance of considering the co-adsorption of H* in reaching good agreement with experiments. We have summarized the experimental and theoretical trends in Figures 3.1, 3.2 and 3.3 in Figure 3.4. This figure contains the adsorption energies of CH_3CH_2O* and CH_3*CHOH with and without coadsorbed *H and the additive inverse of the experimental onset potentials which, according to the results in Figure 3.1, corresponds to experimental free energy of adsorption of the adsorbed intermediate of acetaldehyde reduction.

3.5 Mechanistic implications

It is important to discuss the mechanistic implications of our observations for the reduction of CO/CO_2 to ethanol and other C_2 products such as ethylene. We have previously proposed the mechanism shown in Figure 3.5 for the reduction of CO to C_2 species on Cu(100) on the basis of DFT calculations [107]. In that mechanism, ethanol, acetaldehyde and ethylene share the same intermediates up to the fifth proton-electron transfer, which is supported by the experiments of Hori and coworkers, who observed that the nature of the metallic cations from the electrolyte affects similarly the Faradaic efficiencies of ethylene and ethanol production [65].

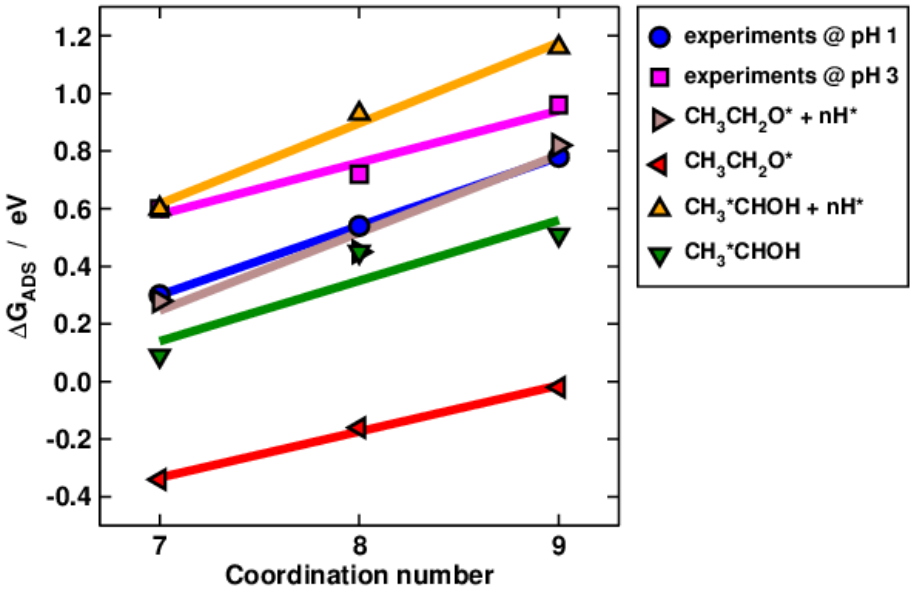

Figure 3.4: Experimental (●, ■) and theoretical (►, ◄, ▲, ▼) trends in adsorption energies of the adsorbed intermediates of acetaldehyde reduction as a function of the coordination number of the active sites on Cu(322) (step edge, cn = 7), Cu(100) (cn = 8), and Cu(111) (cn = 9).

The product of the fifth proton-electron transfer is the "selectivity-determining" intermediate (SDI in Figure 3.5). The sixth proton-electron transfer favors the formation of ethylene (orange pathway in Figure 3.5) over acetaldehyde (grey pathway in Figure 3.5) at the onset of ethylene formation, that is at -0.4 V_{RHE} [107]. The results in Figures 3.1 and 3.2 indicate that the onset of acetaldehyde reduction to ethanol requires -0.54 V_{RHE} on Cu(100) (-0.45 V from DFT calculations). Such onset for the formation of ethanol from acetaldehyde is in contrast to previous experimental and theoretical results on the reduction of ethylene oxide to ethylene on polycrystalline copper, the onset of which is less negative than -0.4 V_{RHE} (-0.35 V from the backward scan in experiments and -0.33 V from DFT calculations on Cu(100)) [107, 109]. Unlike acetaldehyde reduction, the potential-determining step for ethylene oxide reduction is the second proton-electron transfer, which implies that desorption of adsorbed intermediates limits the onset of the reaction. In the case of a

desorption-limited reaction, structure sensitivity affects the trends in onset potentials differently: undercoordinated sites binding adsorbates more strongly increase the onset potential.

The conjunction of the findings for ethylene oxide and acetaldehyde reduction suggests that, although ethylene and ethanol share common intermediates in the early stages of CO/CO_2 reduction, the protonation of the SDI favours ethylene formation compared to ethanol formation on Cu(100). Importantly, we have shown here that undercoordinated sites at stepped surfaces are able to lower those barriers by virtue of their stronger adsorption energies. Step sites, on the other hand, affect adversely the production of ethylene on Cu(100).

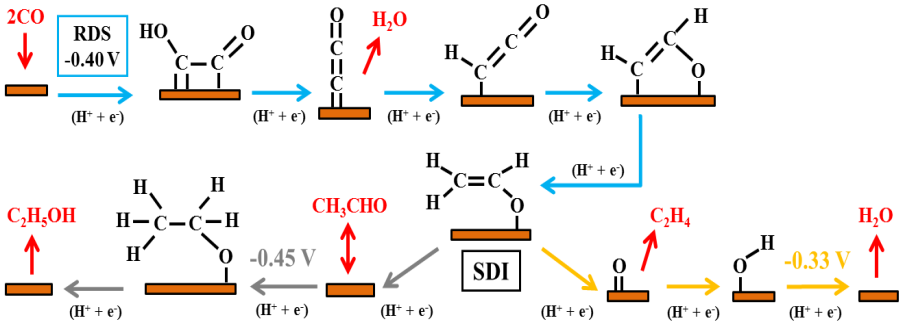

Figure 3.5: Mechanism of the electrochemical reduction of CO on copper to C_2 species on Cu(100), adapted from ref. [107]. The pathways for the production of acetaldehyde, ethanol and ethylene are identical up to the fifth proton-electron transfer (blue arrows). The rate-determining step (RDS at -0.40 V) is the first proton-electron transfer and CH_2CHO^* is the selectivity-determining intermediate (SDI). Protonation of the SDI on the β-C requires -0.45 V and leads to acetaldehyde and ethanol (grey arrows). Protonation on the α-C requires -0.33 V and leads to ethylene and water (orange arrows). On Cu(100) the protonation of the SDI is inclined towards the ethylene pathway (orange arrows).

3.6 Conclusions

Elucidation of the reaction mechanism of CO/CO_2 reduction to C_2 species is not trivial, as it involves the transfer of several proton-electron pairs and numerous adsorbed intermediates. A possible way of simplifying the problem is to analyze separate reactions involving fewer proton-electron transfers. In that vein, we have considered here the structure-sensitive reduction of acetaldehyde to ethanol on copper, which corresponds to the late stages of CO/CO_2 reduction to ethanol. Our results suggest that ethanol formation is more favourable on open copper surfaces, which is explained by the preference of $CH_3CH_2O^*$ for undercoordinated sites. Therefore, a plausible way of inclining the selectivity of copper electrodes towards the formation of ethanol from CO/CO_2 is the use of undercoordinated square sites: square ensembles because they catalyze the formation of C-C bonds, and undercoordinated sites because they incline the selectivity towards ethanol instead of ethylene.

Chapter 4

Spectroscopic Observation of a Hydrogenated CO Dimer Intermediate During CO Reduction on Cu(100) Electrodes

Carbon dioxide and carbon monoxide (CO) can be electrochemically reduced to useful products such as ethylene and ethanol on copper electrocatalysts. The process is yet to be optimized and the exact mechanism and the corresponding reaction intermediates are under debate or unknown. In particular, it has been hypothesized that the C-C bond formation proceeds via CO dimerization and further hydrogenation. Although computational support for this hypothesis exists, direct experimental evidence has been elusive. In this work, we detect a hydrogenated dimer intermediate (OCCOH) using Fourier transform infrared spectroscopy at low overpotentials in LiOH solutions. Density functional theory calculations support our assignment of the observed vibrational bands. The formation of this intermediate is structure sensitive, as it is observed only during CO reduction on Cu(100) and not on Cu(111), in agreement with previous experimental and computational observations.

This chapter has been published as: E Pérez-Gallent, MC Figueiredo, F Calle-Vallejo, MTM Koper, Angewandte Chemie, 2017, 129 (13), 3675-3678

4.1 Introduction

A considerable number of experimental observations as well as density functional theory (DFT) calculations have established that CO_2 and CO reduction on copper electrodes forms C_1 and C_2 products through different reaction pathways.[47, 49-50, 52, 57] The formation of C_1 and C_2 products has been shown to be highly sensitive to copper surface structure and electrolyte pH.[51, 59, 61, 63-64, 91, 127] Hori et al[61] showed that the CO to CH_4 reduction follows a concerted proton-electron transfer mechanism, in stark contrast with C_2H_4 production, the rate-limiting step of which is not sensitive to pH and only involves an electron transfer. As a result, on the pH corrected RHE reference scale, the formation of ethylene from CO depends on pH while that of CH_4 does not.[61, 63] Furthermore, Schouten et al. showed that C_2H_4 formation takes place preferentially at Cu(100) electrodes without simultaneous CH_4 formation, which indicates that the reaction paths towards CH_4 and C_2H_4 must bifurcate in the early stages of CO reduction.[61] Specifically, a C_2 intermediate that requires only electron transfer to be formed, namely a negatively charged CO dimer, has been proposed as the first C-C coupled intermediate.[49, 51, 53] Various recent computational works have studied the structural sensitivity of this intermediate, and concluded that the formation of the dimer is indeed favored both thermodynamically and kinetically on Cu(100) sites compared to Cu(111).[53-54, 58]

However, there is still no direct experimental evidence that proves CO dimerization in aqueous solution during CO reduction on copper electrodes, and the existence of the dimer is mostly a logical deduction from experimental and computational results. In this chapter, we provide experimental evidence for the formation of a hydrogenated CO dimer (OCCOH) at low overpotentials during CO reduction on Cu(100) electrodes in LiOH solution, employing in situ Fourier transform infrared spectroscopy (FTIR), and support our interpretation by detailed DFT calculations.

4.2 Experimental

Prior to each electrochemical experiment, the glassware used was stored overnight in a solution of $KMnO_4$ that was rinsed with a mixture of ultra clean water (Millipore MilliQ, resistivity > 18.2 MΩ), 20 ml/l of hydrogen peroxide and 1 ml/l of concentrated sulfuric acid. The glassware was further cleaned by boiling 4 times in Millipore MilliQ water. A coiled platinum wire was used as counter electrode and a reversible hydrogen electrode (RHE) in the same electrolyte was used as reference electrode.

The copper electrodes used were 99.99% copper disks with a diameter of 6mm, purchased from Mateck and aligned to < 0.5° accuracy. Prior to every experiment, the electrodes were electropolished and characterized as described elsewhere.[91]

The electrolytes were made from ultra-pure water (Millipore MilliQ, resistivity > 18.2 MΩ) and high purity reagents (Sigma Aldrich TraceSelect). Before every experiment, Argon (Linde, 6.0) was bubbled through the electrolyte for 15 minutes in order to remove air from the solution, and during the experiments argon was kept flowing above the solution.

FTIR measurements were performed with a Bruker Vertex 80 V Infrared spectrophotometer.[128] The electrochemical cell was assembled on top of a 60° CaF_2 prism, and the electrode was situated against this prism to form a thin layer. The measurements were performed under external reflection. FTIR spectra were obtained from an average of 100 scans with a resolution of 8 cm^{-1} at the selected potentials. Every spectrum was obtained by applying single potential steps compared to the reference potential (+0.1 V). The spectra are shown as $(R-R_0)/R_0$ where R is the reflectance at the sample potential and R_0 is the reflectance at the reference potential. Thereby the ratio $\Delta R/R_0$ gives positive bands for the formation of species at the sample potential, while negative bands correspond to the loss of species at the sample potential. P-polarized

light was used to probe species both near the electrode surface and in solution.

The vibrational frequencies were calculated by means of DFT calculations using the VASP code[112] with the PBE exchange-correlation functional[113] and the projector augmented wave (PAW) method.[114] The Cu(100) surfaces were modelled with (3×2) 4-layer-thick slabs. The vertical separation between periodically repeated images was more than 16 Å and dipole corrections were applied. The structures were optimized allowing the adsorbates and the two topmost layers to relax in all directions, while fixing the 2 bottom layers at the optimized bulk positions. The relaxations were carried out with a plane-wave cut-off of 450 eV, using the conjugate-gradient scheme until the maximum force on any atom was below 0.05 eV $Å^{-1}$. The Brillouin zones were sampled with 6×8×1 Monkhorst-Pack meshes.[115] The Fermi level of the surfaces was smeared using the Methfessel-Paxton method[116] with an k_BT = 0.2 eV, and all energies were extrapolated to 0 K.

The vibrational frequency analysis was made using the harmonic oscillator approximation with two displacements in each direction plus the ground state.

4.3 Results and discussion

Figure 4.1 shows the potential-dependent absorbance spectra of Cu(100) in 0.1 M LiOH solutions in Argon atmosphere (Fig.4.1a, left panel) and in CO atmosphere (Fig.4.1b, right panel). The reference spectrum is taken at +0.1 V and additional spectra are provided for +0.05, 0.00, -0.05, -0.10, -0.15 and -0.2 V (all reported potentials are on the RHE scale). First of all, in Argon atmosphere the absorption spectra do not display any bands. After CO is bubbled through the solution, three bands appear at 1677, 1600 and 1191 cm^{-1}. The band at 1600 cm^{-1} corresponds to the O-H bending mode of H_2O. This band causes fluctuations in the baseline of the spectra making it difficult to identify

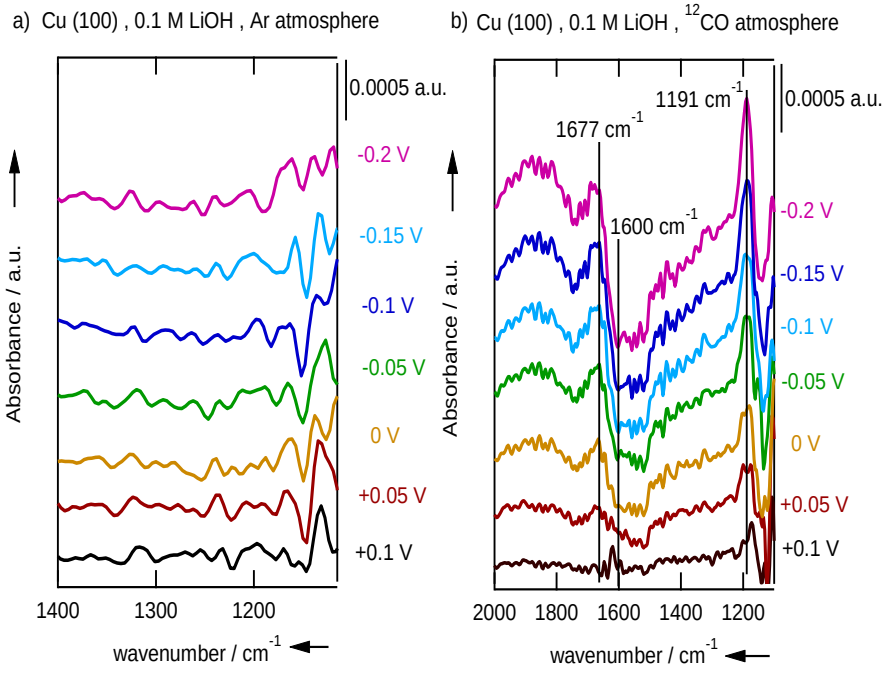

Figure 4.1: . Potential-dependent absorbance spectra for Cu(100) in the a) absence and b) presence of CO in a 0.1 M LiOH solution. Reference spectrum recorded at +0.1 V vs. RHE. Highlighted bands and their corresponding frequencies are indicated with a vertical line at 1191 cm^{-1} for ^{12}C-OH stretching, 1145 cm-1 for ^{13}C-OH stretching, 1677 cm^{-1} for C=O stretching and 1600 cm-1 for O-H

other bands in this wavenumber range. The band at 1677 cm^{-1} corresponds to the C=O stretching[129-131] of CO adsorbed on hollow sites on Cu(100), in agreement with DFT calculations (see Figure 3 below). The intensity of the band for CO at multi bonded sites increases with more negative electrode potential. In alkaline media, the absolute potential (on the SHE scale) is more negative compared to acidic conditions and, consequently, the band for CO at multifold sites dominates the spectra.[132-135]

Simultaneously with the CO-related band, a band at 1191 cm^{-1} associated with C-OH stretching[136] grows in the spectra.

Importantly, when CO reduction was performed under the exact same conditions on a Cu(111) electrode (see Appendix III, Figure AIII.1), the band at 1191 cm^{-1} and the band corresponding to C=O stretching at 1677 cm^{-1} were not observed. In order to ensure that the band at 1191 cm^{-1} comes from a C-containing species, both the blank spectrum and a spectrum taken with isotopically labeled carbon ^{13}CO were recorded. Figure 4.1a shows the absorbance spectra on Cu(100) without CO. The absence of the band at 1191 cm^{-1} strongly suggests that the signal appearing in CO atmosphere comes from a C-containing species. Moreover, when the absorbance spectra were obtained in ^{13}CO atmosphere (see Figure 4.2, left panel), the band shifts from 1191 cm^{-1} to 1145 cm^{-1}. The shift of approximately 45 cm^{-1} matches the expected shift for the absorption spectra of ^{13}C compared to ^{12}C,[137] confirming that the band at 1191 cm^{-1} comes from a C-containing species.

As mentioned before, water exhibits a wide O-H bending band in the 1650-1450 cm^{-1} range, which prevents the straightforward observation of vibrations from other species in this wavenumber range. For this reason, CO reduction on Cu(100) was performed in D_2O; the corresponding spectra are shown in Figure 4.2b (right panel). In D_2O electrolyte, the range of 1650-1450 cm^{-1} is free of water bands, allowing for the identification of additional bands. Unfortunately, D_2O has an O-D bending band at 1209 cm^{-1} masking the C-OH stretching band. Interestingly, Figure 4.2b shows that in D_2O electrolyte at +0.05 V and more negative potentials a band appears around 1584 cm^{-1}, which corresponds to a C=O stretch but is not adsorbed CO.

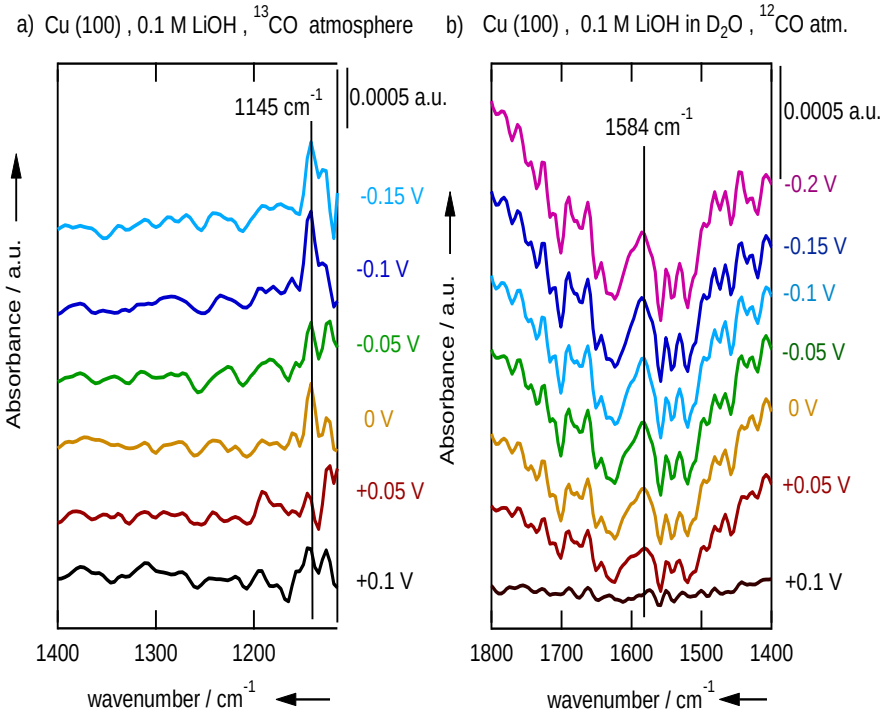

Figure 4.2: Potential dependent absorbance spectra for Cu (100) in the presence of a) 13CO (left) and with b) D2O as electrolyte (right) in a 0.1 M LiOH solution. Reference spectrum recorded at +0.1 V vs. RHE. Highlighted bands and their corresponding frequencies are indicated with a vertical line at 1191 cm-1 for 12C-OH stretching, 1145 cm-1 for 13C-OH stretching and 1584 cm-1 for 12C=O stretching.

From the combined results of the experiments in H_2O and D_2O, we observe two vibrational bands coming from C-containing species that are formed at low overpotentials on Cu(100) only. It is important to note that at the low overpotentials considered in our experiments, namely +0.1 to -0.15 V, no products are observed (for instance, the earliest onset potential on Cu(100) is that of C_2H_4 at -0.4 V).[59, 138] Thus, the bands in question should, in principle, be assigned to vibrations of adsorbed intermediates of CO reduction rather than to species in solution. To verify this hypothesis, we have scrutinized the IR spectra of

various possible species in solution, including various C_1 and C_2 species. Transmission spectra of species in solution such as formaldehyde, formate and methanol (C_1 molecules), and acetaldehyde and acetic acid (C_2 molecules) were recorded, shown in Appendix III, figure AIII.2. The absence of the bands at 1191 and 1584 cm^{-1} in the transmission spectra rules out the possibility that the bands observed during the reduction of CO on Cu(100) correspond to these species in solution. Although methanol has a C-OH vibration at 1195 cm^{-1} in 0.1 M LiOH, the vibration at 1584 cm^{-1} is absent (see Appendix III, figure AIII.2c) and its substantially negative onset potential (-0.95 V[50]) precludes the presence of methanol at the low overpotentials at which this work was performed (+0.1 to -0.15 V). The transmission spectra of acetaldehyde also displays a band at 1195 cm^{-1}, however, this band is associated with the C-OH stretching from the methanol present in the acetaldehyde solution as a stabilizer. In addition, acetaldehyde presents other two bands at 1712 and 1666 cm^{-1}. The absence of these bands in the spectra obtained during CO reduction rules out the possibility of acetaldehyde as a product. Another compound that could have vibrational frequencies close to those in Figures 1 and 2 is acetylenediol (HOC≡COH). Maier et al collected the infrared spectra of this double alcohol[139] and reported a single C-OH stretching band at 1212 cm^{-1}.

Having verified that the observed bands at 1191 and 1584 cm^{-1} do not correspond to species in solution, we now resort to DFT calculations to see whether a given adsorbed intermediate or a combination of them exhibit such bands. Since both CH_4 and C_2H_4 production from CO possess relatively early rate-limiting steps[57, 140-141], we have limited our analysis to C_1 and C_2 species with no or a low content of hydrogen atoms (see Figure 4.3). First, consider the C_1 species CHO and COH (Figure 4.3b-c), which are the two possible products of the first hydrogenation of CO. They both have bands close to the band observed during the adsorption/reduction of ^{12}CO on Cu(100) at 1191 cm^{-1} (Figure 4.1b, right panel), but none of them exhibit the additional vibrational band at 1584 cm^{-1} (Figure 4.2, right panel). The same is true for the CO dimer (OCCO, Figure 4.3d), which presents a vibrational band at 1200 cm^{-1} but

does not exhibit a band around 1584 cm^{-1}. Besides, a lithiated dimer (Figure 4.3e) features two C-O stretching frequencies that are not close to either of the bands at 1191 and 1584 cm^{-1}. Conversely, a CO dimer in which one of the oxygen atoms has been hydrogenated (OCCOH, Figure 4.3f) exhibits bands close to both experimental bands. In addition, we have calculated the vibrational signatures of a CO dimer of which one of the carbon atoms has been hydrogenated (OCCHO, Figure 4.3g). This adsorbate has vibrational bands around 1313, 1200,1071 cm^{-1} but no band close to 1584 cm^{-1}. Adsorbed acetylenediol, namely a doubly hydrogenated CO dimer (HOCCOH, Figure 4.3h) was also considered in our DFT calculations. The predicted vibrational frequencies for C-OH stretching are 1397,1229 and 1150 cm^{-1}. We also considered a simultaneously hydrogenated and lithiated dimer (HOCCOLi) and its vibrational frequencies were found at 1427 and 1246 cm^{-1}. Finally, a doubly lithiated dimer (LiOCCOLi) possesses C=O stretching frequencies at 1329 and 1261 cm^{-1}.

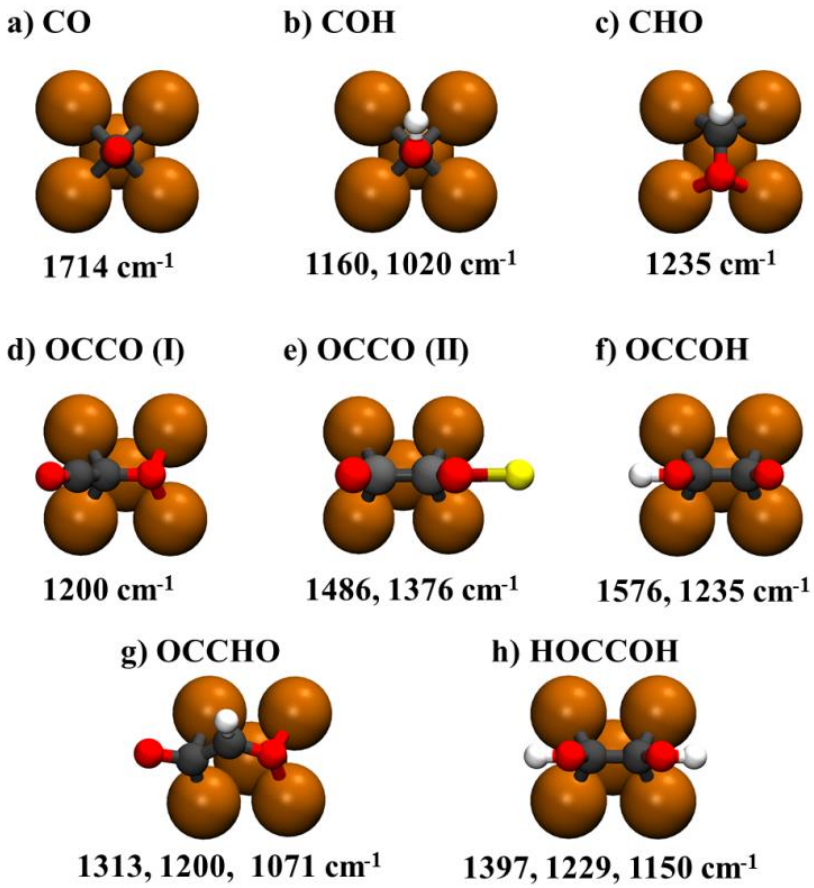

Figure 4.3: Schematic structures of possible adsorbed intermediates on Cu(100) and their calculated infrared-active vibrational frequencies in the 1100-1600 cm-1 wavenumber region. Cu, C, O, and H atoms are depicted as orange, gray, red and white spheres

Therefore, we conclude that the bands at 1191 and 1584 cm^{-1} arise from C-O-H and C-O stretching vibrations and correspond, in the simplest case, to a hydrogenated dimer (OCCOH), or in general to this adsorbate in combination with other C_1 and C_2 adsorbates. This is in line with previous computational works showing that OCCOH is the most stable intermediate formed after the first hydrogenation of CO on Cu(100).[53]. In Chapter 5 we performed further experiments and calculations to examine the influence of various alkaline cations on CO dimerization and their impact on the CO reduction pathway.

4.4 Conclusion

In conclusion, we have shown experimentally that Cu(100) electrodes in LiOH solutions host a C-containing adsorbate at low overpotentials with vibrational bands at 1191 and 1584 cm^{-1}. Based on DFT calculations of a wide variety of C_1 and C_2 intermediates, we ascribe these bands to the C-O-H and C=O stretching modes of a hydrogenated CO dimer (OCCOH). These results provide for the first time direct confirmation of an important hypothesis in the electrocatalysis of CO_2 reduction on copper, namely that the C-C coupling to C_2 species on Cu(100) takes place through a reductive dimerization step at the early stages of the reaction mechanism. The fact that the vibrational features ascribed to the CO dimer could not be observed on Cu(111) under identical conditions confirms that CO dimerization is a structure-sensitive process favored by sites with square symmetry, in agreement with previous experimental[64] and theoretical studies.[54]

Chapter 5
Structure and potential dependent cation effects on CO reduction at copper single crystal electrodes

The complexity of the electrocatalytic reduction of CO to CH_4 and C_2H_4 on copper electrodes prevents a straightforward elucidation of the reaction mechanism and the design of new and better catalysts. Although structural and electrolyte effects have been separately studied, there are no reports on structure-sensitive cation effects on the catalyst's selectivity over a wide potential range. Therefore, we investigated CO reduction on Cu(100), Cu(111) and Cu(polycrystalline) electrodes in 0.1 M alkaline hydroxide electrolytes (LiOH, NaOH, KOH, RbOH, CsOH) between 0 and -1.5 V vs RHE. We used Online Electrochemical Mass Spectrometry (OLEMS) and High-Performance Liquid Chromatography (HPLC) to determine the product distribution as a function of electrode structure, cation size and applied potential. First, cation effects are potential dependent, as larger cations increase the selectivity of all electrodes towards ethylene at E > -0.45 V vs RHE, but methane is favored at more negative potentials. Second, cation effects are structure-sensitive, as the onset potential for C_2H_4 formation depends on the electrode structure and cation size, whereas that for CH_4 does not. Fourier Transform Infrared Spectroscopy (FTIR) and Density Functional Theory (DFT) help to understand how cations favor ethylene over methane at low overpotentials on Cu(100). The rate determining step to methane and ethylene formation is CO hydrogenation, which is considerably easier in presence of alkaline cations for a CO dimer compared to a CO monomer. For Li^+ and Na^+, the stabilization is such that hydrogenated dimers are observable with FTIR at low overpotentials. Thus, potential-dependent, structure-sensitive cation effects help steer the selectivity towards specific products.

This chapter has been published as: E Pérez-Gallent, G Marcandalli, MC Figueiredo, F Calle-Vallejo, MTM Koper, 2017, , 139, 16412–16419

5.1 Introduction

Electrocatalytic reduction of CO_2 is an attractive strategy for the conversion of renewable energy into fuels, which helps in closing the biogeochemical carbon cycle. Several metals and other types of electrodes have been studied for the electrochemical reduction of CO_2[142]. However, copper remains the only metal to produce hydrocarbons (primarily methane and ethylene) with reasonable faradaic efficiencies[42, 86]. For instance, Jaramillo et al reported the formation of 16 different species from CO_2 reduction in aqueous bicarbonate solution, where complex molecules including C_2 (e.g. acetaldehyde, acetate, ethylene glycol, glycolaldehyde) and C_3 species (e.g. n-propanol, propionaldehyde, allyl alcohol, acetone) were detected with current efficiencies lower than 5 % [50]. Several studies of Cu-based catalysts[48, 143] have shown higher selectivity for C_2 products. However, the mechanistic reasons for their selectivity remain elusive. Here we examine the combined role of electrolyte cations, potential window and catalyst structure on the selectivity towards C_1 vs C_2 products during CO reduction on Cu.

Hori et al showed that CO_2 reduction on Cu electrodes is structure sensitive[144]: Cu(100) electrodes are most efficient for the conversion of CO_2 to C_2H_4, Cu(111) favors the formation of CH_4 and HCOOH, and Cu(110) gives the highest current efficiencies for secondary C_2 products (e.g. acetic acid, acetaldehyde and ethanol). Similar results were obtained by Schouten et al. during the reduction of CO[64]. While Hori et al concluded that the introduction of steps on (100) terraces enhances C_2H_4 evolution and suppresses CH_4 formation[144], Schouten et al. attributed the selective formation of C_2H_4 to pristine (100) terraces[64]. Moreover, they showed that CO reduction to C_2H_4 takes place preferentially at Cu(100) electrodes without simultaneous CH_4 evolution, which indicates that the reaction paths towards CH_4 and C_2H_4 bifurcate in the early stages of CO reduction[59]. On the other hand, it has been shown that C_2 species such as ethylene and ethanol are formed in a

common pathway that bifurcates at the late stages of the reaction[53, 65, 127]. The favorable formation of C_2H_4 on Cu(100) is supported by density functional theory (DFT) calculations, which demonstrate that C-C bond formation proceeds via CO dimerization and has a lower activation barrier on Cu(100) than on Cu(111).[54, 58] In addition to structural effects, there is an important role of the electrolyte, especially through the pH. The onset potential on the NHE scale of CH_4 evolution depends on pH, while C_2H_4 evolution does not. Hori et al concluded that CO reduction to CH_4 proceeds as a series of concerted proton-electron transfers, in contrast with C_2H_4 evolution for which the rate limiting step only involves an early electron transfer, justifying its pH-independent onset[138-139]. We showed previously with DFT calculations that the electron transfer to form a negatively charged $(CO)_2$ dimer is the potential-limiting step of CO reduction to C_2H_4 on Cu(100),[53] in contrast with studies that assume only concerted proton-electron transfers[57], which cannot explain the pH independence of C_2H_4 formation.

In addition to pH, the activity and selectivity of Cu for CO_2 reduction also depends on the nature of the anions and/or cations in the electrolyte. Strasser et al showed that the selectivity of the major products of CO_2 reduction depends on the size and concentration of halides[56]: while Cl^- and Br^- enhance the production of CO, I^- lowers CO evolution and increases the selectivity towards methane. The effects were attributed to halide adsorption on copper, which alters the negative charge on the surface and favors the protonation of CO towards CH_4. Furthermore, Lee et al showed that the presence of Cl^- enhances the catalytic activity toward multiple C_2-C_4 species on Cu-oxide derived catalysts, due to the presumed advantageous affinity between reaction intermediates and catalytic surface in presence of Cl^-[145]. Hori et al reported that alkaline cations affect the selectivity of CO_2 and CO reduction on polycrystalline copper[65], so that larger cations favor the formation of C_2 and C_3 species such as C_2H_4, C_2H_5OH and C_3H_7OH. Cation effects were explained by Hori et al in terms of a variation in the potential in the outer Helmholtz plane (OHP), which originates from a difference in the hydration number of the different cations. Larger cations are less hydrated and expected to

adsorb more easily on the cathode surface, shifting the potential to more positive values thereby steering the selectivity towards C_2H_4 instead of CH_4. Such experimental observations were confirmed by Kyriacou et al.[146]. Bell and coworkers explained cation effects on CO_2 reduction in terms of the different pKa values for cation hydrolysis, which lower the local pH at the surface from Li^+ to Cs^+ and lead to an increase in CO_2 concentration near the electrode surface.[147] However, this model cannot explain the fact that similar cation effects are observed during CO reduction[65], the concentration of which is not affected by pH.

All previous studies concerning cation effects in the reduction of CO_2 and CO on copper have used only polycrystalline electrodes and did not cast light on their potential dependence. In this chapter we will argue that such effects depend on the electrode structure, the applied potential and the size of the cation. To this end, we used two single-crystalline copper surfaces (Cu(100), Cu(111)) together with polycrystalline Cu in LiOH, NaOH, KOH, RbOH and CsOH solutions. Online Electrochemical Mass Spectrometry (OLEMS) and High-Performance Liquid Chromatography (HPLC) were used to investigate the product distribution over a wide potential range. In addition, in situ Fourier Transform Infrared (FTIR) spectroscopy and Density Functional Theory (DFT) calculations are used to identify early reaction intermediates of CO reduction on Cu(100) and explain the cation-mediated enhancement of ethylene formation over methane. Understanding how the structural and potential-dependent cation effects impact the catalytic performance provides insight for devising efficient and selective catalysts for CO reduction.

5.2 Experimental

Prior to every experiment, the glassware was placed overnight in a $KMnO_4$ solution which was then rinsed with a mixture of MilliQ water (resistivity > 18.2 MΩ), 1 mL/L of H_2SO_4 98% and 20 mL/L of H_2O_2. All the glassware was boiled 4 times in MilliQ water for further cleaning. A

platinum wire was used as counter electrode, and a reversible hydrogen electrode (RHE) was used as reference electrode. The RHE electrode was placed in a Luggin capillary that contains only supporting electrolyte, and thus it is not affected by the presence of CO. All potentials in this chapter are referred to the RHE scale. The potential was controlled by an Ivium A06075 potentiostat. The copper electrodes were 99.99% copper disks (5.8 mm diameter), purchased from Mateck and aligned to < 0.5° accuracy. The electrodes were electropolished in a 10:5:2 solution of H_3PO_4:H_2O:H_2SO_4 at +3 V vs. Cu for 10 s. The surface of the electrode was characterized by cyclic voltammetry in a 0.1 M NaOH solution as explained elsewhere[91]. Electrolytes were made of high purity reagents (Sigma Aldrich TraceSelect) in ultra-pure water (MilliQ). The purity of the hydroxides was >99.9 % for all hydroxides except for Rb. The amount of impurities present in RbOH sometimes led to questionable and non-reproducible results. Before every experiment, argon (Linde, 6.0) was bubbled through the electrolyte for 20 minutes to remove air from the solution, after which CO (Linde, 6.0) was bubbled through the solution for another 20 minutes until saturation was reached. During the experiment, CO was kept flowing through the solution.

The gaseous products formed during the reaction were detected by Online Electrochemical Mass Spectroscopy (OLEMS)[92]. The volatile products formed on the surface of the electrode were collected by a hydrophobic tip situated at 0.05 mm from the electrode. The distance was kept constant for every experiment with the help of a holder with micrometric precision. The Teflon tip with a diameter of 5.4 mm and an average pore size of 10-14 μm is connected through a PEEK capillary to the mass spectrometer. The bigger tip diameter compared to our previous OLEMS setup[92] allows for the detection of more products, thus increasing the sensitivity of the apparatus. However, this new configuration does not allow to perform experiments in the hanging meniscus configuration, with the possibility that some products not formed on the single-crystal surface might as well reach the tip. Prior to each use, the tip was cleaned in a solution of 0.2 M $K_2Cr_2O_7$ in 2 M H_2SO_4

and then boiled 4 times in MilliQ water. A Balzers Quadrupole mass spectrometer with a secondary electron multiplier (SEM) voltage of 1500 V with an ionization potential of 70 V was used for the detection of every mass. The different mass signals were followed while changing the electrode potential from +0.1 V to -1.5 V vs. RHE at a scan rate of 1 mVs^{-1}. The results obtained with OLEMS are qualitative. A direct comparison between the concentrations of the different products formed is challenging due to changing factors such as the collection efficiency or the current intensity of the signal for different masses. However, for a given product and different electrodes and/or electrolytes, it is possible to compare the formation of such species through their ratio (e.g. on Cu(100) the m/z=26 signal is larger for CsOH than for LiOH, which attests to a larger production of ethylene in Cs-containing electrolytes). On the other hand, the ratio of formation of two different products (e.g. C_2/C_1) offers a fair qualitative comparison.

The liquid products formed during the reduction of CO were collected and analyzed by High Performance Liquid Chromatography (HPLC) with a RID detector (Shimadzu). A 0.005 M H_2SO_4 solution was used as an eluent in an Aminex HPX-87H (Biorad) column with a flow rate of 0.6 mL/min. Samples were taken after 2 h of long-term electrolysis carried out in a H-cell with a Nafion membrane that separates the cathode from the anode compartment. CO was constantly bubbled through the solution to ensure its constant concentration. Chronoamperometry experiments were performed at -0.5, -0.7 and -0.9 V vs RHE on a polycrystalline copper electrode of 16.85 mm diameter.

Fourier Transform Infrared Spectroscopy (FTIR) was used to detect intermediates in the early stages of CO reduction. FTIR measurements were performed with a Bruker Vertex 80 V Infrared spectrophotometer[128]. The electrochemical cell was assembled on top of a 60° CaF_2 prism, and the electrode was situated against this prism to form a thin layer. The measurements were performed under external reflection. FTIR spectra were obtained from an average of 100 scans with a resolution of 8 cm^{-1} at the selected potentials. Every spectrum

was obtained by applying single potential steps compared to the reference potential (+0.1 V). The spectra are shown as $(R-R_0)/R_0$ where R is the reflectance at the sample potential and R_0 is the reflectance at the reference potential. Therefore, the ratio $\Delta R/R_0$ gives positive bands for the formation of species at the sample potential, while negative bands correspond to the loss of species at the sample potential. P-polarized light was used to probe species both near the electrode surface and in solution. The experiments were performed in a thin-layer configuration, which implies some experimental limitations. Any appreciable changes in the thin layer (such as the formation of gaseous products, change in local pH by production or consumption of H or OH species, etc.) result in spectral deformation. This is particularly important at negative potentials for CO reduction because of competitive hydrogen evolution, so that the potential range where spectra can be obtained is in fact narrow and justifies our choice of potentials ranging from -0.2 to +0.1 V. As the thin layer cannot be rigorously controlled, the in situ FTIR is only a qualitative method and definitely cannot be used for quantification. The intensity of the bands cannot be directly compared between experiments as different thin layers are involved

5.3 Results and discussion

5.3.1 OLEMS and HPLC

Cu(111), Cu(100) and Cu(poly) were characterized by voltammetry before and after experiments to control the morphology of the surface[91], see Appendix IV Figure AIV.8. The activity and selectivity of the three electrodes towards CO reduction were investigated with OLEMS by varying the alkaline cation in the 0.1 M hydroxide supporting electrolyte. A linear sweep voltammetry between 0 and -1.5 V vs RHE at a scan rate of 1 mVs^{-1} was carried out while simultaneously the volatile products were detected with OLEMS. Figure 5.1 displays the volatile products formed during the reduction of CO on Cu(100), Cu(111) and polycrystalline Cu for different alkaline hydroxide solutions of identical concentration (0.1 M). Figure 5.1a-5.1c shows the results of CO reduction for Cu(100). The middle panel (b) shows the mass fragment m/z = 15 associated with CH_4, and the top panel (a) shows the mass fragment m/z = 26 associated with C_2H_4. It is important to note that the reported amounts of products formed are in fact lower than the amounts expected if a purification process of the electrolyte would have been performed, according to the results obtained by Surendranath[148]. The onset potential for CH_4 at ca. -0.65 V is independent of the cation in solution. For all cations, except Cs^+, the formation of methane reaches a plateau around -0.9 V vs RHE. The general trend is that larger cations increase methane production. Figure 5.1b also shows that the formation of C_2H_4 on Cu(100) starts at ca. -0.3 V regardless of the cation. The amount of ethylene formed, as well as its formation rate, increase with the size of the cation. Especially Cs^+ shows a significant increase in ethylene production.

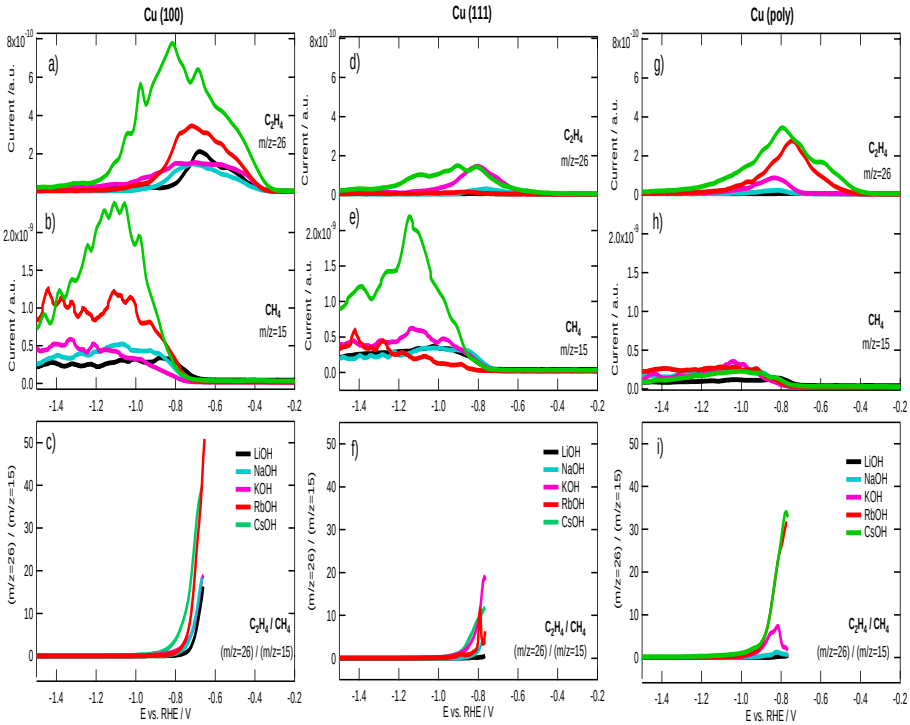

Figure 5.1: OLEMS mass fragments measured during CO reduction associated with the formation C2H4 (top panel, a, d and g) and CH4 (middle panel, b, e, and h) on a) Cu(100) , b) Cu(111) and c) polycrystalline Cu for different 0.1 M alkaline hydroxide solutions. Bottom panel (c, f and i) shows the potential-dependent ratio (m/z = 26) / (m/z = 15) of OLEMS mass fragments associated with the formation of C2H4 and CH4 during CO reduction.

On Cu(111) (Fig 5.1d-f), the onset potential for CH_4 is ca. -0.65 V regardless of the cation, with trends in activity similar to Cu(100). (Rb^+ deviates from this trend but, as mentioned in section 5.2 RbOH frequently showed problems with purity and reproducibility). The formation of C_2H_4 starts around -0.4 V regardless of the cation, which is 0.1 V more negative than on Cu(100). The amount of ethylene formed, as well as its formation rate, is highest with Cs^+ in the electrolyte. It is important to point out the differences observed with the previous work by Schouten et al,[59] where the formation of ethylene and methane on Cu(111) displayed a similar profile having both an onset potential of

approximately -0.8 V. Similar results were obtained by Nilsson et al,[143] who found onset potentials for methane and ethylene on Cu(111) close to -0.9 V. However, in this work ethylene formation on Cu(111) starts at lower overpotentials (-0.4 to -0.5 V), which we attribute to the higher sensitivity achieved by using a larger OLEMS tip in combination with the non-meniscus configuration. Although it is not possible to rule out the contribution of other facets present on the electrode, the significantly higher activity and lower onset potential of Cu(100) surface for ethylene formation is also clearly observed in this work.

On polycrystalline Cu (Fig. 5.1g-i) the onset potential for CH_4 production is around -0.65 V regardless of the cation in solution. The plateau is less pronounced than on the single crystals, and the trend with the size of the cation is less evident. C_2H_4 formation is strongly dependent on the cation, with the smallest cation (Li^+) showing essentially no ethylene formation and the largest cation Cs^+ showing the strongest selectivity towards ethylene. Though we remark again that it is currently impossible to perform fully quantitative selectivity measurements using OLEMS, the results in Figure 5.1 allow us to conclude that (i) larger cations enhance CO reduction to ethylene at low overpotentials, and that the effect is significantly stronger on Cu(100), (ii) larger cations enhance methane production at high overpotentials.

To support these conclusions, we consider in Figure 5.1 bottom panels (c, f and i) the potential dependence of the ratio of the mass signals corresponding to ethylene (m/z = 26) and methane (m/z = 15) for the three different Cu electrodes. The ratio was plotted as I(m/z = 26)/I(m/z = 15), so a high value expresses a larger production of ethylene over methane. Since at potentials more positive than -0.65 V there is no methane production and the value of the ratio C2/C1 is infinite, the ratio was only calculated in the potential region where both products coexist or the amount of C_2H_4 detected is null. At low overpotentials, all copper surfaces show a higher selectivity towards ethylene with increasing cation radius, with the highest selectivity achieved for Cu(100), especially with Rb^+ and Cs^+ in solution. In

particular, for a fixed potential of -0.75 V, the ethylene/methane ratio for Cu(100) are 1.59 for Li^+, 3.93 for Na^+, 4.32 for K^+, 7.54 for Rb^+ and 14.8 for Cs^+ (see Appendix IV Figure AIV.2a). These values show a clear cation effect towards ethylene formation that monotonically follows the cation sizes. In addition, the selectivity for ethylene is enhanced in a larger potential range when larger cations are in solution. Figure AIV.2b in appendix IV shows that larger cations maintain the same selectivity for ethylene at more negative potentials compared to smaller cations: the potentials for which a fixed value of 5 for the ethylene/methane ratio are -0.70, -0.72, -0.72, -0.74 and -0.79 V for Li^+, Na^+, K^+, Rb^+, and Cs^+. Similar tendencies are observed for Cu(111) and polycrystalline Cu but with significantly lower ratios. The ratio C_2/C_1 on Cu(111) and polycrystalline Cu in LiOH solution is almost zero over the whole potential range in which both species coexist, indicating low selectivity for ethylene formation over methane in this electrolyte.

Figure AIV.1 in appendix IV shows the mass fragment m/z = 2 associated with the formation of H_2 from the competitive hydrogen evolution reaction (HER). For all copper surfaces, hydrogen evolution starts at ca. -0.4 V for all different cations except Cs^+, for which it starts at slightly less negative potentials. The amount of hydrogen produced as well as its formation rate increases with the size of the cation in the electrolyte for all copper electrodes.

The minor liquid products obtained during CO reduction on polycrystalline copper and their dependence on the nature of the cation were collected and analyzed with HPLC. Due to the low amount of products formed, chronoamperometry experiments for 2 h were carried out using a large copper disk (16.85 mm diameter). Given the long duration of this set of experiments, we did not perform these experiments with single-crystal electrodes, since the stability of the surface structure may be compromised. Chronoamperometry experiments were carried out at three different potentials: -0.5, -0.7 and -0.9 V vs RHE, with different alkaline hydroxides. The concentrations of the obtained products and their cation dependence are summarized in

Figure AIV.3 in appendix IV. The only liquid product detected for CO reduction at -0.5 V was formic acid. At more negative potentials (-0.7 v and -0.9 V) the products obtained were: formic acid as C_1 product; acetic acid, glycolic acid, ethylene glycol and ethanol as C_2 products; and propionaldehyde, 1-propanol and allyl alcohol as C_3 products. Such C_2 and C_3 products obtained during CO reduction have been reported previously[50, 61]. In general, larger cations such as Cs^+ promote CO reduction to C_{2+} compounds compared to small cations (Li^+ and Na^+), in agreement with the results of Hori et al [65]. A detailed description of the concentration of the products depending on the cation in solution can be found in appendix IV, section IV.2.

Further analysis by ^{1}H-NMR was carried out for the samples obtained after 2 h of chronoamperometry at -0.9 V with Na-, K- and Cs-containing electrolytes (Appendix IV, Figure AIV.4). The ^{1}H-NMR spectra confirmed the products detected with HPLC and their higher concentration with K^+ and Cs^+ compared to Na^+. In addition, methanol was also detected as a reduction product of CO for those three cations. Identification of methanol was not possible with HPLC due to an overlap with the intense peaks of the eluent.

Note that we were unable to consistently detect aldehydes as products, while acetaldehyde and propionaldehyde have been reported to be products of CO_2 reduction on copper[50]. This is probably due to the fact that our experiments were carried out at pH 13, and it is known that aldehydes are unstable at such high pH and disproportionate following a Cannizzaro reaction, giving the corresponding carboxylic acid and alcohol[149].

5.3.2 FTIR

FTIR spectra were recorded during the early stages of CO reduction on Cu(100) and Cu(111) in different alkaline hydroxide solutions, to gain insight into the dependence of the reaction mechanism on to the surface structure of the electrode as well as the cation in the electrolyte. FTIR experiments carried out in Li-containing electrolytes (see Chapter 4) indicated a structure-sensitive process in the early stages of CO reduction[150], which together with DFT calculations led us to hypothesize the formation of a hydrogenated CO dimer intermediate in the pathway leading to ethylene, in agreement with previous experimental[64] and theoretical[54] studies. Figure 5.2a-f shows the potential-dependent absorbance spectra of Cu(100) and Cu(111) under CO atmosphere for different 0.1 M alkaline hydroxide solutions. The spectra recorded on Cu(100) in LiOH solution were previously reported by our group[150].

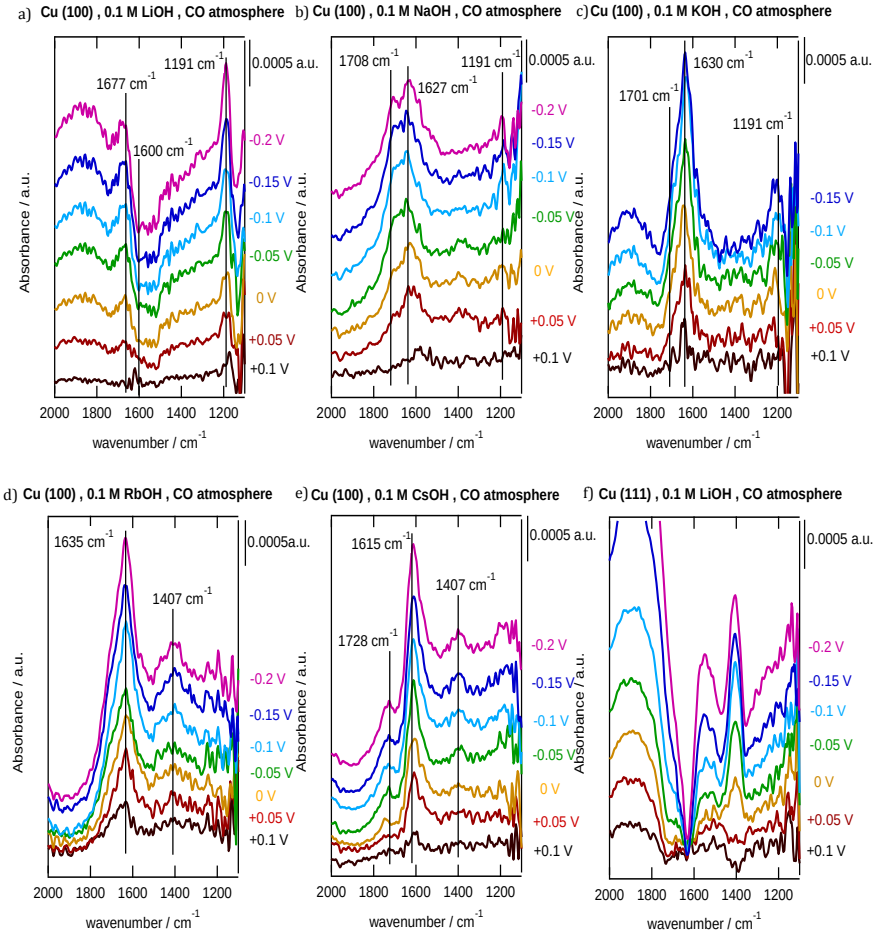

Figure 5.2: Potential-dependent absorbance spectra of Cu(100) in CO atmosphere in 0.1 M solution of a) LiOH, b) NaOH, c) KOH, d) RbOH, e) CsOH. f) LiOH on Cu(111), provided for comparison. Reference spectrum recorded at +0.1 V vs. RHE.

The reference spectrum was taken at +0.1 V vs RHE and additional spectra are provided for +0.05, 0.00, -0.05, -0.10, -0.15 and -0.2 V vs. RHE. Due to experimental limitations, it was not possible to record spectra at more negative potentials where the hydrogen evolution reaction starts, as this destabilizes the thin layer formed between the electrode and the prism of the spectrometer resulting in unstable spectra. These limitations are explained in section 5.2. CO reduction in

different alkaline hydroxide solutions was also studied on Cu(111) (a representative spectrum is shown in Fig. 5.2f). The FTIR spectra for CO interacting with Cu(100) exhibit two common bands for all alkaline electrolytes. The first band, in the range of 1635-1600 cm^{-1}, corresponds to the O-H bending mode of H_2O. This band causes fluctuations in the baseline of the spectra making it difficult to identify other bands in this wavenumber range. The second band, in the range of 1730-1670 cm^{-1}, corresponds to the C-O stretching[129-131] of CO adsorbed on hollow sites on Cu(100) [132-135] . Apart from these two bands, two other bands arise depending on the electrolyte used. For Li, Na and K hydroxides, a band at 1191 cm^{-1} attributed to the C-O stretching of a hydrogenated dimer (OCCOH)[150] is observed. Note that the assignment of this band to the hydrogenated dimer and the exclusion of other species were discussed extensively in Chapter 4.[150] Besides, in appendix IV section IV.7 we also provide arguments to discard the presence of oxalates. In contrast, the band at 1191 cm^{-1} is not observed when Rb^+ and Cs^+ are in solution, a feature that will be explained in the next section with DFT calculations. The intensity of the band assigned to C-O stretching of the hydrogenated dimer diminishes from Li to K (Figs. 5.2a-c). For Rb and Cs (Figs. 5.2d-e), a band at 1407 cm^{-1} is observed, which according to the transmission spectra obtained for various species in solution might correspond to formaldehyde. Formaldehyde has been suggested to be an intermediate of the reduction of CO to CH_4 on Cu(211)[151-152]. The spectra obtained during the reduction of CO on Cu(111) (Fig. 5.2f) also shows the band at 1407 cm^{-1}. However, on Cu(111) this band is more intense for smaller cations than for larger cations.

5.3.3 DFT calculations

To rationalize some of the observed cation effects, we resort now to DFT calculations. We will focus on Cu(100), as ethylene is formed at low overpotentials and the FTIR results in Figure 5.2 suggest the presence of a hydrogenated dimer intermediate. Since CO hydrogenation is critical for both methane[57] and ethylene production,[53, 62], in the following we will focus only on this step. Figure 5.3 shows the energetics of the first electrochemical steps in the reduction of one CO molecule to C_1 species and two CO molecules to C_2 species in vacuum and in presence of Li, Na and Cs (the energies shown are the averages of the separate values found for the three cations, for details see appendix IV Figures AIV.11 and AIV.12). The first proton-electron transfer for a single CO molecule proceeds as:

$$* + CO(g) + H^+ + e^- \rightarrow *CHO \qquad (5.1)$$

This step consists of CO adsorption and hydrogenation. On the other hand, the first proton-electron transfer for two CO molecules proceeds as:

$$* + 2CO(g) + H^+ + e^- \rightarrow *OCCOH \qquad (5.2)$$

This step comprises successive CO adsorption (denoted *CO and 2*CO in Figure 5.3), dimerization (*OCCO), and hydrogenation (*OCCOH). The adsorption configurations of C_1 and C_2 species are provided in appendix IV Figures AIV.9 and AIV.10.

From Figure 5.3 it is clear that all intermediates, namely *CO, 2*CO, *OCCO, *CHO and *OCCOH, are significantly stabilized by the presence of the alkaline cations, but the strength of the effect depends both on the particular adsorbate. Essentially, the overall cation effect is due to the larger stabilization of adsorbates containing C-C bonds (*OCCO and *OCCOH) with respect to the C_1 adsorbates (*CO, 2*CO, *CHO). Importantly, the presence of the cations changes the binding mode of the CO dimer, as shown in appendix IV, Figure AIV.9, and the adsorption sites of the adsorbates (appendix IV, Figures AIV.9 and AIV.10).

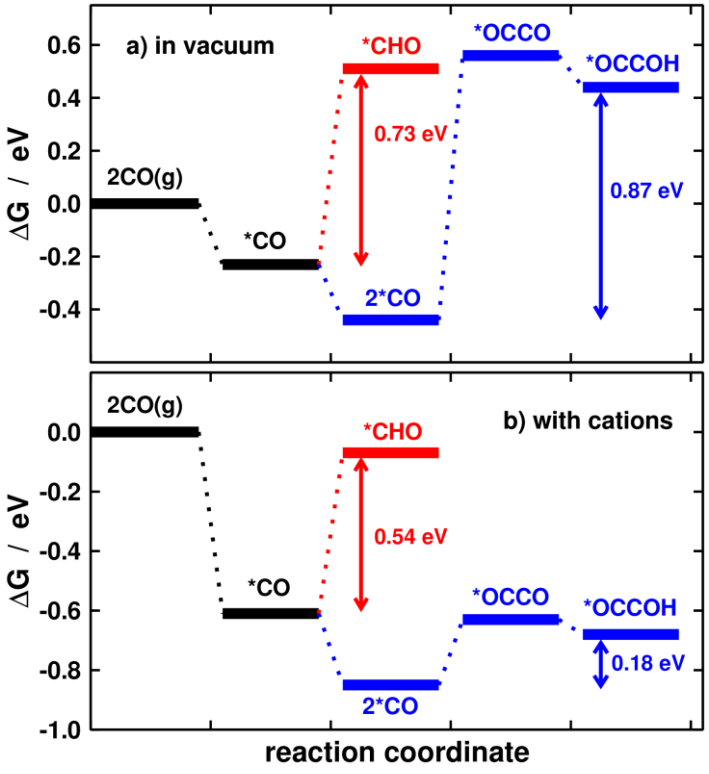

Figure 5.3: Energetics of the first electrochemical steps of CO reduction for the C_1 and C_2 pathways on Cu(100) at 0 V vs RHE. a) In vacuum, and b) with cations, averaging the energies for Li, Na and Cs in appendix IV Figures AIV.11 and AIV.12. While in vacuum both pathways are highly endothermic, the C_2 pathway is remarkably promoted by alkaline cations.

Note that both steps described by Equations (5.1) and (5.2) are highly endothermic in the absence of cations, so that the reaction energies for *CO hydrogenation are 0.73 and 0.87 eV for the C_1 and C_2 pathways (see appendix IV, Tables AIV.2 and AIV.3). In presence of the cations, the energetics of *CO hydrogenation are lowered from 0.73 to 0.54 eV. This change is dwarfed by the dramatic lowering in the C2 pathway from 0.87 to 0.18 eV. This attests to a substantial enhancing effect of the alkaline cations by decreasing the energy barriers for *CO reductive coupling. The enhancement of *OCCO with respect to 2*CO clearly illustrates cation effects: the adsorption energy of *OCCO is made more negative by the cations by ∼1.2 eV, whereas the adsorption energy of 2*CO is stabilized by ∼0.4 eV. In sum, Figure 5.3b explains well the experimentally observed preference of Cu(100) for ethylene formation over methane.

There is also another manifestation of the cation effect, related to the stability of *OCCOH. Similar to the dimer, the hydrogenated counterpart is significantly stabilized (1.16 eV in average) by the presence of alkaline cations. Following the model of Nørskov et al[57] in which the onset potential is linked to the largest uphill reaction energy in a given pathway, the potential to go from 2*CO to *OCCOH is -0.10 V for Li^+, -0.16 for Na^+, and -0.28 eV for Cs^+ (see appendix IV, Figure AIV.12). Therefore, the hydrogenated dimer should only be observable with FTIR at low potentials (> -0.2 V) in presence of Li^+ and Na^+, but not in the case of Cs^+, in agreement with the experimental results in Figure 5.2. This shows that cation effects can be averaged to observe overall trends, but important subtleties pertaining to each cation can only be captured by separate analyses. In addition to the quantitative considerations on the cation effect provided in Figure 5.3, in appendix IV, section IV.6 we also discuss some qualitative features of Li^+, Na^+ and Cs^+ co-adsorption with C_1 and C_2 species.

5.3.4 Mechanistic implications

The OLEMS results in Figure 5.1 suggest a relation between m/z = 15 and m/z = 26 (associated with methane and ethylene formation, respectively). Figure 5.4 illustrates the relation between these two masses for the specific case of CO reduction on Cu(100), although the trend is also observable for Cu(111) and polycrystalline Cu (see appendix IV, Figure AIV.5). Importantly, the mass fragment associated with the formation of ethylene drops when the signal associated with the formation of methane starts to rise. Moreover, the m/z = 15 signal increases faster in the electrolytes for which the m/z = 26 signal decreases faster, leading to a delay in the potential where the maximum current for methane is observed, depending on the size of the cation. For example, while the decay in ethylene formation in LiOH is acute and the rise of the mass fragment associated with methane is steep, in CsOH solutions the decay of ethylene and the formation of methane are both more gradual. In this order of ideas, larger cations enhance the selectivity towards C_2H_4 over a wider potential range.

This behavior could be understood if, for instance, methane formation would be the result of C_2H_4 reduction. However, we discarded this hypothesis because ethylene reduction experiments did not lead to the formation of methane (see appendix IV, Figure AIV.6). It is also important to note that ethane was not detected as a reduction product of ethylene in these experiments.

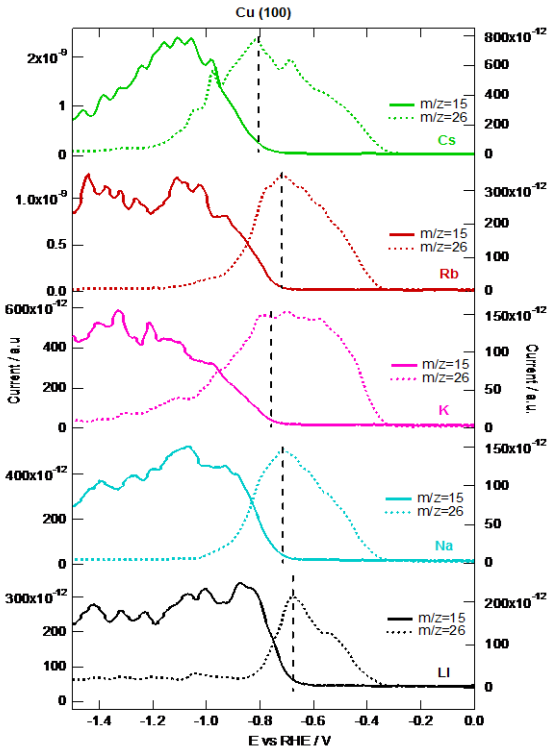

Figure 5.4: OLEMS mass fragments associated with the reduction products formed during CO reduction on Cu (100) electrode in different 0.1 M alkaline hydroxide solutions. Dashed lines correspond with m/z=26 associated with the formation of ethylene, plotted against the right axis and full lines correspond with m/z=15 associated with the formation of methane, plotted against the left axis. Vertical lines highlight the potential at which the m/z=26 signal associated with ethylene starts to decay.

Therefore, we believe that a cation-, potential-, and facet-dependent picture such as the one in Figure 5.5 is needed to portray the mechanistic effects of alkaline cations on CO reduction. The figure shows a schematic representation of the structure- and potential-dependency of the cation effects for CO reduction towards the two main products, methane and ethylene. The onset potential for ethylene formation depends on the facet, being lower for copper single crystals than for polycrystalline copper. In addition, the onset potential for ethylene is not affected by the cation nature when CO reduction is performed on

copper single crystals (see appendix IV, Figure AIV.7), whereas on polycrystalline copper the onset potential varies alongside the cation size, being -0.6 V for Li^+ and Na^+, -0.4 V for K^+ and -0.35 V for Rb^+ and Cs^+. On the other hand, the onset potential for methane formation is independent of both cation size and surface structure. In the range from -0.3 V to -0.65 V, larger cations enhance the formation of ethylene, whereas at potentials more negative than -0.65 V the formation of methane is favored. Figure 5.4 suggests that this phenomenon is due to a shutting down of the C_2 pathway at large overpotentials in which the C_1 pathway becomes favorable.

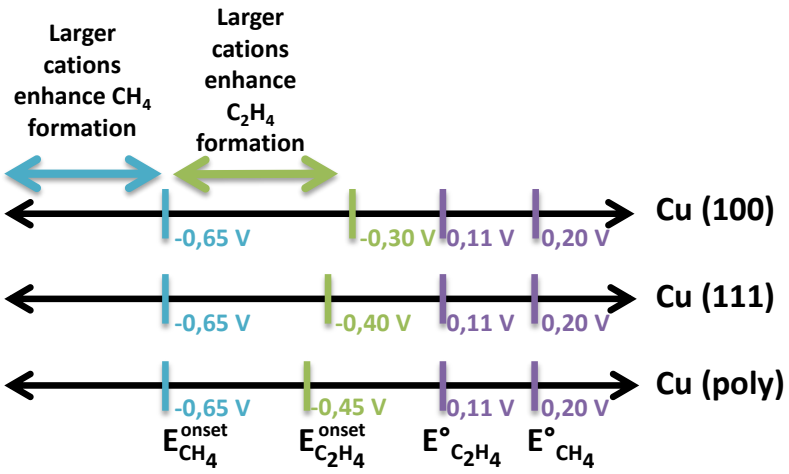

Figure 5.5: Schematics of the structure- and potential-dependent cation effects for CO reduction towards methane and ethylene in alkaline hydroxide electrolytes (pH=13). Potentials vs RHE. E^0 are standard equilibrium potentials

Hori et al explained the differences in product distribution on the nature of the cation based on the potential distribution at the electrode surface in terms of changes in the outer Helmholtz plane (OHP) potential[65]. The OHP potential varies with the cations according to their particular adsorption features. Specific adsorption of cations supposedly shifts the OHP potential to more positive values, the OHP potential being higher for Cs^+ than for Li^+ in view of their dissimilar hydration shells. In this

model, a more negative OHP potential translates into a higher H^+ concentration, such that the pH at the electrode will decrease as the size of the cation decreases. At higher pH values the formation of ethylene vs methane is enhanced.

On the other hand, in the model proposed by Bell et al[147] for the cation enhancement of CO_2 reduction, the pH near the electrode is lower when larger cations are in solution, leading to a higher local CO_2 concentration that results into a higher cathodic activity. They attribute the decrease of pH when larger cations are present to a decrease of the pKa for the cations hydrolysis. When the pKa is sufficiently low, hydrated cations serve as buffering agents, decreasing the pH near the electrode and thereby increasing the local concentration of CO_2. Note that this model is in agreement with experimental data for potentials lower than -1.1 V vs RHE. However, this model cannot explain the fact that similar cation effects are observed during CO reduction[65], the concentration of which is not affected by (local) pH. In their model, Bell et al explained that the hydrolysis of hydrated cations is only effective in mildly basic or acidic electrolytes. However, our experimental results showed a cation enhancement for the production of ethylene during CO reduction in strongly alkaline media (pH=13).

Our explanation of cation effects is based on Figures 5.3, AIV.11, and AIV.12. We believe that cations are essentially catalytic promoters, their presence altering substantially the free-energy landscape of CO reduction. They especially stabilize C_2 species by means of strong O-cation interactions, justified by the strong tendency of those species (e.g. *OCCO and *OCCOH) to be negatively charged, unlike isolated *CO monomers. Our perspective on cation effects is in line with that of Janik and coworkers[153], who explicitly included cation, anion and solvation effects in their calculations and reported similar effects for CO_2 reduction in presence of K^+. The averaging in Figure 5.3 is close to that of Nørskov and coworkers[154-155] who have shown that cations at the double layer induce local field effects that alter the adsorption energies. Although overall cation effects can be averaged, we stress that subtle yet

important details such as differences in adsorption sites, adsorption configurations (appendix IV, Figures AIV.9 and AIV.10) and onset potentials as a function of cation size (appendix IV, Figures AIV.11 and AIV.12) are only captured when modelling the cations explicitly.

Finally, it is important to note that the present work is devoted only to "fully metallic" Cu electrodes, while "oxide-derived" Cu electrodes also exist and, due to their high activity for CO reduction, are the subject of extensive research [55, 143, 156-157]. "Fully metallic" Cu(100) and oxide-derived Cu electrodes produce both large amounts of C_2 products, although the former is inclined towards ethylene, while the latter favors ethanol. Previous works provided a plausible explanation for such dissimilar behavior: there is a selectivity-determining intermediate in the CO reduction pathway to C_2 products, namely $*CH_2CHO$[53]. If hydrogenation leads to $*CH_3CHO$ (i.e. adsorbed acetaldehyde), ethanol is the major final product [127]. Conversely, if hydrogenation leads to $*CH_2CH_2O$, then ethylene is favored [53]. Whereas acetaldehyde is reduced to ethanol at larger rates at steps and grain boundaries[127, 158] compared to terraces, pristine (100) terraces are known to favor ethylene production [59, 64].

5.4 Conclusions

In this chapter, we have shown that the combined effect of alkaline cations and catalyst morphology can steer the selectivity of CO reduction towards ethylene or methane, depending on the potential. Specifically, our results suggest the following conclusions:

1) In general, larger cations enhance CO reduction to ethylene at low overpotentials, especially on Cu(100). With smaller cations in solution, CO reduction on Cu(111) and Cu(polycrystalline) shows low selectivity for ethylene formation over methane over the whole potential range in which both species coexist. The formation of other minor C2 and C3

products (such as acetic acid, glycolic acid, ethanol and propanol) is also enhanced by the presence of larger cations.

2) A correlation between the decline of ethylene formation and the onset potential for methane formation was observed. Furthermore, methane formation reaches its plateau when ethylene formation drops to zero. This suggests that the C_2 pathway is blocked by the enhancement of the C_1 pathway. This correlation depends on the cation size, so that larger cations enhance the selectivity towards ethylene over a wider potential range.

3) For the two major products, methane and ethylene, differences in the onset potential were found as a function of the cation size and the surface structure. While the onset potential of ethylene formation depends on these two factors, the onset potential of methane does not.

4) FTIR and DFT calculations were used to gain insight into the origin of cation effects on Cu(100). As described in chapter 4[150], FTIR suggests the presence of a hydrogenated dimer intermediate (OCCOH) at low overpotentials. The formation of this intermediate depends on the size of the cation, so that the hydrogenated dimer can be detected with FTIR in presence of Li^+, Na^+ and K^+, but not in presence of Rb^+ or Cs^+. DFT calculations explain that the potential necessary to form *OCCOH from *CO in presence of Cs^+ is more negative compared to Li^+ or Na^+. Besides, the adsorption energies of species containing C-C bonds are dramatically stabilized by cations with respect to C_1 species, justifying the selectivity towards ethylene at low overpotentials.

5) The role of cations in CO reduction is that of a catalytic promoter, changing the free energy landscape of CO reduction and specifically stabilizing certain intermediates, especially those with a favorable (electrostatic) interaction with the cation. Larger cations such as Cs promote pathways with these intermediates more effectively than smaller cations such as Li.

Chapter 6

Mechanistic study of the electrosynthesis of propylene carbonate from propylene oxide and CO_2 on copper electrodes

Efficient and selective electrosynthesis of propylene carbonate can be performed by the reaction of carbon dioxide with propylene oxide at copper electrodes. In this paper, we investigate this electrochemical reaction by Cyclic Voltammetry (CV), Fourier Transform Infrared Spectroscopy (FTIR) and High Performance Liquid Chromatography (HPLC) in order to unravel the catalytic mechanism of the reaction. The combination of the results obtained by these different techniques, allows the exclusion of different reduced forms of CO_2, such as CO and (bi)carbonates, as possible carboxylation agents. Moreover, the results also indicate that electrochemical activation of the propylene oxide by the ring opening is not the initial step for this reaction since no product was detected if a current was not applied in presence of "activated propylene oxide" and CO_2. We propose an electrochemical reaction initiated by the activation of CO_2 to CO_2^- which then attacks the epoxide to form the cyclic carbonate. This work also gives evidence for the non-electrocatalytic nature of the cyclic carbonate synthesis since the formation of propylene carbonate also occurs on other metals such as gold and platinum in the same range of applied currents. These results clearly indicate the potential of in situ electrochemical techniques in the mechanistic investigation of electrosynthesis reactions.

This chapter has been submitted as : E Pérez-Gallent, MC Figueiredo, MTM Koper

6.1 Introduction

The accelerated increase of CO_2 atmospheric levels in the last decades due to the consumption of fossil fuels is causing an acute environmental problem[39]. Compared to CO_2 storage solutions, the fixation of CO_2 into organic molecules offers an attractive alternative [159]. Carbon dioxide can be used as a C1 feedstock in organic synthesis due to its abundant, cheap, renewable and non-toxic nature[70]. Among the different valuable products obtained from carbon dioxide, cyclic carbonates offer wide applications in the chemical industry. Cyclic carbonates can be utilized as fuel additives, as electrolytes for Li ion batteries, as plastics, as green reagents[160] and as raw material for the production of dimethyl carbonate[69], which is considered as a replacement for more toxic solvents in paints and coatings since it is exempt from the restrictions placed on most volatile organic products. Many catalyst systems have been developed for the conversion of CO_2 to cyclic carbonates[72-74, 161]. High temperature and high pressure are frequently required due to the relatively low reactivity of CO_2 at low energy input. Electrochemistry would provide an alternative manner to activate carbon dioxide at atmospheric pressure and low temperature. Electrosynthesis of cyclic carbonates has been performed under mild conditions with the achievement of an efficient and selective process[80, 84, 162]. Several metals such as copper[80], stainless steel[79], graphite[79], silver[81] and nickel[81], have been tested for the conversion of propylene oxide and CO_2 to propylene carbonate, obtaining the highest conversion (99%) on copper[79]. Although substantial efforts have been invested towards the achievement of a highly efficient process, the mechanism of this reaction is still under debate. Several studies attribute the opening of the propylene oxide ring as the rate-determining step, meaning that the catalyst activates the epoxide before the attack of CO_2[72, 74, 83, 161, 163], whereas other studies support the need of the activation of CO_2 as a key step to complete the reaction[80-81, 84]. In this work, we study the conversion of propylene oxide and CO_2 to propylene carbonate on copper electrodes in tetraethyl ammonium perchlorate ($TEAClO_4$) in

acetonitrile solutions by in situ Fourier Transform Infrared (FTIR) spectroscopy, in order to investigate the mechanism of the reaction. We will show that the activation of propylene oxide can be ruled out as the rate determining step for propylene carbonate synthesis, and that the electro-activation of CO_2 to a CO_2 radical anion is the likely key step for this process. We also show that undesired by-products may be formed from the reduction of the propylene oxide and the acetonitrile solvent.

6.2 Experimental

Prior to every experiment, the glassware was boiled in MilliQ water to remove possible salts, and subsequently rinsed with acetone. Next, the glassware was then dried in the oven at 100°C for 20 minutes. Electrolytes were made of tetraethyl ammonium perchlorate (Alfa Aesar, 98%) dissolved in acetonitrile (Sigma Aldrich, 99.8%). The electrolyte solutions still contain ca. 50-100 ppm water[164-165].

A flamed annealed platinum wire was used as a counter electrode, and an $Ag/AgClO_4$ in acetonitrile was used as a reference electrode[165]. Copper disc electrodes were used as working electrode (99.99%, from Mateck). The electrodes were electropolished in a 10:5:2 solution of H_3PO_4:H_2O:H_2SO_4 at +3 V vs. Cu for 10 s. The applied current was controlled by an Ivium A06075 potentiostat. Before every experiment, argon (Linde, 6.0) was bubbled through the electrolyte for 25 minutes to de-aerate the solution, after which CO_2 (Linde, 6.0) was bubbled through the solution for another 25 minutes until saturation was reached.

Fourier Transform Infrared Spectroscopy (FTIR) was used to detect intermediates, adsorbed species and species in solution during the reaction. The measurements were performed with a Bruker Vertex 80 V Infrared spectrophotometer[128]. The electrochemical cell was assembled on top of a 60° CaF_2 prism, and the electrode was situated against this prism to form a thin layer. The measurements were performed under external reflection. FTIR spectra were obtained from an average of 100

scans with a resolution of 8 cm^{-1} at selected currents every 4 minutes. The spectra are shown as $(R-R_0)/R_0$ where R is the reflectance at the sample and R_0 is the reflectance at the reference at zero current. Therefore, the ratio $\Delta R/R_0$ gives positive bands for the formation of species near the electrode, while negative bands correspond to the loss of species. P-polarized light was used to probe species both near the electrode surface and in solution. The experiments in the thin layer configuration have some experimental limitations. As the thin layer cannot be rigorously controlled, spectra cannot be used for quantification. The intensity of the bands cannot be directly compared between experiments since different thin layers are involved. However, within a single experiment, trends in intensity are reliable semi-quantitative indicators of changes in concentration. The electrode potential was controlled with a Potentiostat 466 System (Model ER466) from E-DAQ. All the experiments were performed at room temperature. The transmission spectra of the solution species were collected using a SeZn window with an incident angle of 60° and obtained by averaging 100 scans with a resolution of 8 cm^{-1}.

The liquid products formed during the electrosynthesis of propylene carbonate were collected and analyzed by High Performance Liquid Chromatography (HPLC) with a RID detector (Shimadzu). A 0.005 M H_2SO_4 solution was used as an eluent in an Aminex HPX-87H (Biorad) column with a flow rate of 0.6 mL/min. Samples were taken at different times of electrolysis carried out in a H-cell with separate cathode and anode compartments.

6.3 Results and discussion

6.3.1 Cyclic voltammetry

Fig. 6.1 shows the cyclic voltammetry of polycrystalline copper in a 0.1 M $TEAClO_4$ solution in acetonitrile under various conditions. The voltammograms were recorded in the absence of carbon dioxide and propylene oxide PO (black curve), in the presence of propylene oxide (blue curve), in the presence of carbon dioxide (red curve) and in the presence of both propylene oxide and carbon dioxide (green curve).

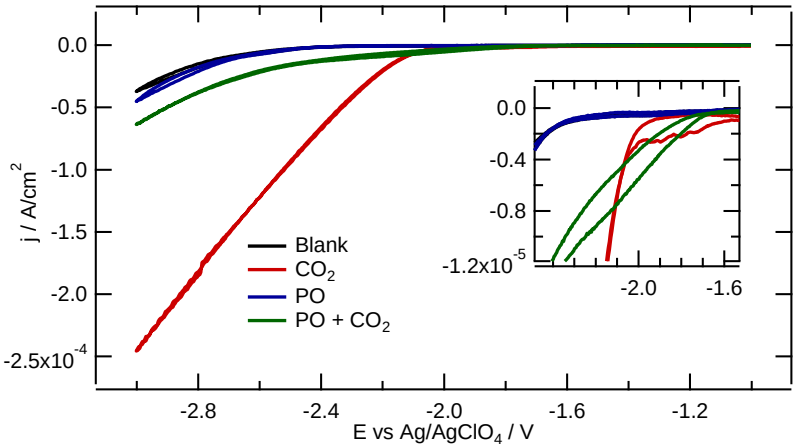

Figure 6.1: Cyclic voltammograms of polycrystalline copper in 0.1 M $TEAClO_4$ in acetonitrile solution in the absence of CO2 and propylene oxide (black) and in the presence of CO_2 (red), 0.1 M propylene oxide (blue) and a combination of propylene oxide (0.1 M) and CO2 (green), with $Ag/AgClO_4$ as reference electrode. Scan rate = 50 mV/s. Inset displays a zoom-in between -1.5 V and -2.5 V vs $Ag/AgClO_4$.

The comparison between the black and blue curves in Fig.6.1 indicates that propylene oxide does not undergo significant reduction under these conditions (though FTIR measurements to be discussed below show some formation of a PO reduction product). On the other hand, when

CO_2 is present in the solution (red curve), a reduction current is observed with an onset potential ca. -1.8 V vs. $Ag/AgClO_4$[164]. When both propylene oxide and carbon dioxide are present in the solution (green curve), a similar onset potential to CO_2 reduction is observed (red curve), but with a higher current between -1.8 and -2.2 V. This observation suggests that a reaction other than mere CO_2 reduction is occurring, with a faster reaction rate in the early stages of the reaction at potentials lower than -2.2 V. At more negative potentials than -2.2 V, the reaction is favored when only CO_2 is present. The lower reduction current observed when both substances are present in comparison with only CO_2 in solution suggests that the presence of propylene oxide hinders the reduction of CO_2, possibly because it reacts with it to form a new compound different from the reduction product of CO_2.

6.3.2 FTIR and HPLC characterization of intermediates and products

The reaction of propylene oxide with carbon dioxide on copper electrodes in $TEAClO_4$ prepared in acetonitrile solutions was analyzed by FTIR and HPLC. Fig.6.2 shows the transmission spectra for the reactant (PO) and for the expected product propylene carbonate (PC). The results show that PO does not have any vibrational mode active in IR, while PC clearly shows features that can lead to its identification with vibrational bands at 1800, 1392, 1184, 1118 and 1053 cm^{-1}. The absorbance spectrum of propylene carbonate in Fig. 6.2 shows that PC is best identified by the characteristic C=O stretching band at 1800 cm^{-1}.

Fig. 6.3 shows the time dependent absorbance spectra of the copper electrode in the presence of 0.1 M propylene oxide and saturated CO_2 atmosphere with an applied reduction current of – 5 mA cm^{-2}. The assignment of the different bands was done with the help of the transmission spectra and previous reports on CO_2 electrochemical reduction in acetonitrile[164] and is summarized in table 6.1. In addition,

vibrational bands for possible decomposition products for PO where also investigated by performing FTIR spectra of a copper electrode with a $TEAClO_4$ solution containing only propylene oxide under reductive conditions (data not shown). The assignment of the decomposition products is also included in Table 6.1.

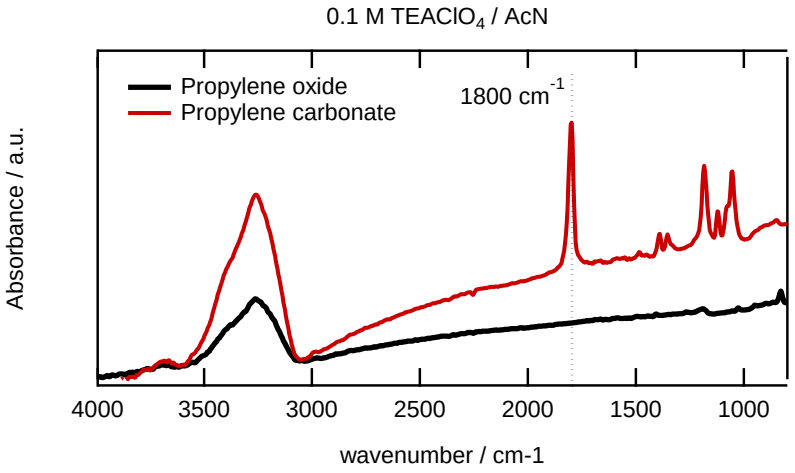

Figure 6.2: Absorbance spectra of a 0.1 M $TEAClO_4$ solution prepared in acetonitrile with propylene oxide (black) and with propylene carbonate (red). Band at 1800 cm^{-1} indicates the C=O stretching band of propylene carbonate.

Fig. 6.3 displays the absorbance spectra taken at different times during the electrosynthesis of propylene carbonate from propylene oxide and carbon dioxide at an applied current of -5 mA/cm^2. After one minute, CO_2 (2333cm^{-1}) starts to be consumed and several bands corresponding with the formation of products start to rise at 1647, 1481, 1361 and 1334 cm^{-1}. These latter bands can be attributed to (bi)carbonate species, CO_3^{2-}, HCO_2^-, CO_3^{2-} and CO_3^{2-} respectively, as described by Figueiredo et al.[164]. Previous studies suggested that the existence of different vibrational bands for C=O and C-O bonds on bicarbonates and carbonates is due to the presence of different ion pairs of the anions with TEA^+ cations or solvation shells with residual water[166]. At longer times (5, 9, 13 and 17 minutes) during the electroreduction of propylene oxide and carbon dioxide, the

spectra show a band at 1800 cm^{-1} growing with time. Fig. 3b shows a zoom-in of the spectral region where this band is observed. The band at 1800 cm^{-1} is attributed to the C=O stretching mode of propylene carbonate, according to the absorbance spectra of propylene carbonate displayed in Fig. 6.2.

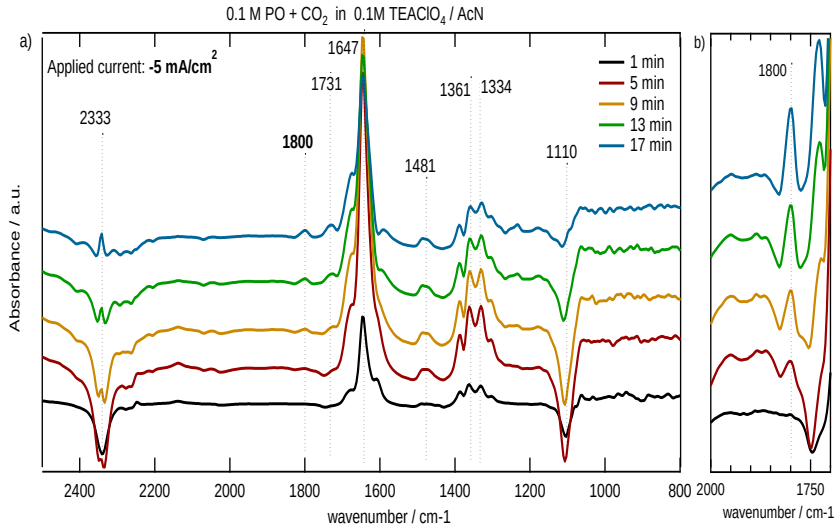

Figure 6.3: a) Time dependent absorbance spectra of a copper electrode in the presence of 0.1 M propylene oxide and saturated carbon dioxide atmosphere in 0.1M $TEAClO_4$ in acetonitrile solution at -5 mA/cm^2 after 1 minute (black), 5 minutes (red), 9 minutes (orange), 13 minutes (green) and 17 minutes (blue). b) zoom-in of spectra shown in a) between 2000-1720 cm^{-1}.

Importantly, simultaneously with the band 1800 cm^{-1}, a band at 1731 cm^{-1} is observed. In order to evaluate if this band is due to byproducts, the absorbance spectra of several species such as benzeneacetaldehyde, ethylene glycol, 1-methoxy 2- propanol and 2-propanol were recorded (data not shown). The absence of a band around 1731 cm^{-1} rules out that the band comes from one of this species. Moreover, the band at 1731 cm^{-1} does not come from a species originating from further reduction of propylene carbonate, since reduction of propylene carbonate does not lead to a band at 1731 cm^{-1} (data not shown). We suggest that the band at 1731 cm^{-1} might be due to the reductive decomposition of propylene oxide. The attribution is done based on the

observation that this band appears during the reduction of propylene oxide in the absence of carbon dioxide. However, further studies must be carried out to identify the nature of this species.

The electroreduction of propylene oxide and carbon dioxide on copper was also carried out at different current densities (-2,-3,-4,-5 and -6 mA/cm^2). Fig.6.4 displays the integrated areas of the band at 1800 cm^{-1} (attributed to propylene carbonate) as a function of the applied current and time. The formation of propylene carbonate is observed after only 5 minutes of electrolysis giving increasing product formation with time for all the different applied current densities. Moreover, applying higher current densities leads to more product formation.

Table 6.1. Assignment of the FTIR bands

v(cm^{-1})	assignment	compound
2333	s C=O	CO_2
2295	s C-N	acetonitrile
2252	s C-N	acetonitrile
1800	**s C=O**	**propylene carbonate**
1731	s C=O	Possible propylene oxide decomposition product
1647	s C=O	CO_3^{2-}
1674	s C=O	acetamide (acetonitrile decomposition product)
1628	b O-H	Water
1585	s N-H	acetamide (acetonitrile decomposition product)
1481	s C-O	HCO_3^-
1361	s C-O	CO_3^{2-}
1334	s C-O	CO_3^{2-}
1178	s N-H	acetamide (acetonitrile decomposition product)
1107	s Cl-O	ClO_4^-

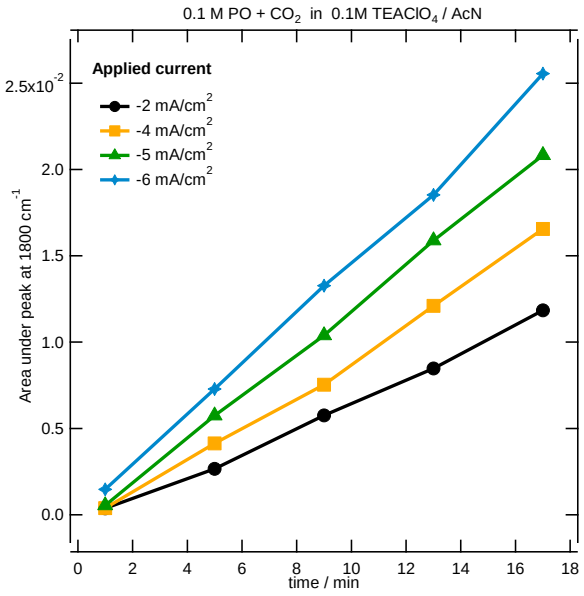

Figure 6.4: Area measured under the band at 1800 cm^{-1} (corresponding to propylene carbonate) observed during the reduction of PO and CO_2 on copper in 0.1 M $TEAClO_4$ in acetonitrile solution at different current densities and different times.

Fig. 6.5 shows the time dependent HPLC chromatograms obtained during the reduction of 0.1 M propylene oxide and CO_2 on a copper electrode in a 0.1 M $TEAClO_4$ in acetonitrile solution at -5 mA/cm^2. Due to large differences in peak intensities, the spectra are displayed in three different panels for a better interpretation. Fig 6.5a shows the peak corresponding to propylene oxide at 16.8 min. The intensity of the peak decreases over time, indicating that propylene oxide is being consumed. Fig 6.5b shows several peaks at 11.2, 13.1, 13.7, 14.9 and 15.4 minutes. We attribute these peaks to the decomposition of propylene oxide and/or decomposition of acetonitrile. This peak attribution is based on comparison of the spectra obtained under the same conditions but in the absence of CO_2 and in the absence of CO_2 and propylene oxide.

In the absence of CO_2, the peaks at 11.2, 13.1 and 13.7 minutes were present, suggesting that this species results from decomposition of propylene oxide. When the spectra were recorded in the absence of CO_2 and propylene oxide, the peaks at 14.9 and 15.4 were present, suggesting that the species comes from the decomposition of the electrolyte. It is known that acetonitrile under reductive conditions in the presence of residual amounts of water decomposes in acetamide, as suggested by previous studies[164, 167]. However, the species have not been characterized with certainty and further studies would be necessary to identify them.

Finally, Fig.6.5c shows the peak attributed to the formation of propylene carbonate at 25.5 min. The double-peak nature of the peak can be tentatively attributed to different solvations of propylene carbonate. As explained before, experiments were performed in acetonitrile solutions but for the HPLC analysis, an eluent of aqueous base is used. This might cause the presence of propylene carbonate solvated by water and also solvated by acetonitrile, that will have slightly different retention times causing the split of the peak in two contributions. Nevertheless, the results show that the production of propylene carbonate during electrolysis at -5 mA/cm^2 increases with time. Different current densities were applied (-2 and -4 mA/cm^2) to evaluate the effect of the applied current to the formation of propylene carbonate. The integrated area under the peak at 25.5 min and the applied current are displayed in Fig.6.6 as a function of time. As expected, the amount of product formed increases with time and with the applied current density.

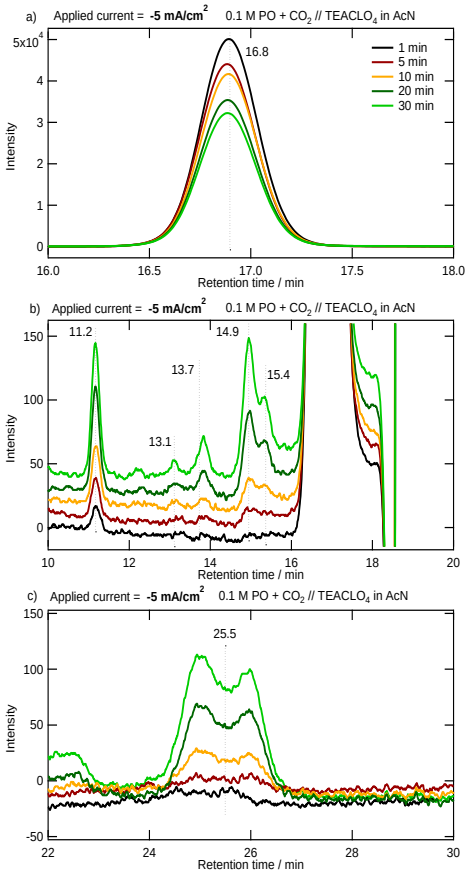

Figure 6.5: Time dependent chromatograms obtained by HPLC during the reduction of 0.1 M propylene oxide and CO_2 on copper in a 0.1 M $TEAClO_4$ in acetonitrile solution at -5 mA/cm². a) Displays the region between 16 and 18 minutes. b) Displays the region between 10 and 20 minutes. c) Displays the region between 22 and 30 minutes.

The combination of the FTIR and HPLC experiments confirm the formation of propylene carbonate from propylene oxide and carbon dioxide on copper electrodes. However, as the used organic solvents were not dry and contain residual water, reduction of water can also take place at these applied currents and potentials, leading to the generation of OH^-. In order to ensure that this is an electrochemical process and not a chemical synthesis catalyzed by the presence of OH^-,

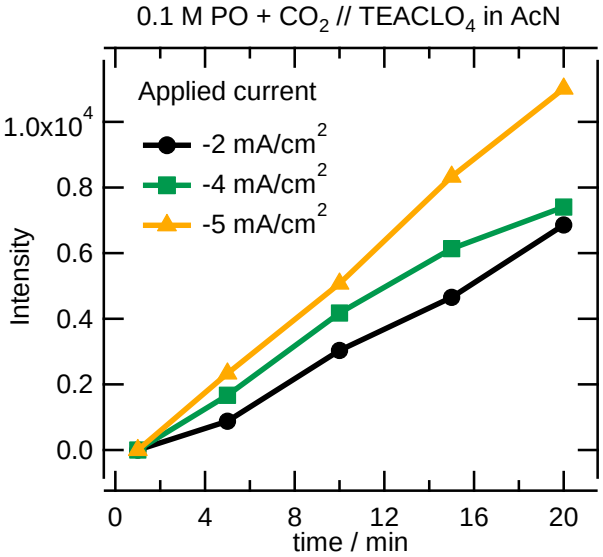

Figure 6.6: Area measured under the peak at 25.5 minutes (corresponding to propylene carbonate) observed during the reduction of PO and CO_2 on copper in 0.1 M $TEAClO_4$ in acetonitrile solution at different current densities and different times.

the spectra of propylene oxide and CO_2 in the presence of a strong base (TEAOH) were recorded (see appendix V, Figure AV.1). The spectra show an intense band at 2341 cm^{-1} corresponding to C=O stretching from CO_2 in solution. Less intense bands at 1670 cm^{-1} corresponding to decomposition products from the acetonitrile were also observed. However, the absence of a band at 1800 cm^{-1} that would correspond to propylene carbonate, supports the electrochemical nature of the synthesis of propylene carbonate instead of a chemical reaction catalyzed by the electrogenerated OH^-, in accordance with the results observed by Yang et al.[78]

6.3.3 Proposed mechanism

In the interest of understanding the mechanism of electrochemical formation of propylene carbonate from propylene oxide and CO_2 on copper, CO and carbonates (two known products from CO_2 electroreduction) were tested as the possible electroactive species for the synthesis of propylene carbonate.

Fig. 6.7 shows the time dependent absorbance spectra of copper in the presence of 0.1 M propylene oxide and saturated carbon monoxide atmosphere in 0.1 M $TEAClO_4$ in acetonitrile solution at -5 mA/cm^2. Carbon monoxide is known to be an intermediate of CO_2 reduction on copper electrodes in aqueous electrolytes[60, 168-169]. However, the absence of the band at 1800 cm^{-1} (corresponding with propylene carbonate) when CO_2 is exchanged for CO, discards CO as the electroactive species in the mechanism of propylene carbonate formation.

Previous studies of CO_2 reduction in non-aqueous solvents showed that the main products formed at high overpotentials are bi(carbonates)[164]. In our work, (bi)carbonates were indeed formed during the electrochemical reaction of propylene oxide and CO_2, identifiable by the bands observed at 1647, 1481, 1361 and 1334 cm^{-1} in Fig.6.3. The bands attributed to (bi)carbonate formation during the electroreduction of propylene oxide and CO_2 decrease with time (see Fig.6.3) while the formation of propylene carbonate (band at 1800 cm^{-1}) increases with time. A possible explanation of these observations would be that (bi)carbonates are being first formed by reduction of CO_2 and then consumed by reacting with propylene oxide to form propylene carbonate.

However, when FTIR spectra were recorded using $TEAHCO_3$ in solution instead of bubbling CO_2, formation of propylene carbonate was not observed (Figure 6.8). Therefore, we rule out (bi)carbonates as the electroactive species for the formation of propylene carbonate on copper. The intensity decrease of the (bi)carbonates bands observed in

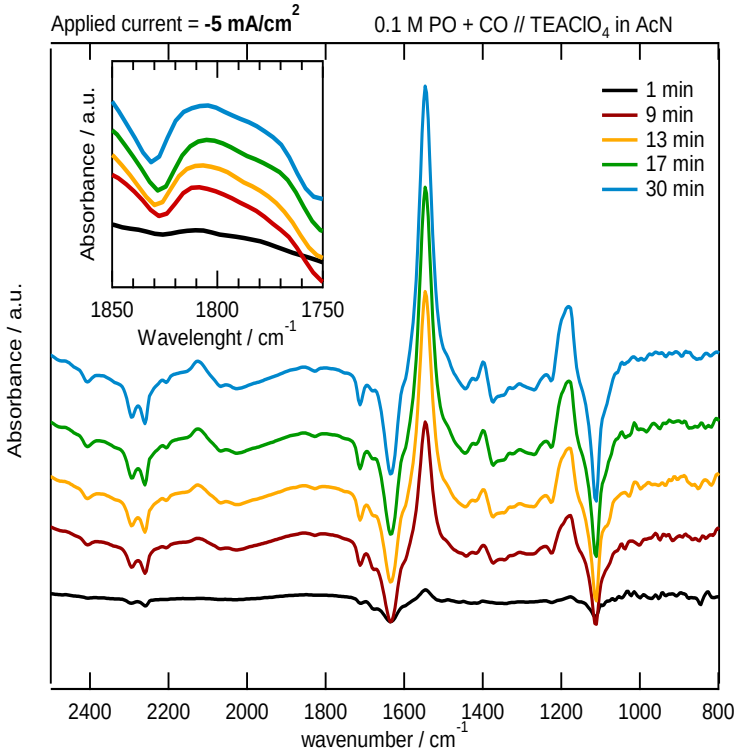

Figure 6.7: Time dependent absorbance spectra of copper in the presence of 0.1 M propylene oxide and saturated carbon monoxide atmosphere in 0.1M $TEAClO_4$ in acetonitrile solution at -5 mA/cm² after 1 minute (black), 9 minutes (red), 13 minutes (yellow), 17 minutes (green) and 30 minutes (blue). Insert displays zoom-in of the region of the spectra between 1850-1750 cm^{-1}.

Fig.6.3 at longer electrolysis times appears to be mirrored by the increase of the intensity of the band at 2333 cm^{-1} corresponding to the C=O stretching mode of CO_2, which is no longer being reduced to (bi)carbonates.

Due to the low solubility of $TEAHCO_3$ in acetonitrile, (bi)carbonates were also generated in situ by reduction of CO_2 on copper. After 30 minutes of electrolysis at saturated carbon dioxide atmosphere at -2.5 V vs $Ag/AgClO_4$ with the subsequent generation of (bi)carbonates,

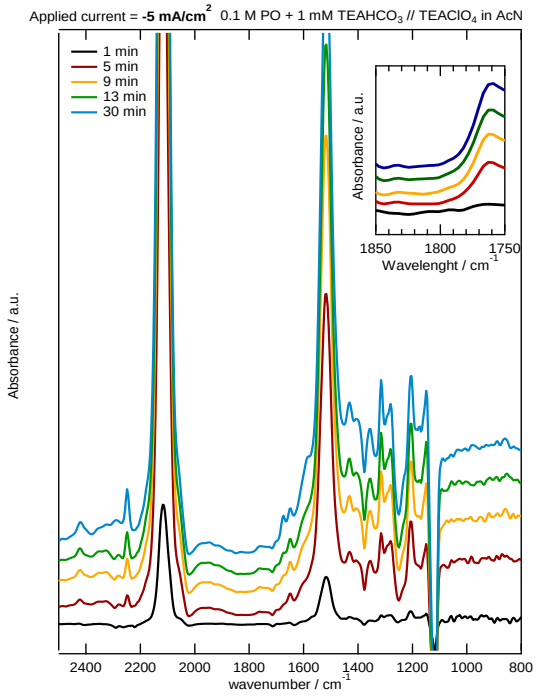

Figure 6.8: Time dependent absorbance spectra of copper in the presence of 0.1 M propylene oxide and 0.01 M $TEAHCO_3$ in 0.1M $TEAClO_4$ in acetonitrile solution at -5 mA/cm^2 after 1 minute (black), 9 minutes (red), 13 minutes (yellow), 17 minutes (green) and 30 minutes (blue). Insert displays zoom-in of the region of the spectra between 1850-1750 cm^{-1}.

propylene oxide was added to the electrochemical cell, and a current density of -5 mA/cm^2 was applied, recording the spectra every 4 minutes (data not shown). In situ generated (bi)carbonates also do not generate the vibrational band characteristic for propylene carbonate at 1800 cm^{-1}. Therefore, we exclude (bi)carbonates as the electroactive species for the formation of propylene carbonate on copper electrodes.

Homogeneous catalysis studies concerning the synthesis of propylene carbonate have proposed the activation of propylene oxide[74, 170] as the rate determining step, in which the catalyst induces a nucleophilic attack on the non-substituted carbon of the epoxide causing the opening

of the ring. Foltran et al. proposed three possible reaction pathways[74]: (1) Catalyst and CO_2 acts simultaneously on the epoxide, (2) Catalyst activates the epoxide before addition of CO_2 and (3) Activation of CO_2 by the catalyst occurs before the activation of the epoxide. Reaction path 1 and 2 were structurally and energetically investigated by Foltran and co-workers using density functional theory (DFT) [74], from which they selected path 2, in which the catalyst activates the epoxide by ring opening before the addition of CO_2 as the most preferable pathway. Path 3, in which the activation of CO_2 by the catalyst occurs before the addition of the epoxide was not investigated due to the high energy needed to activate CO_2.

The activation of propylene oxide as a required step for the synthesis of propylene carbonate on copper electrodes was evaluated in the experiment illustrated in Fig 6.9, which shows time-dependent absorbance spectra at different conditions. First, absorbance spectra were recorded after propylene oxide was reduced at -5 mA/cm^2 for 30 minutes (black line). This first conditioning step was expected to activate the epoxide and thus lead to opening of the ring. The next step was to introduce CO_2 in the electrochemical cell (at a current density of -1 mA/cm^2 at which no propylene carbonate was observed in previous experiments) and spectra was recorded every 4 minutes for 45 minutes (red and yellow lines). If the activated propylene oxide would indeed be the active species, propylene carbonate should form after the addition of CO_2. However, the absence of the band at 1800 cm^{-1} when a mild reduction current was applied with CO_2 present in solution, suggests that CO_2 needs to be activated. Indeed, when in the presence of CO_2 and propylene oxide a higher current is applied (-5mA/cm^2) it results in the formation of propylene carbonate (green line). These experimental results suggest that under electrochemical conditions the reaction pathway starts with the activation of CO_2 by the electrode before the activation of the epoxide, in agreement with the conclusion of Wang et al.[81]. In addition, no evidence of any substance coming from an opening of the epoxide ring prior to the formation of PC has been observed by FTIR (the band at 1731 cm^{-1} does not appear to correspond to a ring-

opening product). Therefore, we suggest the electroreduction of CO_2 to $CO_2^{\bullet-}$ as a key step for the formation of propylene carbonate, in accordance with the work of Xiao et al. and Wang et al.[81, 84]. However, the observation of the CO_2 radical anion as an intermediate of the reaction is not easily confirmed by FTIR due to its short lifetime.

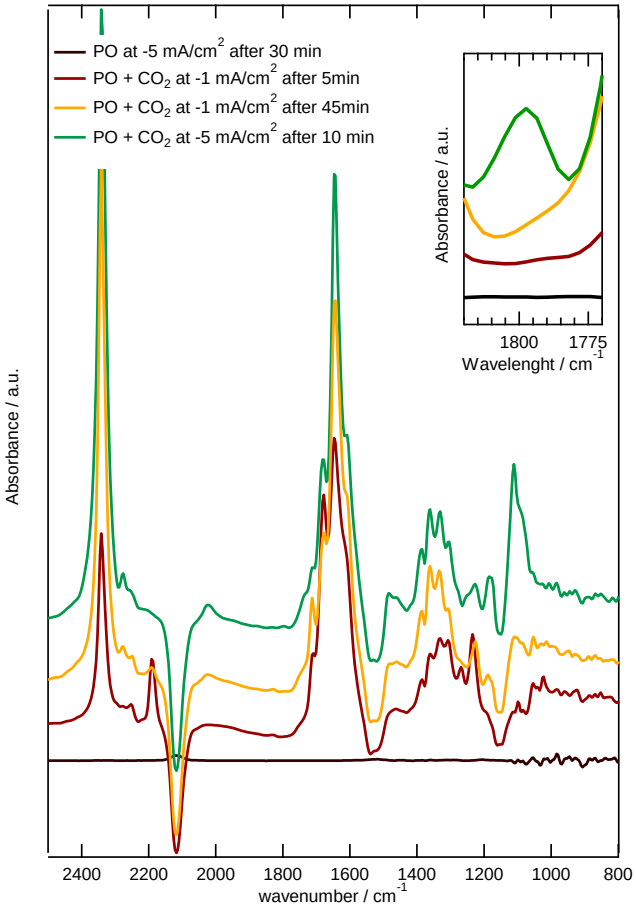

Figure 6.9: Time- and current-dependent absorbance spectra of a copper electrode in the presence of propylene oxide at -5 mA/cm² after 30 minutes (black), in the presence of propylene oxide and carbon dioxide at -1 mA/cm² after 5 minutes (red) and after 45 minutes (yellow) and in the presence of propylene oxide and carbon monoxide at -5 mA/cm² after 10 minutes (green). The inset displays the zoom-in of the region between 1900 - 1750 cm^{-1}.

6.3.3 Electrosynthesis of propylene carbonate on other metals

In the interest of understanding whether the process of propylene carbonate formation is an electrocatalytic reaction or simply a electrochemical process with no strong effect of the electrode material used, Au and Pt were tested as cathodes for the electrochemical conversion of propylene oxide and CO_2 to propylene carbonate.

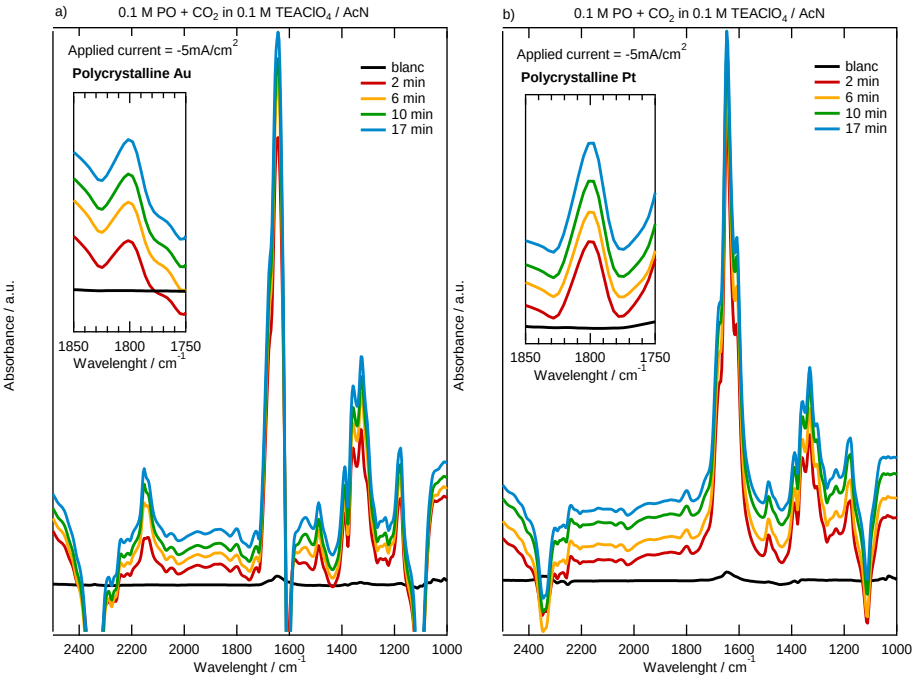

Figure 6.10: Time-dependent absorbance spectra for a) Au and b) Pt in the presence of 0.1 M propylene oxide and saturated carbon dioxide atmosphere in 0.1M $TEAClO_4$ in acetonitrile solution at -5 mA/cm^2 . Inserts display the zoom-in of the region of the spectra between 1900 and 1700 cm^{-1}.

Fig.6.10 shows the time-dependent absorbance spectra for gold (Fig.6.10a) and for platinum (Fig.6.10b) in 0.1M $TEAClO_4$, in the presence of 0.1 M PO and CO_2 atmosphere, in acetonitrile solution at an applied current of -5mA/cm^2. The attribution of the bands observed are

summarized in Table 6.1. On both electrode materials, a band at 1800cm^{-1} corresponding to the C=O stretching mode of propylene carbonate is observed. The results suggest that the reaction is electrochemical but it is not sensitive to the cathode material. Previous studies have reported the synthesis of propylene carbonate on other materials such as stainless steel[84] and nickel[81], in agreement with the non-electrocatalytic character of this reaction.

6.4 Conclusion

The electrosynthesis of propylene carbonate from propylene oxide and carbon dioxide on copper electrodes in $TEAClO_4$ in acetonitrile solutions has been investigated by cyclic voltammetry, FTIR and HPLC. The cyclic voltammogram of copper in the presence of propylene oxide and carbon dioxide shows a reduction current attributed to the formation of propylene carbonate. The formation of propylene carbonate was confirmed by FTIR spectroscopy and HPLC, showing the expected increased product formation at longer times and higher currents. The reaction between propylene oxide and carbon dioxide is an electrochemical reaction, initiated by the activation of CO_2 to CO_2^{-}. Both CO and carbonates were ruled out as intermediates for propylene carbonate synthesis on copper due to the absence of the formation of the cyclic carbonate. Base catalysis was also ruled as a possible mechanism. Moreover, the need of propylene oxide activation via ring opening before the further attack of CO_2 was ruled out since no product was detected if a current was not applied in presence of "activated propylene oxide" and CO_2. Therefore, we suggest that the key step in the synthesis of propylene carbonate is the activation of CO_2 by forming the radical anion $CO_2^{\cdot-}$, which will attack the epoxide to form propylene carbonate. The formation of propylene carbonate also occurs on other metals such as gold and platinum, giving evidence for the non-electrocatalytic nature of the reaction.

Summary

Heterogeneous catalysis is of paramount importance in industrial processes such as the formation of ammonia, the formation of syngas, the catalytic cracking of oil, the formation of sulfuric acid and the formation of nitric acid, among many others. However, these processes require high temperature and pressure to achieve an efficient conversion. In addition, some of these processes lead to undesirable side products which can be environmentally damaging or can affect the catalyst, deteriorating it and thus leading to rapid efficiency loss.

A reasonable alternative for high-temperature industrial processes would be the use of electrocatalysis, which presents several advantages over conventional catalysis. First of all, electrons as reducing/oxidant agents contribute to cleaner processes. Secondly, the use of mild process conditions such as lower temperatures and pressures potentially leads to a higher stability of the starting material or products. Moreover, since the product distribution depends on the applied potential, controlling the potential would in principle allow for the selective formation of the aimed products avoiding harmful and/or undesired by-products. However, the electrochemical synthesis of chemicals is not widespread in industry. The reasons for this limited use of electrochemical techniques can be attributed to a lack of electrochemistry education, a lack of resources for the construction of electrochemical cells and especially to the high costs of electricity and electrochemical cells. The high energy input can be overcome by the use of cheap and abundant catalysts and electricity from renewable sources. Nevertheless, an efficient process must be developed before it has an industrial application. For this purpose, an exhaustive study of the electrochemical reaction must be performed first, in order to understand and control all the different parameters that affect the reaction, its product distribution, selectivity and efficiency.

In this thesis, we have discussed several parameters that affect the electrochemical conversion of environmentally harmful molecules such as nitrates and carbon dioxide to more valuable and less deleterious compounds, in order to cast light onto the mechanism of the reaction to achieve an efficient and selective system.

This thesis is divided in two main parts, the reduction of nitrates (chapter 2) and the mechanistic study of CO_2 conversion to different products such as ethanol (chapter 3), ethylene (chapter 4 and 5) and propylene carbonate (chapter 6).

Numerous previous works have studied the difference in product distribution during the reduction of nitrate on several metals and at several pH's. In chapter 2 of this thesis, we studied the electrocatalytic reduction of nitrate on copper electrodes. The influence of the electrode surface morphology was studied by employing two different copper single crystals, namely Cu(100) and Cu(111). In addition, the experiments were performed in acidic and in alkaline media, providing then a study of the influence of the pH in this reaction. The experiments have shown that the product distribution varies depending on the pH of the electrolyte. While in acidic media the products formed are NO and ammonia, in alkaline media the main product is hydroxylamine. In addition, the reduction of nitrate is structure sensitive only in basic media, with the formation of hydroxylamine favoured on Cu(100).

On the other hand, the electrochemical reduction of carbon dioxide has received considerable attention in the last decades due to the capability of copper to convert CO_2 into fuels such as methane, ethylene and ethanol. Although this process was discovered in the 1980's, the mechanism of the reaction is still under debate.

The reduction of carbon dioxide on copper has ethylene as its main C2 product. Nevertheless, trace amounts of ethanol and acetaldehyde have been also observed. Since acetaldehyde has been confirmed as an intermediary for ethanol formation during the reduction of carbon monoxide, in chapter 3 we discuss the mechanistic implications of

acetaldehyde reduction to ethanol during CO_2 reduction. It is believed that these three compounds share a common intermediate at the early stages of CO_2 reduction. However, the pathway for ethylene and ethanol formation must bifurcate at later stages of the reaction. Our results have shown that the selectivity-determining intermediate is the product of the fifth protonation (CH_2CHO^*). The protonation of this intermediate favours ethanol formation on undercordinated sites. In contrast, square symmetry sites favour the formation of ethylene. Despite the higher energetic barriers found for ethanol compared to ethylene, the selectivity for ethanol can be increased by making use of the structure selectivity of the reaction.

Another interesting step in the mechanism of CO_2 reduction is related to the formation of ethylene. The only intermediate experimentally confirmed during the reduction of CO_2 to ethylene has been CO. Computational studies have hypothesized that the C-C bond formation in the ethylene pathway occurs via a reductive dimerization step and further hydrogenation. In chapter 4 we provided spectroscopic evidence for the formation of a CO hydrogenated intermediate (OCCOH) in the ethylene pathway. The formation of this intermediate has been confirmed to be structure sensitive, being favourable mostly on square symmetry sites.

Several factors such as the pH of the electrolyte, the chemical nature of cations or anions and the morphology of the electrode surface have been previously studied for the reduction of CO_2. All these parameters lead to significant changes in product distribution, selectivity and conversion rate. In chapter 5 we analyse the combined effect of electrode morphology, alkaline cation size and applied potential during CO reduction. In general, larger cations enhance the formation of ethylene at potentials more positive than -0.45V, whereas larger cations enhance the formation of methane at more negative potentials. We suggested that the ethylene pathway shuts down by the enhancement of the methane pathway, this correlation also being dependent on the cation size. Larger cations enhance the ethylene selectivity over a wider

potential range. We suggested that the cations act as catalytic promoters stabilizing intermediates with a favourable electrostatic interaction with the cation. In addition, the formation of the CO hydrogenated dimer explained in chapter 4 (OCCOH) has been found to be dependent on the cation size. Whereas the hydrogenated dimer is observable in FTIR when Li^+, Na^+ and K^+ are present, it is not observable in the presence of Rb^+ or Cs^+. DFT calculations describe the formation of *OCCOH as less favourable in presence of larger cations compared to smaller cations.

Finally, we studied in chapter 6 the conversion of carbon dioxide into larger organic molecules, specifically into cyclic carbonates. We analyzed the mechanism of the formation of propylene carbonate from carbon dioxide and propylene oxide on copper electrodes. We excluded carbon monoxide and (bi)carbonate as possible carboxylation agents. Moreover, we discarded the activation of propylene oxide via ring opening as the key step for this reaction. Our experiments suggest that the electrochemical reaction is initiated by the activation of CO_2 to $CO_2^{\cdot-}$, which attacks propylene oxide to ultimately form propylene carbonate.

In general terms, this thesis has stressed the importance of exhaustive mechanistic studies in order to gain knowledge of all the steps involved in an electrochemical reaction. The understanding of how different factors affect the selectivity and conversion towards a certain product can help in achieving more efficient processes, which can be steered to the formation of desired products by adjusting different parameters involved in the reaction.

References

1. Zumft, W. G., Cell biology and molecular basis of denitrification. *Microbiology and molecular biology reviews* **1997,** *61* (4), 533-616.
2. O'Brien, T. F.; Bommaraju, T. V.; Hine, F., *Handbook of Chlor-Alkali Technology: Volume I: Fundamentals, Volume II: Brine Treatment and Cell Operation, Volume III: Facility Design and Product Handling, Volume IV: Operations, Volume V: Corrosion, Environmental Issues, and Future Developments*. Springer Science & Business Media: 2007; Vol. 1.
3. Gluszcz, P.; Fürch, K.; Ledakowicz, S., Mercury in the chlor-alkali electrolysis industry. In *Bioremediation of Mercury: Current Research and Industrial Applications*, Caister Academic Press Norfolk, UK: 2013; pp 97-118.
4. Grjotheim, K.; Krohn, C.; Malinovsky, M.; Matiasovsky, K.; Thonstad, J., Aluminium electrolysis. Fundamentals of hall-Heroult process. 2-nd edition. *J. Thonstad. Düsseldorf: Aluminium-Verlag* **1982**.
5. Sequeira, C.; Santos, D., Electrochemical routes for industrial synthesis. *Journal of the Brazilian Chemical Society* **2009,** *20* (3), 387-406.
6. Beck, F., Electrosynthesis of adiponitrile in undivided cells. *J. Appl. Electrochem.* **1972,** *2* (1), 59-69.
7. Ding, H.; DeRoy, P. L.; Perreault, C.; Larivée, A.; Siddiqui, A.; Caldwell, C. G.; Harran, S.; Harran, P. G., Electrolytic Macrocyclizations: Scalable Synthesis of a Diazonamide-Based Drug Development Candidate. *Angew. Chem. Int. Ed.* **2015,** *54* (16), 4818-4822.
8. Burgett, A. W.; Li, Q.; Wei, Q.; Harran, P. G., A Concise and Flexible Total Synthesis of (−) ‐ Diazonamide A. *Angew. Chem.* **2003,** *115* (40), 5111-5116.
9. Kita, Y.; Tohma, H.; Kikuchi, K.; Inagaki, M.; Yakura, T., Hypervalent iodine oxidation of N-acyltyramines: synthesis of quinol ethers, spirohexadienones, and hexahydroindol-6-ones. *The Journal of Organic Chemistry* **1991,** *56* (1), 435-438.
10. Martínez-Huitle, C. A.; Rodrigo, M. A.; Sirés, I.; Scialdone, O., Single and Coupled Electrochemical Processes and Reactors for the Abatement of Organic Water Pollutants: A Critical Review. *Chem. Rev.* **2015,** *115* (24), 13362-13407.
11. Ghernaout, D.; Naceur, M. W.; Aouabed, A., On the dependence of chlorine by-products generated species formation of the electrode material

and applied charge during electrochemical water treatment. *Desalination* **2011,** *270* (1), 9-22.
12. Moorcroft, M. J.; Davis, J.; Compton, R. G., Detection and determination of nitrate and nitrite: a review. *Talanta* **2001,** *54* (5), 785-803.
13. Reyter, D.; Chamoulaud, G.; Bélanger, D.; Roué, L., Electrocatalytic reduction of nitrate on copper electrodes prepared by high-energy ball milling. *J. Electroanal. Chem.* **2006,** *596* (1), 13-24.
14. Carpenter, S. R.; Caraco, N. F.; Correll, D. L.; Howarth, R. W.; Sharpley, A. N.; Smith, V. H., Nonpoint pollution of surface waters with phosphorus and nitrogen. *Ecological applications* **1998,** *8* (3), 559-568.
15. Lee, Y. W.; Dahab, M. F.; Bogardi, I., Nitrate risk management under uncertainty. *Journal of Water Resources Planning and Management* **1992,** *118* (2), 151-165.
16. Galloway, J. N.; Schlesinger, W. H.; Levy, H.; Michaels, A.; Schnoor, J. L., Nitrogen fixation: Anthropogenic enhancement-environmental response. *Global Biogeochemical Cycles* **1995,** *9* (2), 235-252.
17. Adam, J., Health aspects of nitrate in drinking-water and possible means of denitrification (literature review). *Water SA* **1980,** *6* (2), 79-89.
18. Wakida, F. T.; Lerner, D. N., Non-agricultural sources of groundwater nitrate: a review and case study. *Water research* **2005,** *39* (1), 3-16.
19. Mani, K., Electrodialysis water splitting technology. *Journal of membrane science* **1991,** *58* (2), 117-138.
20. Panyor, L.; Fabiani, C., Anion rejection in a nitrate highly rejecting reverse osmosis thin-film composite membrane. *Desalination* **1996,** *104* (3), 165-174.
21. Schoeman, J.; Steyn, A., Nitrate removal with reverse osmosis in a rural area in South Africa. *Desalination* **2003,** *155* (1), 15-26.
22. Matějů, V.; Čižinská, S.; Krejčí, J.; Janoch, T., Biological water denitrification—a review. *Enzyme and Microbial Technology* **1992,** *14* (3), 170-183.
23. Duca, M.; Koper, M. T., Powering denitrification: the perspectives of electrocatalytic nitrate reduction. *Energy Environ. Sci.* **2012,** *5* (12), 9726-9742.
24. Rosca, V.; Duca, M.; de Groot, M. T.; Koper, M. T., Nitrogen cycle electrocatalysis. *Chem. Rev.* **2009,** *109* (6), 2209-2244.
25. Da Cunha, M.; De Souza, J.; Nart, F., Reaction Pathways for Reduction of Nitrate Ions on Platinum, Rhodium, and Platinum− Rhodium Alloy Electrodes. *Langmuir* **2000,** *16* (2), 771-777.

26. De Groot, M.; Koper, M., The influence of nitrate concentration and acidity on the electrocatalytic reduction of nitrate on platinum. *J. Electroanal. Chem.* **2004,** *562* (1), 81-94.
27. Tucker, P. M.; Waite, M. J.; Hayden, B. E., Electrocatalytic reduction of nitrate on activated rhodium electrode surfaces. *J. Appl. Electrochem.* **2004,** *34* (8), 781-796.
28. Li, M.; Feng, C.; Zhang, Z.; Sugiura, N., Efficient electrochemical reduction of nitrate to nitrogen using Ti/IrO 2–Pt anode and different cathodes. *Electrochim. Acta* **2009,** *54* (20), 4600-4606.
29. Pletcher, D.; Poorabedi, Z., The reduction of nitrate at a copper cathode in aqueous acid. *Electrochim. Acta* **1979,** *24* (12), 1253-1256.
30. Dima, G.; Beltramo, G.; Koper, M., Nitrate reduction on single-crystal platinum electrodes. *Electrochim. Acta* **2005,** *50* (21), 4318-4326.
31. Taguchi, S.; Feliu, J. M., Electrochemical reduction of nitrate on Pt (S)[n (111)×(111)] electrodes in perchloric acid solution. *Electrochim. Acta* **2007,** *52* (19), 6023-6033.
32. Dima, G.; De Vooys, A.; Koper, M., Electrocatalytic reduction of nitrate at low concentration on coinage and transition-metal electrodes in acid solutions. *J. Electroanal. Chem.* **2003,** *554*, 15-23.
33. Yang, J.; Sebastian, P.; Duca, M.; Hoogenboom, T.; Koper, M. T., pH dependence of the electroreduction of nitrate on Rh and Pt polycrystalline electrodes. *Chemical Communications* **2014,** *50* (17), 2148-2151.
34. Brylev, O.; Sarrazin, M.; Bélanger, D.; Roué, L., Rhodium deposits on pyrolytic graphite substrate: Physico-chemical properties and electrocatalytic activity towards nitrate reduction in neutral medium. *Appl. Catal. B* **2006,** *64* (3), 243-253.
35. Duca, M.; van der Klugt, B.; Koper, M., Electrocatalytic reduction of nitrite on transition and coinage metals. *Electrochim. Acta* **2012,** *68*, 32-43.
36. Badea, G. E., Electrocatalytic reduction of nitrate on copper electrode in alkaline solution. *Electrochim. Acta* **2009,** *54* (3), 996-1001.
37. Reyter, D.; Bélanger, D.; Roué, L., Study of the electroreduction of nitrate on copper in alkaline solution. *Electrochim. Acta* **2008,** *53* (20), 5977-5984.
38. Bouzek, K.; Paidar, M.; Sadilkova, A.; Bergmann, H., Electrochemical reduction of nitrate in weakly alkaline solutions. *J. Appl. Electrochem.* **2001,** *31* (11), 1185-1193.
39. Yang, H.; Xu, Z.; Fan, M.; Gupta, R.; Slimane, R. B.; Bland, A. E.; Wright, I., Progress in carbon dioxide separation and capture: A review. *Journal of environmental sciences* **2008,** *20* (1), 14-27.

40. Yamasaki, A., An overview of CO2 mitigation options for global warming—emphasizing CO2 sequestration options. *Journal of Chemical Engineering of Japan* **2003,** *36* (4), 361-375.
41. Huijgen, W. J. J.; Comans, R. N. J. *Carbon dioxide sequestration by mineral carbonation. Literature Review*; Energy research Centre of the Netherlands ECN: 2003.
42. Hori, Y.; Kikuchi, K.; Suzuki, S., Production of CO and CH4 in electrochemical reduction of CO2 at metal electrodes in aqueous hydrogencarbonate solution. *Chem. Lett.* **1985,** *14* (11), 1695-1698.
43. Noda, H.; Ikeda, S.; Oda, Y.; Imai, K.; Maeda, M.; Ito, K., Electrochemical reduction of carbon dioxide at various metal electrodes in aqueous potassium hydrogen carbonate solution. *Bull. Chem. Soc. Jpn.* **1990,** *63* (9), 2459-2462.
44. Hansen, H.; Varley, J.; Peterson, A.; Norskov, J.; Nørskov, J., Understanding Trends in the Electrocatalytic Activity of Metals and Enzymes for CO2Reduction to CO. *J. Phys. Chem. Lett.* **2013,** *4* (3), 388-392.
45. Sullivan, B. P.; Krist, K.; Guard, H., *Electrochemical and electrocatalytic reactions of carbon dioxide*. Elsevier: 2012.
46. Summers, D. P.; Leach, S.; Frese, K. W., The electrochemical reduction of aqueous carbon dioxide to methanol at molybdenum electrodes with low overpotentials. *J. Electroanal. Chem. Interfacial Electrochem.* **1986,** *205* (1-2), 219-232.
47. Hori, Y.; Takahashi, I.; Koga, O.; Hoshi, N., Selective formation of C2 compounds from electrochemical reduction of CO2 at a series of copper single crystal electrodes. *J. Phys. Chem. B* **2002,** *106* (1), 15-17.
48. Li, C. W.; Ciston, J.; Kanan, M. W., Electroreduction of carbon monoxide to liquid fuel on oxide-derived nanocrystalline copper. *Nature* **2014,** *508* (7497), 504-507.
49. Gattrell, M.; Gupta, N.; Co, A., A review of the aqueous electrochemical reduction of CO 2 to hydrocarbons at copper. *J. Electroanal. Chem.* **2006,** *594* (1), 1-19.
50. Kuhl, K. P.; Cave, E. R.; Abram, D. N.; Jaramillo, T. F., New insights into the electrochemical reduction of carbon dioxide on metallic copper surfaces. *Energy Environ. Sci.* **2012,** *5* (5), 7050-7059.
51. Schouten, K.; Kwon, Y.; Van der Ham, C.; Qin, Z.; Koper, M., A new mechanism for the selectivity to C 1 and C 2 species in the electrochemical reduction of carbon dioxide on copper electrodes. *Chem. Sci.* **2011,** *2* (10), 1902-1909.

52. Kortlever, R.; Shen, J.; Schouten, K. J. P.; Calle-Vallejo, F.; Koper, M. T., Catalysts and reaction pathways for the electrochemical reduction of carbon dioxide. *J. Phys. Chem. Lett.* **2015,** *6* (20), 4073-4082.
53. Calle‐Vallejo, F.; Koper, M., Theoretical considerations on the electroreduction of CO to C2 species on Cu (100) electrodes. *Angew. Chem. Int. Ed.* **2013,** *52* (28), 7282-7285.
54. Li, H.; Li, Y.; Koper, M. T.; Calle-Vallejo, F., Bond-making and breaking between carbon, nitrogen, and oxygen in electrocatalysis. *J. Am. Chem. Soc.* **2014,** *136* (44), 15694-15701.
55. Verdaguer-Casadevall, A.; Li, C. W.; Johansson, T. P.; Scott, S. B.; McKeown, J. T.; Kumar, M.; Stephens, I. E.; Kanan, M. W.; Chorkendorff, I., Probing the active surface sites for CO reduction on oxide-derived copper electrocatalysts. *J. Am. Chem. Soc.* **2015,** *137* (31), 9808-9811.
56. Varela, A. S.; Ju, W.; Reier, T.; Strasser, P., Tuning the Catalytic Activity and Selectivity of Cu for CO2 Electroreduction in the Presence of Halides. *ACS Catal.* **2016,** *6* (4), 2136-2144.
57. Peterson, A. A.; Abild-Pedersen, F.; Studt, F.; Rossmeisl, J.; Nørskov, J. K., How copper catalyzes the electroreduction of carbon dioxide into hydrocarbon fuels. *Energy Environ. Sci.* **2010,** *3* (9), 1311-1315.
58. Montoya, J. H.; Shi, C.; Chan, K.; Nørskov, J. K., Theoretical Insights into a CO Dimerization Mechanism in CO2 Electroreduction. *J. Phys. Chem. Lett.* **2015,** *6* (11), 2032-2037.
59. Schouten, K. J. P.; Qin, Z.; Gallent, E. P.; Koper, M. T. M., Two Pathways for the Formation of Ethylene in CO Reduction on Single-Crystal Copper Electrodes. *J. Am. Chem. Soc.* **2012,** *134* (24), 9864-9867.
60. Hori, Y.; Wakebe, H.; Tsukamoto, T.; Koga, O., Electrocatalytic process of CO selectivity in electrochemical reduction of CO2 at metal electrodes in aqueous media. *Electrochim. Acta* **1994,** *39* (11–12), 1833-1839.
61. Hori, Y.; Takahashi, R.; Yoshinami, Y.; Murata, A., Electrochemical reduction of CO at a copper electrode. *J. Phys. Chem. B* **1997,** *101* (36), 7075-7081.
62. Hori, Y.; Murata, A.; Takahashi, R.; Suzuki, S., Electroreduction of CO to CH/sub 4/and C/sub 2/H/sub 4/at a copper electrode in aqueous solutions at ambient temperature and pressure. *J. Am. Chem. Soc.;(United States)* **1987,** *109* (16).
63. Schouten, K. J. P.; Gallent, E. P.; Koper, M. T., The influence of pH on the reduction of CO and CO2 to hydrocarbons on copper electrodes. *J. Electroanal. Chem.* **2014,** *716*, 53-57.

64. Schouten, K. J. P.; Pérez Gallent, E.; Koper, M. T., Structure sensitivity of the electrochemical reduction of carbon monoxide on copper single crystals. *ACS Catal.* **2013,** *3* (6), 1292-1295.
65. Murata, A.; Hori, Y., Product selectivity affected by cationic species in electrochemical reduction of CO2 and CO at a Cu electrode. *Bull. Chem. Soc. Jpn.* **1991,** *64* (1), 123-127.
66. Kas, R.; Kortlever, R.; Milbrat, A.; Koper, M. T.; Mul, G.; Baltrusaitis, J., Electrochemical CO 2 reduction on Cu 2 O-derived copper nanoparticles: controlling the catalytic selectivity of hydrocarbons. *Phys. Chem. Chem. Phys.* **2014,** *16* (24), 12194-12201.
67. Christophe, J.; Doneux, T.; Buess Herman, C., Electroreduction of Carbon Dioxide on Copper-Based Electrodes: Activity of Copper Single Crystals and Copper–Gold Alloys. *Electrocatalysis* **2012,** *3* (2), 139-146.
68. Angamuthu, R.; Byers, P.; Lutz, M.; Spek, A. L.; Bouwman, E., Electrocatalytic CO2 conversion to oxalate by a copper complex. *Science* **2010,** *327* (5963), 313-315.
69. Tundo, P.; Selva, M., The chemistry of dimethyl carbonate. *Acc. Chem. Res.* **2002,** *35* (9), 706-716.
70. Sakakura, T.; Choi, J.-C.; Yasuda, H., Transformation of carbon dioxide. *Chem. Rev* **2007,** *107* (6), 2365-2387.
71. Evison, D.; Hinsley, D.; Rice, P., Chemical weapons. *BMJ : British Medical Journal* **2002,** *324* (7333), 332-335.
72. North, M.; Pasquale, R., Mechanism of cyclic carbonate synthesis from epoxides and CO2. *Angew. Chem.* **2009,** *121* (16), 2990-2992.
73. Korosteleva, I.; Markova, N.; Kolesnichenko, N.; Ezhova, N.; Khadzhiev, S.; Trukhmanova, N., Catalytic synthesis of propylene carbonate from propylene oxide and carbon dioxide in the presence of rhodium complexes modified with organophosphorus ligands and chitosan. *Petroleum Chemistry* **2013,** *53* (6), 412-417.
74. Foltran, S.; Mereau, R.; Tassaing, T., Theoretical study on the chemical fixation of carbon dioxide with propylene oxide catalyzed by ammonium and guanidinium salts. *Catal. Sci. Technol.* **2014,** *4* (6), 1585-1597.
75. Baiker, A., Utilization of carbon dioxide in heterogeneous catalytic synthesis². **2000**.
76. Darensbourg, D. J.; Holtcamp, M. W., Catalysts for the reactions of epoxides and carbon dioxide. *Coordination Chemistry Reviews* **1996,** *153*, 155-174.
77. Shaikh, A.-A. G.; Sivaram, S., Organic carbonates. *Chem. Rev.* **1996,** *96* (3), 951-976.

78. Yang, H.; Gu, Y.; Deng, Y.; Shi, F., Electrochemical activation of carbon dioxide in ionic liquid: synthesis of cyclic carbonates at mild reaction conditions. *Chemical Communications* **2002,** (3), 274-275.
79. Buckley, B. R.; Patel, A. P.; Wijayantha, K. U., Electrosynthesis of cyclic carbonates from epoxides and atmospheric pressure carbon dioxide. *Chemical Communications* **2011,** *47* (43), 11888-11890.
80. Wu, L.; Yang, H.; Wang, H.; Lu, J., Electrosynthesis of cyclic carbonates from CO 2 and epoxides on a reusable copper nanoparticle cathode. *RSC Adv.* **2015,** *5* (30), 23189-23192.
81. Wang, H.; Wu, L.-X.; Lan, Y.-C.; Zhao, J.-Q.; Lu, J.-X., Electrosynthesis of cyclic carbonates from CO2 and diols in ionic liquids under mild conditions. *Int. J. Electrochem. Sci* **2011,** *6*, 4218-4227.
82. Kihara, N.; Nakawaki, Y.; Endo, T., Preparation of 1, 3-oxathiolane-2-thiones by the reaction of oxirane and carbon disulfide. *The Journal of Organic Chemistry* **1995,** *60* (2), 473-475.
83. Calo, V.; Nacci, A.; Monopoli, A.; Fanizzi, A., Cyclic carbonate formation from carbon dioxide and oxiranes in tetrabutylammonium halides as solvents and catalysts. *Organic letters* **2002,** *4* (15), 2561-2563.
84. Xiao, Y.; Chen, B.-L.; Yang, H.-P.; Wang, H.; Lu, J.-X., Electrosynthesis of enantiomerically pure cyclic carbonates from CO 2 and chiral epoxides. *Electrochem. Commun.* **2014,** *43*, 71-74.
85. Schmitz, C., The Rise of Big Business in the World Copper Industry 1870-1930. *The Economic History Review* **1986,** *39* (3), 392-410.
86. Hori, Y.; Kikuchi, K.; Murata, A.; Suzuki, S., Production of methane and ethylene in electrochemical reduction of carbon dioxide at copper electrode in aqueous hydrogencarbonate solution. *Chem. Lett.* **1986,** *15* (6), 897-898.
87. Vitousek, P. M.; Howarth, R. W., Nitrogen Limitation on Land and in the Sea: How Can It Occur? *Biogeochemistry* **1991,** *13* (2), 87-115.
88. Galloway, J. N.; Townsend, A. R.; Erisman, J. W.; Bekunda, M.; Cai, Z.; Freney, J. R.; Martinelli, L. A.; Seitzinger, S. P.; Sutton, M. A., Transformation of the Nitrogen Cycle: Recent Trends, Questions, and Potential Solutions. *Science* **2008,** *320* (5878), 889-892.
89. Duca, M.; Kavvadia, V.; Rodriguez, P.; Lai, S. C. S.; Hoogenboom, T.; Koper, M. T. M., New insights into the mechanism of nitrite reduction on a platinum electrode. *J. Electroanal. Chem.* **2010,** *649* (1–2), 59-68.
90. Bae, S.-E.; Gewirth, A. A., Differential reactivity of Cu (111) and Cu (100) during nitrate reduction in acid electrolyte. *Faraday Discuss.* **2009,** *140*, 113-123.

91. Schouten, K. J. P.; Gallent, E. P.; Koper, M. T., The electrochemical characterization of copper single-crystal electrodes in alkaline media. *J. Electroanal. Chem.* **2013,** *699*, 6-9.
92. Wonders, A. H.; Housmans, T. H. M.; Rosca, V.; Koper, M. T. M., On-line mass spectrometry system for measurements at single-crystal electrodes in hanging meniscus configuration. *J. Appl. Electrochem.* **2006,** *36* (11), 1215-1221.
93. Yang, J.; Kwon, Y.; Duca, M.; Koper, M. T., Combining Voltammetry and Ion Chromatography: Application to the Selective Reduction of Nitrate on Pt and PtSn Electrodes. *Analytical chemistry* **2013,** *85* (16), 7645-7649.
94. Figueiredo, M. C.; Souza-Garcia, J.; Climent, V.; Feliu, J. M., Nitrate reduction on Pt (111) surfaces modified by Bi adatoms. *Electrochem. Commun.* **2009,** *11* (9), 1760-1763.
95. Bae, S.-E.; Stewart, K. L.; Gewirth, A. A., Nitrate adsorption and reduction on Cu (100) in acidic solution. *J. Am. Chem. Soc.* **2007,** *129* (33), 10171-10180.
96. Petrii, O. A.; Safonova, T. Y., Electroreduction of nitrate and nitrite anions on platinum metals: a model process for elucidating the nature of the passivation by hydrogen adsorption. *J. Electroanal. Chem.* **1992,** *331* (1), 897-912.
97. Horanyi, G.; Rizmayer, E., Role of adsorption phenomena in the electrocatalytic reduction of nitric acid at a platinized platinum electrode. *J. Electroanal. Chem. Interfacial Electrochem.* **1982,** *140* (2), 347-366.
98. Koper, M. T., Non-linear phenomena in electrochemical systems. *Journal of the Chemical Society, Faraday Transactions* **1998,** *94* (10), 1369-1378.
99. Rosca, V.; Beltramo, G. L.; Koper, M. T. M., Hydroxylamine electrochemistry at polycrystalline platinum in acidic media: a voltammetric, DEMS and FTIR study. *J. Electroanal. Chem.* **2004,** *566* (1), 53-62.
100. Rodes, A.; Gomez, R.; Orts, J.; Feliu, J.; Perez, J.; Aldaz, A., In situ FTIR spectroscopy characterization of the NO adlayers formed at platinum single crystal electrodes in contact with acidic solutions of nitrite. *Langmuir* **1995,** *11* (9), 3549-3553.
101. Hughes, M.; Nicklin, H.; Shrimanker, K., Autoxidation of hydroxylamine in alkaline solutions. Part II. Kinetics. The acid dissociation constant of hydroxylamine. *Journal of the Chemical Society A: Inorganic, Physical, Theoretical* **1971**, 3485-3487.

102. Dumas, P.; Suhren, M.; Chabal, Y.; Hirschmugl, C.; Williams, G., Adsorption and reactivity of NO on Cu (111): a synchrotron infrared reflection absorption spectroscopic study. *Surf. Sci.* **1997,** *371* (2), 200-212.
103. Kim, C.; Yi, C.-W.; Goodman, D., Adsorption and reaction of NO on Cu (100): an infrared reflection absorption spectroscopic study at 25 K. *J. Phys. Chem. B* **2002,** *106* (28), 7065-7068.
104. Santos, E.; Pötting, K.; Lundin, A.; Quaino, P.; Schmickler, W., Hydrogen Evolution on Single‐Crystal Copper and Silver: A Theoretical Study. *ChemPhysChem* **2010,** *11* (7), 1491-1495.
105. Gattrell, M.; Gupta, N.; Co, A., A review of the aqueous electrochemical reduction of CO2 to hydrocarbons at copper. *Journal of Electroanalytical Chemistry* **2006,** *594* (1), 1-19.
106. Hori, Y.; Murata, A.; Takahashi, R., Formation of hydrocarbons in the electrochemical reduction of carbon dioxide at a copper electrode in aqueous solution. *Journal of the Chemical Society, Faraday Transactions 1: Physical Chemistry in Condensed Phases* **1989,** *85* (8), 2309-2326.
107. Calle-Vallejo, F.; Koper, M. T. M., Theoretical Considerations on the Electroreduction of CO to C2 Species on Cu(100) Electrodes. *Angewandte Chemie International Edition* **2013,** *52* (28), 7282-7285.
108. Schouten, K. J. P.; Calle-Vallejo, F.; Koper, M. T. M., A Step Closer to the Electrochemical Production of Liquid Fuels. *Angewandte Chemie International Edition* **2014,** *53* (41), 10858-10860.
109. Schouten, K. J. P.; Kwon, Y.; van der Ham, C. J. M.; Qin, Z.; Koper, M. T. M., A new mechanism for the selectivity to C1 and C2 species in the electrochemical reduction of carbon dioxide on copper electrodes. *Chemical Science* **2011,** *2* (10), 1902.
110. P. Schouten, K. J.; Gallent, E. P.; Koper, M. T. M., The electrochemical characterization of copper single-crystal electrodes in alkaline media. *Journal of Electroanalytical Chemistry* **2013,** *699* (0), 6-9.
111. Kwon, Y.; Koper, M. T. M., Combining Voltammetry with HPLC: Application to Electro-Oxidation of Glycerol. *Analytical Chemistry* **2010,** *82* (13), 5420-5424.
112. Kresse, G.; Furthmüller, J., Efficient iterative schemes for ab initio total-energy calculations using a plane-wave basis set. *Physical Review B* **1996,** *54* (16), 11169-11186.
113. Perdew, J. P.; Burke, K.; Ernzerhof, M., Generalized Gradient Approximation Made Simple. *Physical Review Letters* **1996,** *77* (18), 3865-3868.

114. Kresse, G.; Joubert, D., From ultrasoft pseudopotentials to the projector augmented-wave method. *Physical Review B* **1999,** *59* (3), 1758-1775.
115. Monkhorst, H. J.; Pack, J. D., Special points for Brillouin-zone integrations. *Physical Review B* **1976,** *13* (12), 5188-5192.
116. Methfessel, M.; Paxton, A. T., High-precision sampling for Brillouin-zone integration in metals. *Physical Review B* **1989,** *40* (6), 3616-3621.
117. Lide, D. R., *CRC Handbook of Chemistry and Physics. ed. CD-ROM version*. 90th ed.; CRC Press/Taylor and Francis: Boca Raton, FL, 2010.
118. Calle-Vallejo, F.; Koper, M. T. M., First-principles computational electrochemistry: Achievements and challenges. *Electrochimica Acta* **2012,** *84*, 3-11.
119. Norskov, J. K.; Rossmeisl, J.; Logadottir, A.; Lindqvist, L.; Kitchin, J. R.; Bligaard, T.; Jonsson, H., Origin of the overpotential for oxygen reduction at a fuel-cell cathode. *Journal of Physical Chemistry B* **2004,** *108* (46), 17886-17892.
120. Peterson, A. A.; Abild-Pedersen, F.; Studt, F.; Rossmeisl, J.; Norskov, J. K., How copper catalyzes the electroreduction of carbon dioxide into hydrocarbon fuels. *Energy & Environmental Science* **2010,** *3* (9), 1311-1315.
121. Nørskov, J. K.; Rossmeisl, J.; Logadottir, A.; Lindqvist, L.; Kitchin, J. R.; Bligaard, T.; Jónsson, H., Origin of the Overpotential for Oxygen Reduction at a Fuel-Cell Cathode. *J. Phys. Chem. B* **2004,** *108* (46), 17886-17892.
122. Li, H.; Li, Y.; Koper, M. T. M.; Calle-Vallejo, F., Bond-Making and Breaking between Carbon, Nitrogen, and Oxygen in Electrocatalysis. *Journal of the American Chemical Society* **2014,** *136* (44), 15694-15701.
123. Calle-Vallejo, F.; Martínez, J. I.; García-Lastra, J. M.; Sautet, P.; Loffreda, D., Fast Prediction of Adsorption Properties for Platinum Nanocatalysts with Generalized Coordination Numbers. *Angewandte Chemie International Edition* **2014,** *53* (32), 8316-8319.
124. Calle-Vallejo, F.; Loffreda, D.; KoperMarc, T. M.; Sautet, P., Introducing structural sensitivity into adsorption–energy scaling relations by means of coordination numbers. *Nat Chem* **2015,** *7* (5), 403-410.
125. Calle-Vallejo, F.; Huang, M.; Henry, J. B.; Koper, M. T. M.; Bandarenka, A. S., Theoretical design and experimental implementation of Ag/Au electrodes for the electrochemical reduction of nitrate. *Physical Chemistry Chemical Physics* **2013,** *15* (9), 3196-3202.
126. Zhang, Y.-J.; Sethuraman, V.; Michalsky, R.; Peterson, A. A., Competition between CO2 Reduction and H2 Evolution on Transition-Metal Electrocatalysts. *ACS Catalysis* **2014,** *4* (10), 3742-3748.

127. Ledezma-Yanez, I.; Gallent, E. P.; Koper, M. T.; Calle-Vallejo, F., Structure-sensitive electroreduction of acetaldehyde to ethanol on copper and its mechanistic implications for CO and CO 2 reduction. *Catal. Today* **2016,** *262*, 90-94.
128. Garcia, G.; Rodriguez, P.; Rosca, V.; Koper, M., Fourier transform infrared spectroscopy study of CO electro-oxidation on Pt (111) in alkaline media. *Langmuir* **2009,** *25* (23), 13661-13666.
129. Hori, Y.; Koga, O.; Watanabe, Y.; Matsuo, T., FTIR measurements of charge displacement adsorption of CO on poly-and single crystal (100) of Cu electrodes. *Electrochim. Acta* **1998,** *44* (8), 1389-1395.
130. Ryberg, R., Carbon monoxide adsorbed on Cu(100) Studied by infrared spectroscopy. *Surf. Sci.* **1982,** *114* (2), 627-641.
131. Gajdoš, M.; Hafner, J., CO adsorption on Cu(1 1 1) and Cu(0 0 1) surfaces: Improving site preference in DFT calculations. *Surf. Sci.* **2005,** *590* (2–3), 117-126.
132. Chang, S. C.; Weaver, M. J., In situ infrared spectroscopy of carbon monoxide adsorbed at ordered platinum (100)-aqueous interfaces: double-layer effects upon the adsorbate binding geometry. *J. Phys. Chem.* **1990,** *94* (12), 5095-5102.
133. Arán-Ais, R. M.; Figueiredo, M. C.; Vidal-Iglesias, F. J.; Climent, V.; Herrero, E.; Feliu, J. M., On the behavior of the Pt (100) and vicinal surfaces in alkaline media. *Electrochim. Acta* **2011,** *58*, 184-192.
134. Shaw, S. K.; Berná, A.; Feliu, J. M.; Nichols, R. J.; Jacob, T.; Schiffrin, D. J., Role of axially coordinated surface sites for electrochemically controlled carbon monoxide adsorption on single crystal copper electrodes. *Phys. Chem. Chem. Phys.* **2011,** *13* (12), 5242-5251.
135. Koper, M. T.; van Santen, R. A., Electric field effects on CO and NO adsorption at the Pt (111) surface. *J. Electroanal. Chem.* **1999,** *476* (1), 64-70.
136. Socrates, G., *Infrared and Raman characteristic group frequencies: tables and charts*. John Wiley & Sons: 2004.
137. Severson, M. W.; Stuhlmann, C.; Villegas, I.; Weaver, M. J., Dipole–dipole coupling effects upon infrared spectroscopy of compressed electrochemical adlayers: Application to the Pt (111)/CO system. *J. Chem. Phys.* **1995,** *103* (22), 9832-9843.
138. Calle-Vallejo, F.; Ignacio Martinez, J.; Rossmeisl, J., Density functional studies of functionalized graphitic materials with late transition metals for oxygen reduction reactions. *Phys. Chem. Chem. Phys.* **2011,** *13* (34), 15639-15643.

139. Maier, G.; Rohr, C., Ethynediol: Photochemical Generation and Matrix‐spectroscopic Identification. *Liebigs Ann.* **1996,** *1996* (3), 307-309.
140. Calle-Vallejo, F.; Martínez, J. I.; García-Lastra, J. M.; Abad, E.; Koper, M. T. M., Oxygen reduction and evolution at single-metal active sites: Comparison between functionalized graphitic materials and protoporphyrins. *Surf. Sci.* **2013,** *607*, 47-53.
141. Nie, X.; Esopi, M. R.; Janik, M. J.; Asthagiri, A., Selectivity of CO2 reduction on copper electrodes: the role of the kinetics of elementary steps. *Angew. Chem. Int. Ed.* **2013,** *52* (9), 2459-2462.
142. Hori, Y., Electrochemical CO2 reduction on metal electrodes. In *Modern aspects of electrochemistry*, Springer: 2008; pp 89-189.
143. Roberts, F. S.; Kuhl, K. P.; Nilsson, A., High selectivity for ethylene from carbon dioxide reduction over copper nanocube electrocatalysts. *Angew. Chem. Int. Ed.* **2015,** *54* (17), 5179-5182.
144. Hori, Y.; Takahashi, I.; Koga, O.; Hoshi, N., Electrochemical reduction of carbon dioxide at various series of copper single crystal electrodes. *J. Mol. Catal. A: Chem.* **2003,** *199* (1), 39-47.
145. Lee, S.; Kim, D.; Lee, J., Electrocatalytic Production of C3‐C4 Compounds by Conversion of CO2 on a Chloride‐Induced Bi‐Phasic Cu2O‐Cu Catalyst. *Angew. Chem.* **2015,** *127* (49), 14914-14918.
146. Kyriacou, G.; Anagnostopoulos, A., Influence CO 2 partial pressure and the supporting electrolyte cation on the product distribution in CO 2 electroreduction. *J. Appl. Electrochem.* **1993,** *23* (5), 483-486.
147. Singh, M. R.; Kwon, Y.; Lum, Y.; Ager III, J. W.; Bell, A. T., Hydrolysis of Electrolyte Cations Enhances the Electrochemical Reduction of CO2 over Ag and Cu. *J. Am. Chem. Soc.* **2016,** *138* (39), 13006-13012.
148. Wuttig, A.; Surendranath, Y., Impurity ion complexation enhances carbon dioxide reduction catalysis. *ACS Catal.* **2015,** *5* (7), 4479-4484.
149. Birdja, Y. Y.; Koper, M. T. M., The Importance of Cannizzaro-Type Reactions during Electrocatalytic Reduction of Carbon Dioxide. *J. Am. Chem. Soc.* **2017,** *139* (5), 2030-2034.
150. Pérez‐Gallent, E.; Figueiredo, M. C.; Calle‐Vallejo, F.; Koper, M., Spectroscopic Observation of a Hydrogenated CO Dimer Intermediate During CO Reduction on Cu (100) Electrodes. *Angew. Chem.* **2017,** *129* (13), 3675-3678.
151. Cook, R. L.; MacDuff, R. C.; Sammells, A. F., Evidence for formaldehyde, formic acid, and acetaldehyde as possible intermediates during electrochemical carbon dioxide reduction at copper. *J. Electrochem. Soc.* **1989,** *136* (7), 1982-1984.

152. DeWulf, D. W.; Jin, T.; Bard, A. J., Electrochemical and surface studies of carbon dioxide reduction to methane and ethylene at copper electrodes in aqueous solutions. *J. Electrochem. Soc.* **1989,** *136* (6), 1686-1691.
153. Akhade, S. A.; McCrum, I. T.; Janik, M. J., The impact of specifically adsorbed ions on the copper-Catalyzed electroreduction of CO2. *J. Electrochem. Soc.* **2016,** *163* (6), F477-F484.
154. Sandberg, R. B.; Montoya, J. H.; Chan, K.; Nørskov, J. K., CO-CO coupling on Cu facets: Coverage, strain and field effects. *Surf. Sci.* **2016,** *654*, 56-62.
155. Chen, L. D.; Urushihara, M.; Chan, K.; Nørskov, J. K., Electric Field Effects in Electrochemical CO2 Reduction. *ACS Catal.* **2016,** *6* (10), 7133-7139.
156. Kim, Y.-G.; Javier, A.; Baricuatro, J. H.; Soriaga, M. P., Regulating the product distribution of CO reduction by the atomic-level structural modification of the Cu electrode surface. *Electrocatalysis* **2016,** *7* (5), 391-399.
157. Gao, D.; Zegkinoglou, I.; Divins, N. J.; Scholten, F.; Sinev, I.; Grosse, P.; Roldan Cuenya, B., Plasma-Activated Copper Nanocube Catalysts for Efficient Carbon Dioxide Electroreduction to Hydrocarbons and Alcohols. *ACS nano* **2017,** *11* (5), 4825-4831.
158. Bertheussen, E.; Verdaguer‐Casadevall, A.; Ravasio, D.; Montoya, J. H.; Trimarco, D. B.; Roy, C.; Meier, S.; Wendland, J.; Nørskov, J. K.; Stephens, I. E., Acetaldehyde as an Intermediate in the Electroreduction of Carbon Monoxide to Ethanol on Oxide‐Derived Copper. *Angew. Chem. Int. Ed.* **2016,** *55* (4), 1450-1454.
159. Rochelle, C.; Czernichowski-Lauriol, I.; Milodowski, A., The impact of chemical reactions on CO2 storage in geological formations: a brief review. *Geological Society, London, Special Publications* **2004,** *233* (1), 87-106.
160. Jasinski, R., Bibliography on the uses of propylene carbonate in high energy, density batteries. *J. Electroanal. Chem. Interfacial Electrochem.* **1967,** *15*, 89-91.
161. Bhanage, B. M.; Fujita, S.-i.; Ikushima, Y.; Arai, M., Synthesis of dimethyl carbonate and glycols from carbon dioxide, epoxides, and methanol using heterogeneous basic metal oxide catalysts with high activity and selectivity. *Applied Catalysis A: General* **2001,** *219* (1), 259-266.
162. Zhang, L.; Niu, D.; Zhang, K.; Zhang, G.; Luo, Y.; Lu, J., Electrochemical activation of CO 2 in ionic liquid (BMIMBF 4): synthesis of

organic carbonates under mild conditions. *Green Chemistry* **2008,** *10* (2), 202-206.
163. Lu, X.-B.; Wang, H.; He, R., Aluminum phthalocyanine complex covalently bonded to MCM-41 silica as heterogeneous catalyst for the synthesis of cyclic carbonates. *J. Mol. Catal. A: Chem.* **2002,** *186* (1), 33-42.
164. Figueiredo, M. C.; Ledezma-Yanez, I.; Koper, M. T., In situ spectroscopic study of CO2 electroreduction at copper electrodes in acetonitrile. *ACS Catal.* **2016,** *6* (4), 2382-2392.
165. Ledezma-Yanez, I.; Koper, M. T. M., Influence of water on the hydrogen evolution reaction on a gold electrode in acetonitrile solution. *J. Electroanal. Chem.* **2017,** *793* (Supplement C), 18-24.
166. Christensen, P.; Hamnett, A.; Muir, A.; Freeman, N., CO2 reduction at platinum, gold and glassy carbon electrodes in acetonitrile: An in-situ FTIR study. *J. Electroanal. Chem. Interfacial Electrochem.* **1990,** *288* (1-2), 197-215.
167. Foley, J. K.; Korzeniewski, C.; Pons, S., Anodic and cathodic reactions in acetonitrile/tetra-n-butylammonium tetrafluoroborate: an electrochemical and infrared spectroelectrochemical study. *Canadian journal of chemistry* **1988,** *66* (1), 201-206.
168. Hori, Y.; Murata, A.; Yoshinami, Y., Adsorption of CO, intermediately formed in electrochemical reduction of CO2, at a copper electrode. *Journal of the Chemical Society, Faraday Transactions* **1991,** *87* (1), 125-128.
169. Wuttig, A.; Liu, C.; Peng, Q.; Yaguchi, M.; Hendon, C. H.; Motobayashi, K.; Ye, S.; Osawa, M.; Surendranath, Y., Tracking a common surface-bound intermediate during CO2-to-fuels catalysis. *ACS central science* **2016,** *2* (8), 522-528.
170. Wang, W.; Li, C.; Yan, L.; Wang, Y.; Jiang, M.; Ding, Y., Ionic liquid/Zn-PPh3 integrated porous organic polymers featuring multifunctional sites: Highly active heterogeneous catalyst for cooperative conversion of CO2 to cyclic carbonates. *ACS Catal.* **2016,** *6* (9), 6091-6100.
171. Niu, K.; Xu, Y.; Wang, H.; Ye, R.; Xin, H. L.; Lin, F.; Tian, C.; Lum, Y.; Bustillo, K. C.; Doeff, M. M., A spongy nickel-organic CO2 reduction photocatalyst for nearly 100% selective CO production. *Science Advances* **2017,** *3* (7), e1700921.
172. Mills, J.; McCrum, I.; Janik, M., Alkali cation specific adsorption onto fcc (111) transition metal electrodes. *Phys. Chem. Chem. Phys.* **2014,** *16* (27), 13699-13707.
173. Jović, V. D.; Jović, B. M., EIS and differential capacitance measurements onto single crystal faces in different solutions: Part II: Cu(111) and Cu(100) in 0.1 M NaOH. *J. Electroanal. Chem.* **2003,** *541*, 13-21.

174. Marcus, Y., Thermodynamics of solvation of ions. Part 5.—Gibbs free energy of hydration at 298.15 K. *Journal of the Chemical Society, Faraday Transactions* **1991,** *87* (18), 2995-2999.
175. Ramki, C.; Vizhi, R. E., Growth, optical, electrical and mechanical properties of sodium hydrogen oxalate hydrate (NaHC 2 O 4· H 2 O) single crystal for NLO applications. *Mater. Chem. Phys.* **2017,** *197*, 70-78.

Appendix I

Supporting information to chapter 2

I.1 Results

The reduction of nitrate (NO_3^-) in a 0.1 M NaOH solution prepared in D_2O was also studied by FTIR on both copper surfaces in order to confirm the absence of the bands corresponding to NO. Figure AI.1 shows potential dependent absorbance spectra of Cu(100) (left panel) and Cu(111) (right panel) in 0.1 M NaOH solution in the presence of 10 mM $NaNO_3$. The reference spectrum is taken at +0.35 V and additional spectra are provided for +0.30, +0.25, +0.20, +0.15, +0.10, +0.05, +0.00, -0.05, -0.10, -0.15, -0.20, -0.25, -0.30, -0.35 V (all reported potentials are in the RHE scale). In agreement with the onset potentials for nitrate reduction observed in the CVs (fig. 2.1) ,IC (fig. 2.4) and FTIR (fig. 2.6), the absorbance spectra show that the onset potential for the reduction of nitrate is +0.15 V on Cu (111) and +0.1 V on Cu (100), as observed by a negative band at 1370 cm^{-1} associated with the consumption of nitrate. However, the simultaneous formation of nitrite that was observed by the positive band at 1231 cm^{-1} when the experiments were carried out in H_2O (fig. 2.6) is not observable in the experiment carried out in D_2O because the band corresponding with nitrite (NO_2^-) is masked by the D-O stretching band. There is no band at 1690 cm^{-1} that would correspond to NO, confirming the absence of formation of NO, in agreement with the results obtained with Online Mass Spectrometry (fig. 2.5).

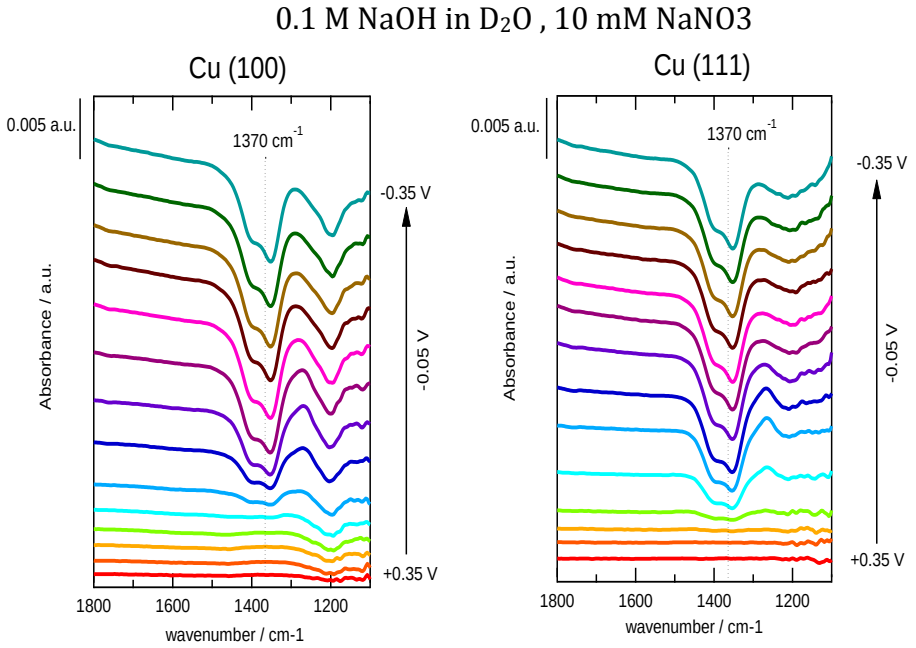

Figure AI.1: Potential dependent absorbance spectra for the reduction of 10 mM $NaNO_3$ on Cu (100) (left panel) and on Cu (111) (right panel) electrode in 0.1 M NaOH solution in D_2O. Reference spectrum recorded at 0.35 V vs. RHE. Potential step is 0.05V.

Appendix II

Supporting information to chapter 3

II.1 Voltammetric characterization of copper single-crystals electrodes

Figure AII.1 shows the characteristic features of the copper single-crystal surfaces, between -0.25 and 0.35 V_{RHE}, in agreement with those previously reported by Schouten et al [91].

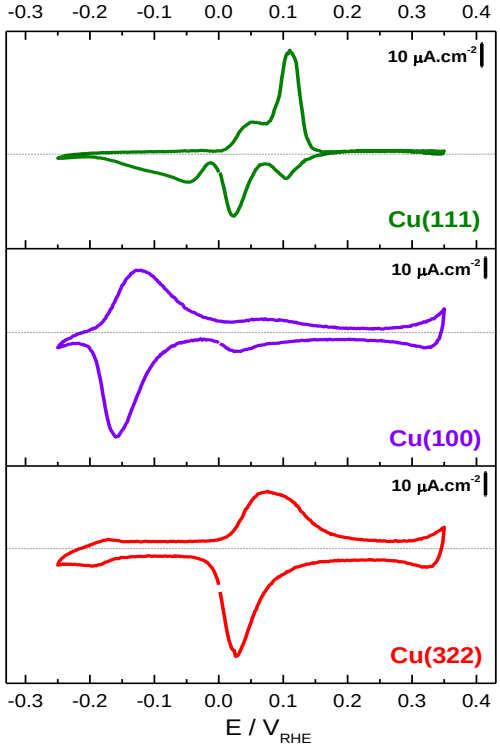

Figure AII.1: Cyclic voltammetries for Cu(111), Cu(100) and Cu(322) electrodes in 0.1 M NaOH; scan rate: 50 mV s^{-1}, Ar-atmosphere.

Figure AII.2 shows the linear sweep voltammetries for acetaldehyde reduction on three copper single-crystal surfaces, between 0.0 and -1.5 V_{RHE}, at pH 1 and 3.

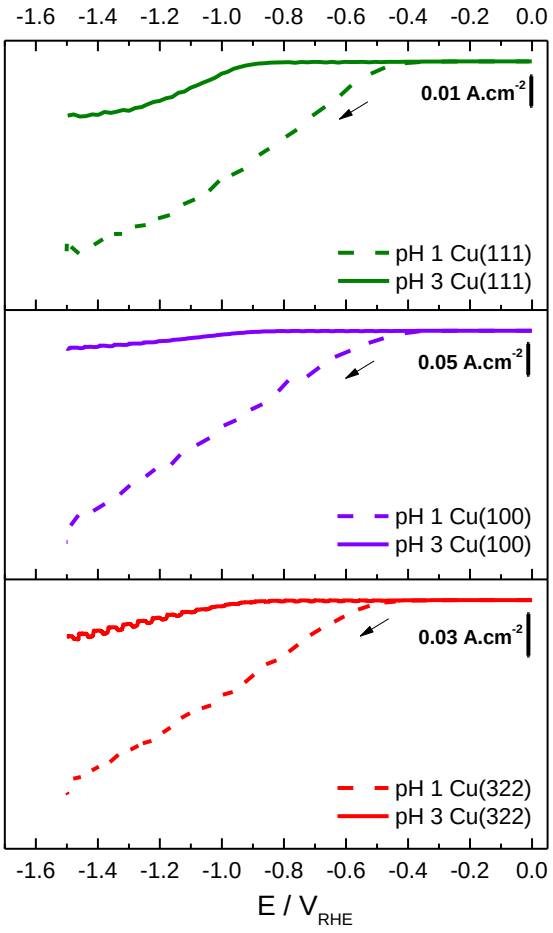

Figure AII.2: Linear sweep voltammetries for acetaldehyde reduction on Cu(111), Cu(100) and Cu(322) electrodes. The solutions used were: 0.1 M $HClO_4$ + 0.1 M acetaldehyde (pH 1), and 0.001 M $HClO_4$ + 0.099 M $KClO_4$ + 0.1 M acetaldehyde (pH 3). Scan rate: 1 mV s^{-1}, Ar-atmosphere.

II.2 DFT simulations in a high H-coverage regime

Figures AII.3 and AII.4 contain the most stable adsorption configurations of CH_3CH_2O* and CH_3*CHOH in the presence of coadsorbed hydrogen on the three crystals under study.

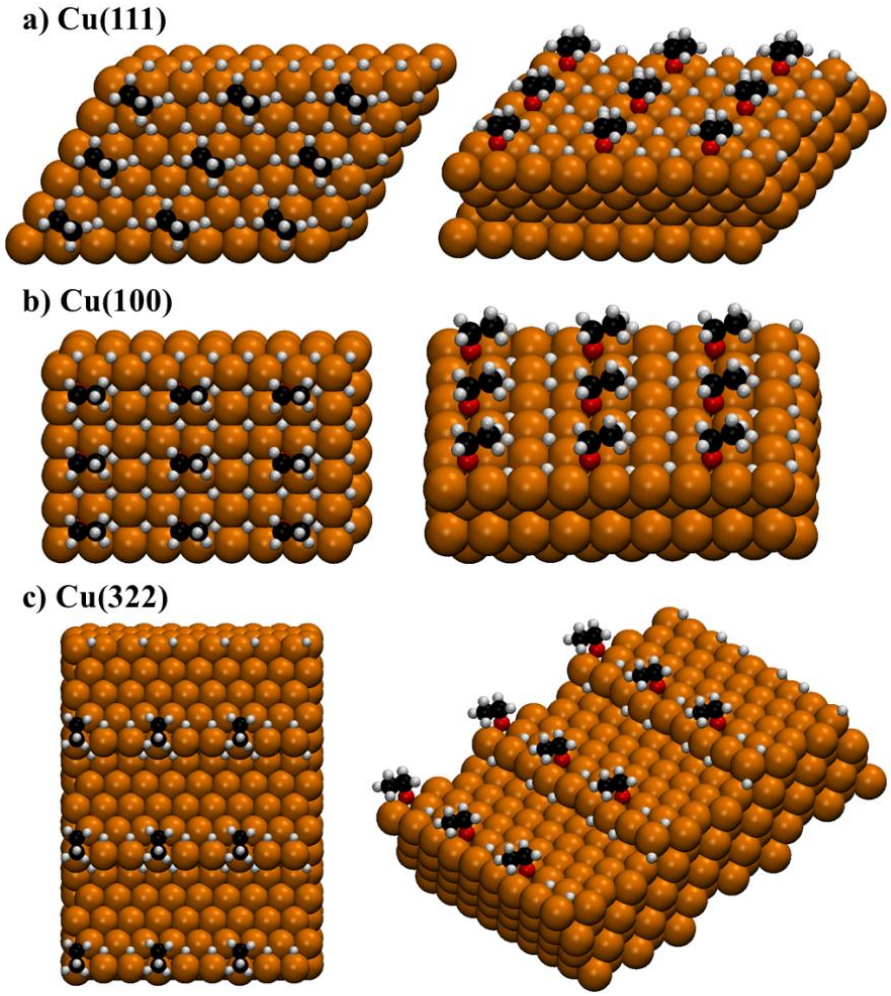

Figure AII.3: Coadsorption of *H and CH_3CH_2O* on a) Cu(111), b) Cu(100), c) Cu(322). Left: top views, right: side views.

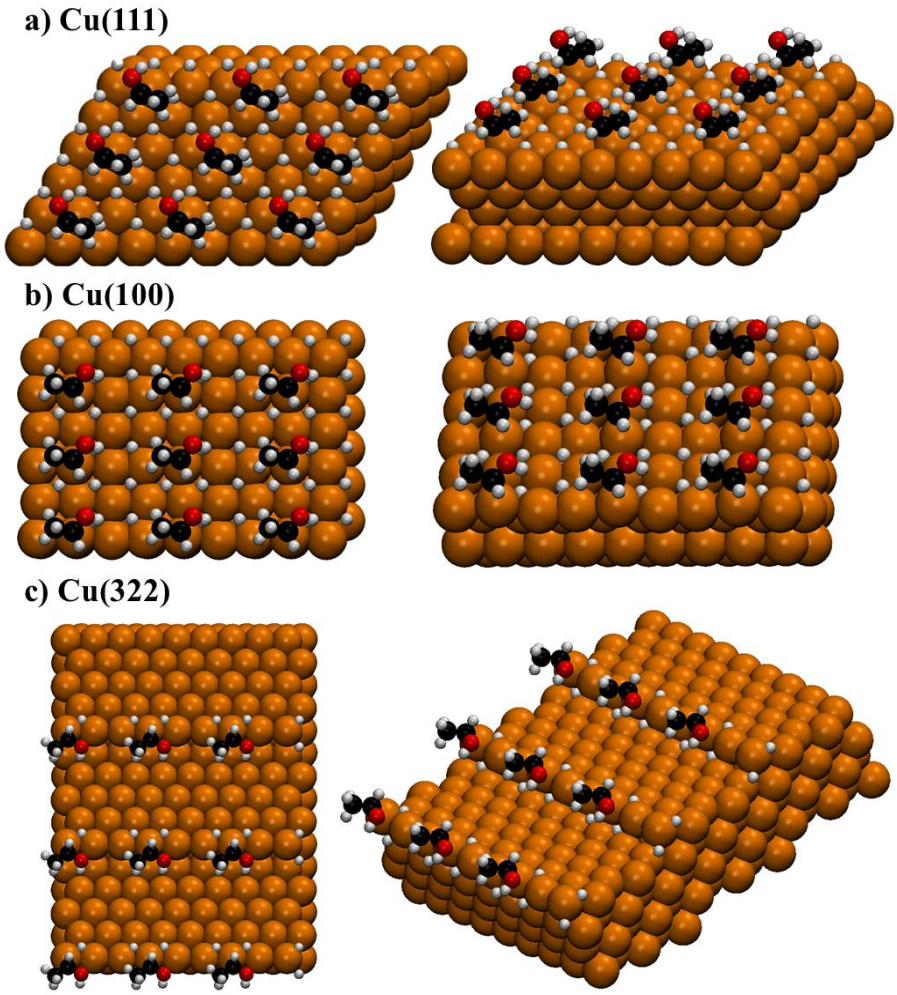

Figure AII.4: Coadsorption of *H and CH_3*CHOH on a) Cu(111), b) Cu(100), c) Cu(322). Left: top views, right: side views.

Appendix III

Supporting information to chapter 4

III.1 Results and discussion

Figure AIII.1 shows the potential-dependent absorbance spectra of Cu(111) in 0.1 M LiOH solutions in CO atmosphere. The reference spectrum is taken at +0.1 V and additional spectra are provided for +0.05, 0.00, -0.05, -0.10, -0.15 and -0.2 V (all reported potentials are on the RHE scale). The spectra show two bands at 1632 and 1407 cm^{-1} . The band at 1632 cm^{-1} corresponds to the OH bending mode of H_2O. This band causes fluctuations in the baseline of the spectra. The band at 1407 cm^{-1} is assigned to formaldehyde according to the transmission spectra obtained for this species in solution (See Figure AIII.2 e). Formaldehyde has been suggested to be an intermediate of the reduction of CO to CH_4 on Cu(211) [57]. During the reduction of CO on Cu(111), there is no band around 1680 cm^{-1} that would correspond to adsorbed CO [131]. The band at 1191 cm^{-1} that is assigned to the C-OH stretching on Cu(100) for the hydrogenated dimer is absent in the spectra obtained on Cu(111), confirming the favorability of square sites for the formation of the hydrogenated dimer as an early intermediate of CO reduction. The transmission spectra of other C1 and C2 species such as acetate, formate, acetaldehyde, formaldehyde and methanol were also recorded (Figure AIII.2). The lack of a match of the bands obtained during CO reduction with the bands observed in the transmission spectra of this C1 and C2 species, rules out the possibility of having these species as intermediates in CO reduction on Cu(100) electrodes.

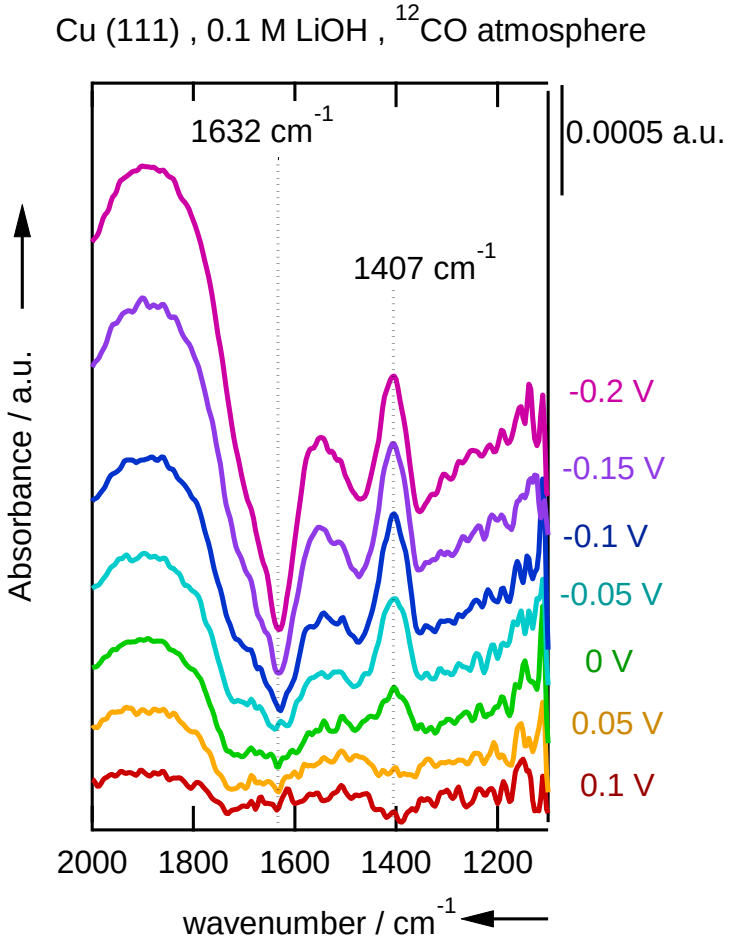

Figure AIII.1: Potential-dependent absorbance spectra for Cu(111) in the presence of CO in a 0.1 M LiOH solution. Reference spectrum recorded at +0.1 V vs. RHE. Highlighted bands and their correspondent frequency are indicated with a vertical line at 1407 cm-1 for ^{12}C-OH stretching and 1632 cm^{-1} for O-H bending.

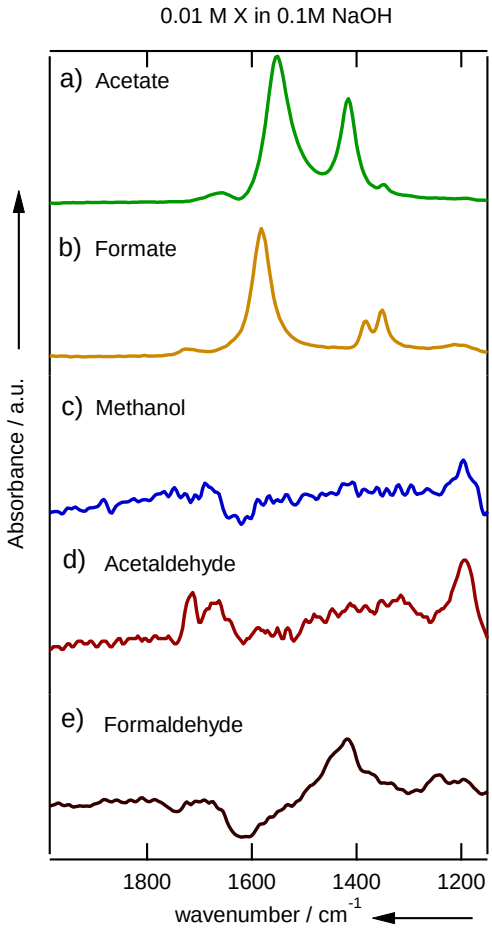

Figure AIII.2: Transmission spectra of 0.01 M of: a) acetate, b) formate, c) methanol, d) acetaldehyde, and e) formaldehyde in 0.1 M NaOH solution.

Appendix IV

Supporting information to chapter 5

IV.1 OLEMS measurements

IV.1.1 Hydrogen evolution reaction

Figure AIV.1 show the mass fragment m/z = 2 associated with the formation of H_2 from the competitive hydrogen evolution reaction (HER) during CO reduction on Cu(100), Cu(111) and polycrystalline Cu. On all copper surfaces, hydrogen evolution starts at ca. -0.4 V for all different cations except Cs^+, for which it starts at slightly less negative potentials. The amount of hydrogen produced as well as its formation rate increases with the size of the cation in the electrolyte for every copper surface

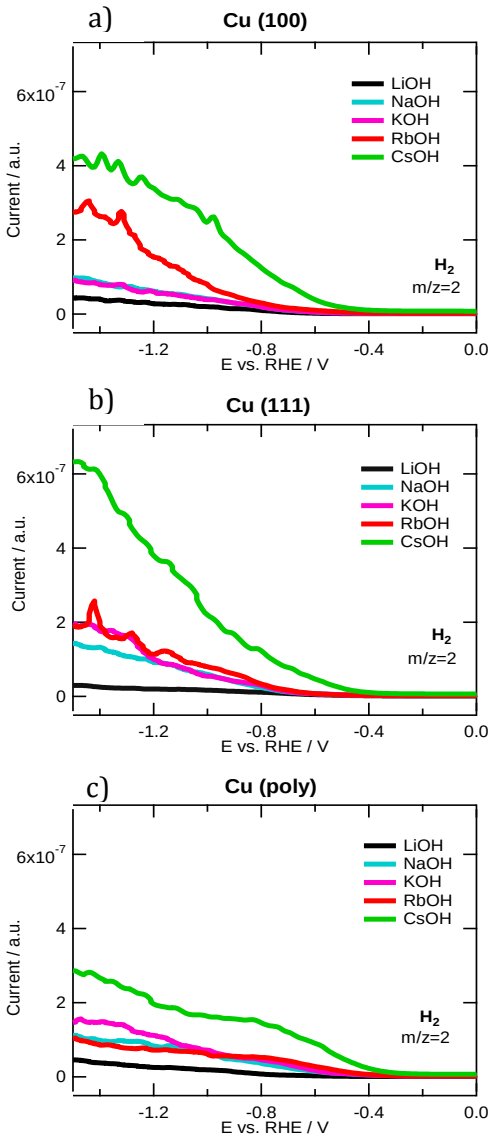

Figure AIV.1: OLEMS mass fragment m/z= associated with the formation of H_2 during CO reduction on a) Cu(100) , b) Cu(111) and c) polycrystalline Cu for different 0.1 M alkaline hydroxide solutions.

IV.1.1 Cation effect for ethylene selectivity

Figure AIV.2 illustrates the cation effect on the selectivity of ethylene versus methane on Cu(100) electrodes during CO reduction. The values in Figure AIV.2 have been extracted from Figure 5.1 for a clearer representation of the cation effect for ethylene selectivity.

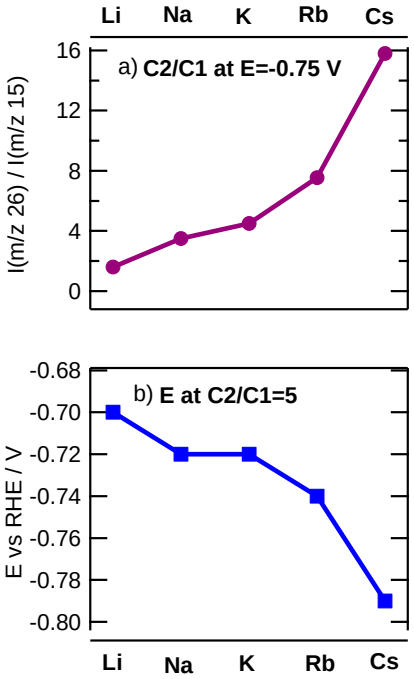

Figure AIV.2: a) ratio ethylene/methane at a representative potential of -0.75 V vs RHE for different alkali cations. b) potential for which a fixed value of 5 for the ratio ethylene/methane is obtained for different alkali cations.

Figure AIV.2a shows the ratio C_2/C_1 at a representative potential of -0.75 V vs RHE for different alkaline cations. Figure AIV.2b shows the potential for which a fixed value of 5 for the ratio ethylene/methane is obtained for the different alkaline cations. The values of the

ethylene/methane ratio at -0.75 V show a clear effect of the cation towards ethylene formation that monotonically follows the cation sizes. In addition, the potentials for wich a fixed value of 5 for the ratio ethylene/methane show that larger cations can maintain the same selectivity for ethylene at more negative potentials compared to smaller cations, suggesting that the selectivity for ethylene is enhanced in a larger potential range when larger cations are used.

IV.2 HPLC measurements

During CO reduction on polycrystalline copper, the minor liquid products formed were collected and analyzed by High- Performance Liquid Chromatography (HPLC).

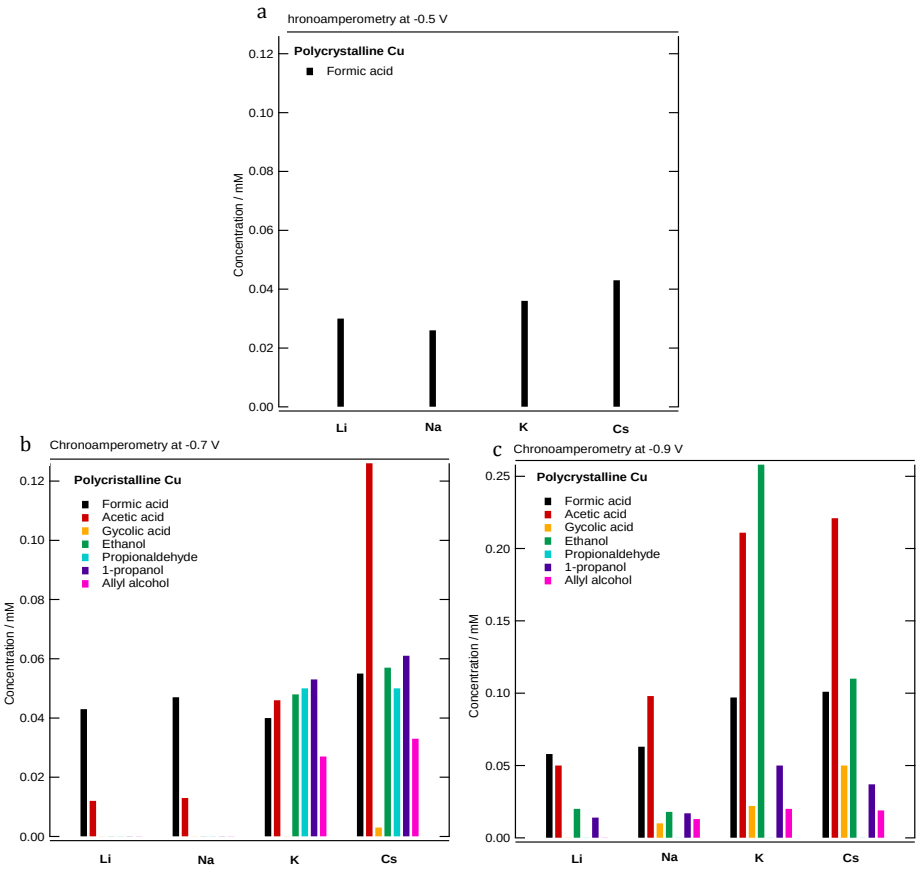

Figure AIV.3: Concentration analyzed with HPLC of different liquid products obtained during the reduction of CO after 2h of electrolysis at a) -0.5 V b) -0.7 V and c) -0.9 V on polycrystalline Cu with 0.1 M solutions of alkaline hydroxides.

Chronoamperometry experiments were carried out at three different potentials: -0.5, -0.7 and -0.9 V, with different alkaline hydroxides as electrolytes. The results are summarize in Figure AIV.2. Experiments with RbOH showed an anomalously low amount of product formation, which we ascribe to the combination of low purity and long experimentation time. Therefore, data obtained with Rb cations are not included in the results described below.

When chronoamperometry experiments were performed at -0.5 V vs RHE for 2 h (See Figure AIV.3a), the only product observed was formic acid. The concentration of this acid does not greatly change along with the cation in solution, being the concentration in the range 0.025 – 0.043 mM. Note that the formation of formic acid has been never reported as a CO reduction product. We attribute its formation here to the Cannizzaro reaction, a base-catalyzed aldehyde disproportionation resulting in the formation of the corresponding acid and alcohol. In this specific case, the formaldehyde formed during CO reduction disproportionates into methanol and formic acid. We recently pointed out the importance of this reaction[149], as it explains the concomitant formation of acids and alcohols observed during CO_2 reduction as a result of a local pH increase due to OH^- generation from the simultaneous hydrogen evolution reaction. Formate might as well be produced after *CO is hydrogenated to *CHO, and *CHO combines with OH^- according to Zheng et al. [171]

At more negative potentials (-0.7 V and -0.9 V), we observed more significant differences in terms of product distribution and concentration. The products obtained were: formic acid as C_1 product; acetic acid, glycolic acid, ethylene glycol and ethanol as C_2 products; propionaldehyde, 1-propanol and allyl alcohol as C_3 products. The C_2 and C_3 products obtained during CO reduction have been reported previously[50, 61].

At -0.7 V, formic acid is formed on all electrolytes with slight differences in concentration. However, the concentration of acetic acid, increases

with the cation size. Ethanol, propionaldehyde, 1-propanol and allyl alcohol were only observed when K^+ and Cs^+ were present in the electrolyte, with slightly higher concentrations observed for the latter. In addition, with Cs^+ a small amount of glycolic acid was produced. Ethylene glycol was also detected in KOH and CsOH, although an accurate quantification was not possible due to an overlap with the intense peak of acetic acid.

During CO reduction at more negative potentials (-0.9 V), higher concentrations of products were generally obtained. Formic acid and acetic acid were formed for all cations, with their concentrations increasing with the cation size. Ethanol and 1-propanol were also detected for every cation with the highest concentration corresponding to K^+. Small amounts of allyl alcohol were detected for Na^+, K^+ and Cs^+, without significant differences in concentration. Glycolic acid was also observed for Na^+, K^+ and Cs^+, with a clearer trend regarding the size of the cation. Ethylene glycol was detected with K^+ and Cs^+, but a clear quantification was not possible. In general, larger cations (Cs^+) promote CO reduction to C_2 species compared to small cations (Li^+ and Na^+), in agreement with the results by Hori et al[65].

IV.3 ^{1}H-NMR

The samples collected after 2h of CO reduction by chronoamperometry at -0.9 V vs. RHE in 0.1 M NaOH, KOH and CsOH solutions were analyzed by ^{1}H-NMR. The ^{1}H-NMR spectra are shown in Figure AIV.4.

Solvent supression was employed to reduce the size of the peak corresponding to water in order to magnify the peaks corresponding to CO reduction products. The product distribution obtained is similar, regardless of the cation size, although differences in the intensity of the peaks were observed.

The products observed were formic acid, acetic acid, ethylene glycol, glycolic acid, ethanol and 1-propanol, in agreement with the products

observed with HPLC. In addition, methanol was also observed as a CO reduction product for all three electrolytes analyzed. The detection of methanol by HPLC analysis was not possible due to the overlap of the corresponding peak with the peaks of the eluent. The amount of these reduction products was higher for CsOH and KOH, compared to NaOH, although an accurate quantification was not made.

Table AIV.1 shows an overview of the products detected by ^{1}H-NMR for the electrolysis experiments performed at -0.9 V vs. RHE in NaOH, KOH and CsOH 0.1 M solutions.

Table AIV.1: 1H-NMR chemical shift for the products detected after reduction of CO at -0.9 V vs. RHE in 0.1 M NaOH, KOH and CsOH solutions.

Compound	**Proton**	**Nb H**	**Mult.**	**Delta / ppm (Na^+)**	**Delta / ppm (K^+)**	**Delta / ppm (Cs^+)**
Formic acid	-H	1	s	8.376	8.367	8.359
Acetic acid	$-CH_3$	3	s	2.206	2.196	2.184
Ethylene glycol	$-CH_2-$	4	t	3.484	3.470	3.462
Glycolic acid	$-CH_2-$	2	s	3.869	3.858	3.845
Methanol	$-CH_3$	3	s	3.278	3.267	3.255
Ethanol	$-CH_2-$	2	q	3.587	3.566	3.558
	$-CH_3$	3	t	1.105	1.104	1.090
1-propanol	$-CH_3$	3	t	0.816	0.806	0.807
	$-CH_2-$	2	qt	1.105	1.098	1.095
	$-CH_2-$	2	t	3.587	3.56	3.473

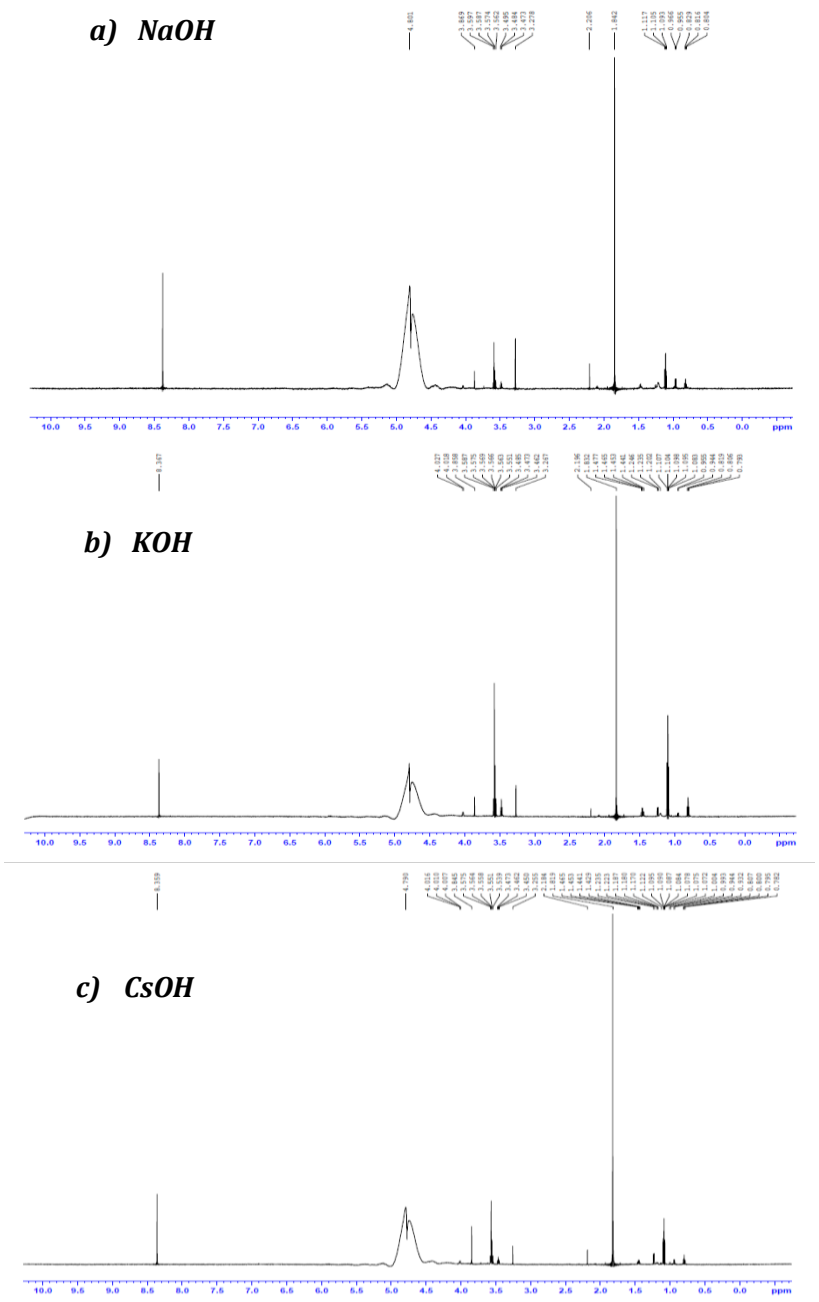

Figure AIV.4: ^{1}H-NMR spectra of the samples obtained during CO reduction on polycrystalline copper after 2h of chronoamperometry at -0.9 V vs RHE in a) NaOH, b) KOH and c) CsOH 0.1 M solutions.

IV. 4 Mechanistic implications

During the electroreduction of CO, a relation between the formation of ethylene and methane was noted: an increase in m/z = 15 (corresponding to methane) occurs when m/z = 26 (corresponding to ethylene) starts to decay. Figure AIV.5 shows the relation between these two mass fragments for Cu(111) and Cu(polycrystalline) in different alkaline hydroxide solutions, which complement Figure 5.4 in chapter 5.

The possibility that methane formation be the result of ethylene reduction has been tested. Figure AIV.6 shows the reduction of ethylene on Cu(100) in 0.1 M CsOH solution. When ethylene is reduced, only the formation of hydrogen from the competitive hydrogen evolution reaction (HER) was observed. The absence of methane formation rules out the possibility that the relation observed between methane and ethylene is due to methane production as a following step in the C_2 pathway. It is important to mention that ethane was not detected during the reduction of ethylene, either.

The decay in m/z = 26 during CO reduction due to the reduction of ethylene has also been considered. The experiments show that ethylene reduction starts at ca. -0.4 V achieving its maximum reduction current at ca. -0.6 V vs RHE, and the decay of m/z = 26 during the reduction of CO occurs at ca. -0.7 V. Thus, the possibility of the decay of the ethylene signal due to its reduction has also been ruled out. Hence, we propose that the C_2 pathway gets blocked by the enhancement of the C_1 pathway and discard the hypothesis that C_2 products are transformed to produce C_1 species.

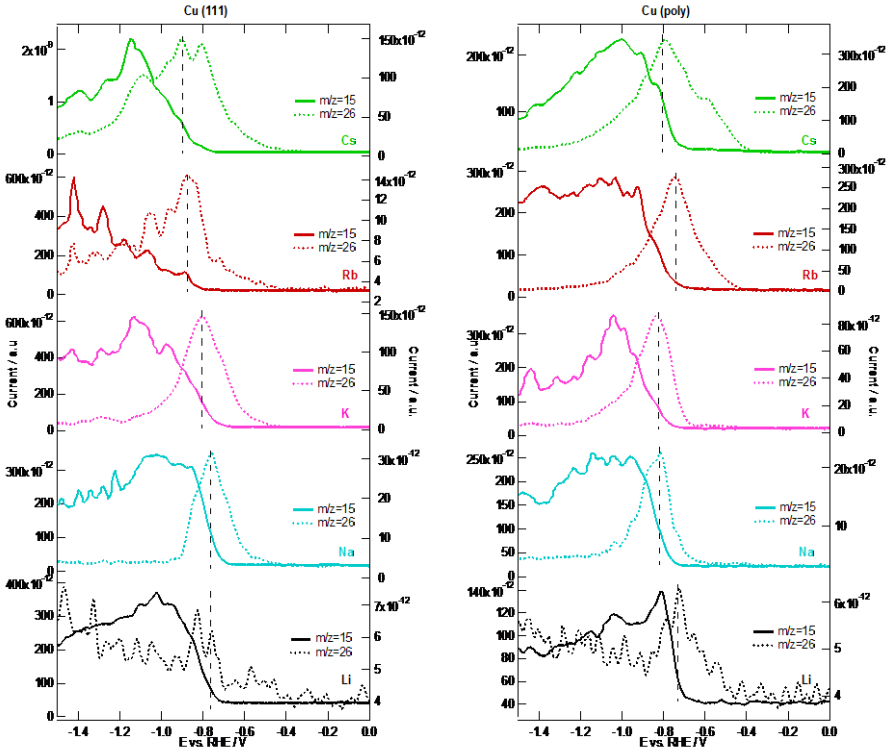

Figure AIV.5: OLEMS mass fragments associated with the reduction products formed during CO reduction on Cu(111) (left panel) in different 0.1 M alkaline hydroxide solutions. Dashed lines correspond to m/z = 26 associated with the formation of ethylene, plotted against the right axis. Full lines correspond to m/z = 15 associated with the formation of methane, plotted against the left axis.

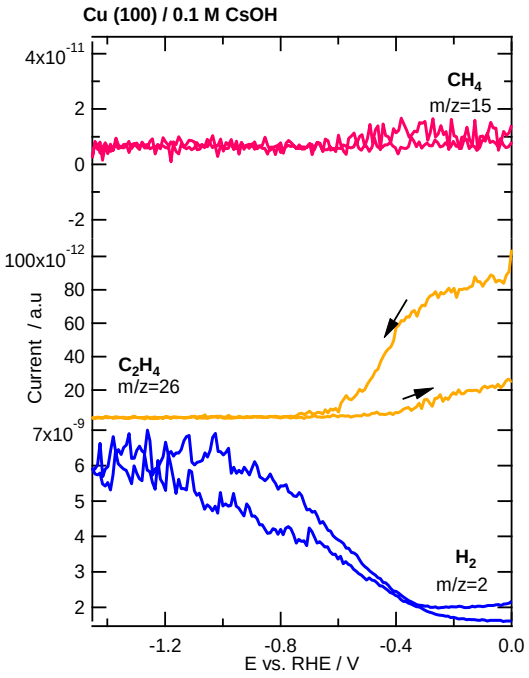

Figure AIV.6: OLEMS mass fragments associated with the reduction of ethylene on Cu(100) in 0.1 M CsOH solution. The bottom panel displays m/z = 2 associated with the formation of H2, the middle panel displays m/z = 26 associated with the reduction of C2H4 and the top panel displays m/z = 15 associated with CH4.

The onset potential for the formation of methane and ethylene during the reduction of CO is displayed in figure AIV.7. The onset potential for ethylene formation depends on the facet, being lower for copper single crystals than for polycrystalline copper. In addition, the onset potential for ethylene is not affected by the cation size when CO reduction is performed on copper single crystals, whereas on polycrystalline copper the onset potential depends on the cation, being -0.6 V for Li^+ and Na^+, -0.4 V for K^+ and -0.35 V for Rb^+ and Cs^+. On the other hand, the onset potential for methane formation is independent of both cation nature and surface structure.

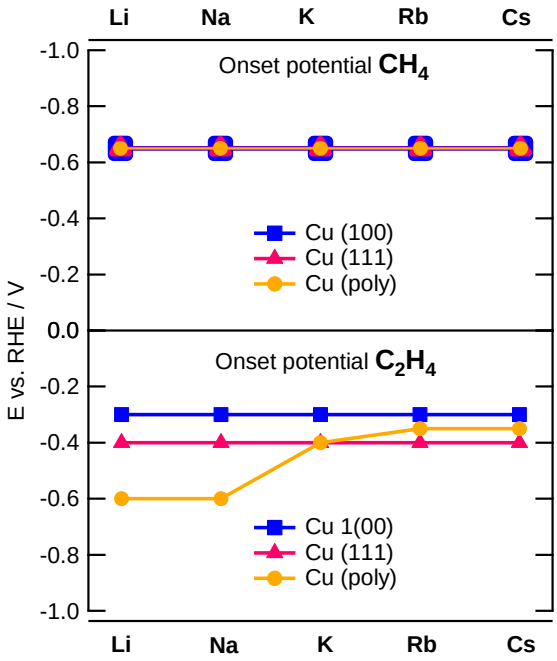

Figure AIV.7: Onset potential for the formation of methane (top panel) and ethylene (bottom panel) dependent on the cation nature and surface structure.

IV.5 Electrode surface characterization

The structure of copper electrodes is a key factor in tuning the selectivity of CO electroreduction.[64, 144] Therefore, cyclic voltammetry before and after the reduction of CO (Figure AIV.8) has been carried out in order to determine the initial state of the electrode surface and to assess its change after CO reduction.

Prior to CO reduction, the voltammograms exhibit the characteristic peaks according to the specific copper surface, in agreement with the study of Schouten et al.[91] However, the state of the electrode surface

at the end of the experiments displays some differences with respect to the initial state. . While the surfaces of Cu(100) and Cu(poly) electrodes remain relatively unchanged, Cu(111) underwent major modifications. Thus, the variation in product distribution is merely due to the nature of the cation in solution and structural factors must not be considered. On Cu(100) OH^- adsorption/desorption peaks at -0.15 V are present before and after the experiment. However, the OH^- adsorption/desorption peaks on Cu(111) decrease in current intensity after the experiment. In addition, a new irreversible anodic peak appears at +0.35 V, suggesting that the well-defined (111) arrangement has been partially lost at the end of the OLEMS experiments. This new anodic peak might be due to specific cation adsorption or to OH^- adsorption on a reconstructed surface.

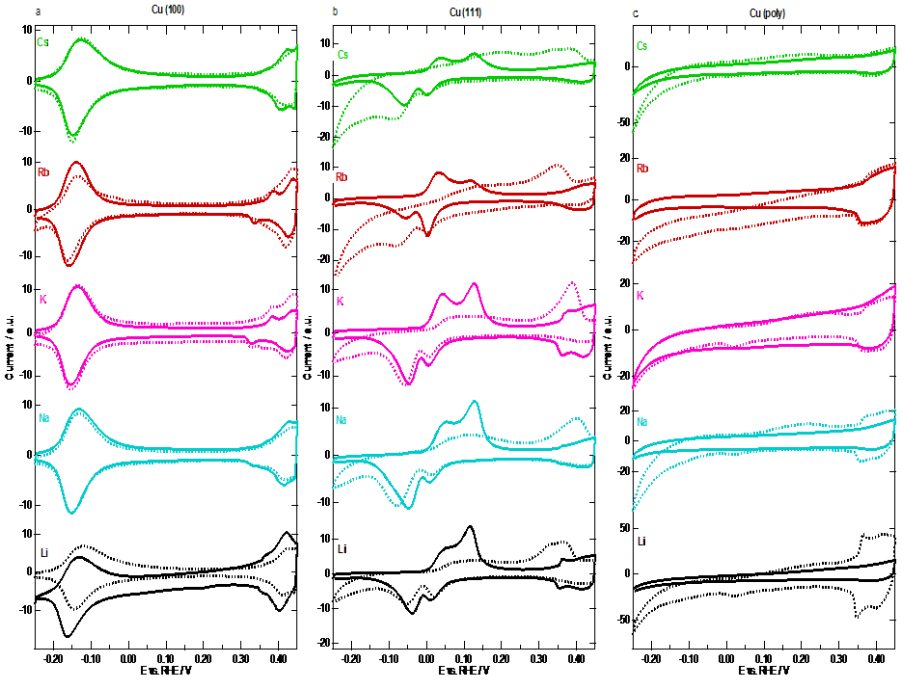

Figure AIV.8: Cyclic voltammetry characterization of a) Cu(100), b) Cu(111) and c) Cu(poly) in different 0.1 M alkaline hydroxide solutions before OLEMS experiments (full lines) and after OLEMS experiments (dashed lines).

First, according to DFT calculations in which solvation effects are considered, the specific adsorption of alkaline cations on fcc (111) transition metals occurs in the same potential range of HER[172]. Secondly, Jović et al. reported the slow Cu(111) surface reconstruction induced by adsorption/desorption of OH^-, when the potential is scanned between -0.25 V and +0.45 V vs. RHE[173]. Both processes might give a possible explanation for the modification of the Cu(111) surface.

IV.6 Computational details

Cu(100) was modeled with (3×2) slabs that contained four atomic layers. For such slabs, we sampled the Brillouin zones with 6×8×1 Monkhorst-Pack grids.[115]. The geometry optimizations were carried out using a plane-wave cut-off of 450 eV, employing the conjugate-gradient scheme until the maximum force on any atom was below 0.05 eV $Å^{-1}$, and allowing the two topmost layers and the adsorbates to relax in all directions, while the 2 bottommost layers were frozen at the optimized bulk distances. The separation between periodical images was more than 16 Å in the z direction and dipole corrections were also applied. The Fermi level in the calculations was smeared using the Methfessel-Paxton method[116] with an electronic temperature of 0.2 eV, and all energies were extrapolated to T = 0 K.

The chemical potential of protons and electrons was calculated from that of H_2(g) using the computational hydrogen electrode[121]. The free energies of the species were calculated as: $G = E_{DFT} + ZPE - TS + E_{solvation}$, where E_{DFT} is the total energy calculated in the manner described before, *ZPE* is the zero-point energy calculated through the harmonic oscillator approximation, and *TS* (with T = 298.15 K) is the total entropy correction for H_2(g) and H_2O(l), whereas it corresponds to the vibrational entropy part for the adsorbed species. We applied the solvation corrections ($E_{solvation}$) reported before for *CO (-0.1 eV/CO)[57], *OCCO (-0.3 eV/*OCCO) and *OCCOH (-0.48 eV/*OCCOH)[53] and included

explicit water in the calculations to solvate only the alkaline cations. Given the known problems of PBE for the description of CO(g)[57], we corrected its total energy by -0.24 eV as described elsewhere[53].

Figure AIV.9 contains the adsorption configurations of 2*CO, $*C_2O_2$ and $*C_2O_2H$ on Cu(100) in vacuum and in presence of the alkaline cations Li^+, Na^+ and Cs^+. Only in the case of Li^+, the calculations included one explicit water molecule, as the adsorption energy of H_2O over adsorbed Li, Na and Cs was -0.32, 0.04, and 0.19 eV, respectively.

This different solvation upon adsorption reflects the fact that in solution, the number of water molecules in the first solvation shell decrease as a function of the cation size, so that Li^+, Na^+, Cs^+ are surrounded by ~5, 3-4 and 2 H_2O molecules, respectively[174]. However, the adsorption energetics in presence of the cations are rather similar in presence and absence of water, as shown in Table AIV.2.

Table AIV.2: Energetics of adsorption on Cu(100) of two CO molecules (2*CO), their dimer ($*C_2O_2$), and hydrogenated dimer ($*C_2O_2H$). All values are in eV.

species	vacuum	Li	Li + H_2O	Na	Na + H_2O	Cs	Cs + H_2O
2*CO	-0.44	-0.77	-0.77	-0.74	-0.81	-1.04	-0.96
*C2O2	0.56	-0.51	-0.48	-0.64	-0.67	-0.76	-0.63
*C2O2H	0.44	-0.54	-0.68	-0.58	-0.72	-0.77	-0.66

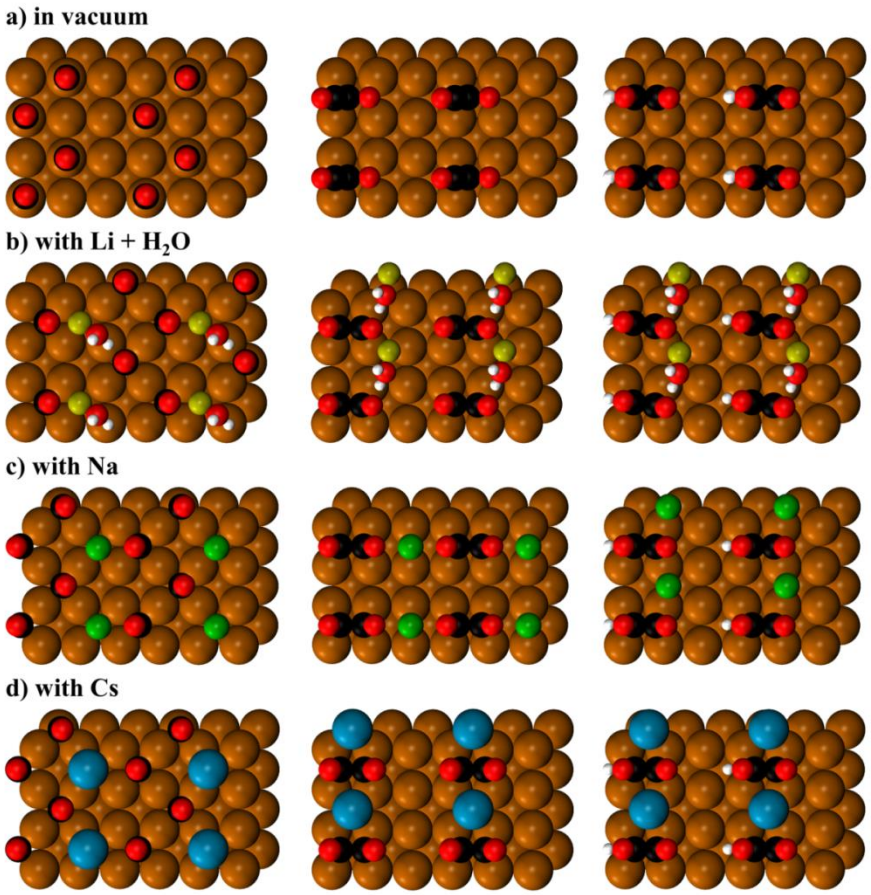

Figure AIV.9: Adsorption on Cu(100) of 2*CO (left), *C_2O_2 (center) and *C_2O_2H (right) in a) vacuum, and with b) Li, c) Na, and d) Cs. Color code: C: black, Cs: blue, Cu: orange, H: white, Li: yellow, Na: green, oxygen: red.

Essentially, the commonality between the three analyzed cations is that their effects are only present when they are relatively close to the adsorbates. The distances to the closest O atoms in the dimer vary considerably with cation: 1.88, 2.37, and 3.08 Å for Li^+, Na^+ and Cs^+, respectively.

Regarding the C_1 pathway, Figure AIV.10 contains the adsorption configurations of *CO and *CHO on Cu(100) in vacuum and in presence of the alkaline cations Li^+, Na^+ and Cs^+. Based on the adsorption energies

of water on the cations provided above, only in the case of Li^+ the calculations included one explicit water molecule. In any case, the adsorption energetics are rather similar in presence and absence of water, as shown below in Table AIV.3 for Li.

Table AIV.3: Energetics of adsorption on Cu(100) of *CO and *CHO. All values are in eV.

species	vacuum	Li	Li + H_2O	Na	Cs
*CO	-0.23	-0.60	-0.58	-0.60	-0.64
*CHO	0.51	-0.10	-0.09	-0.01	-0.10

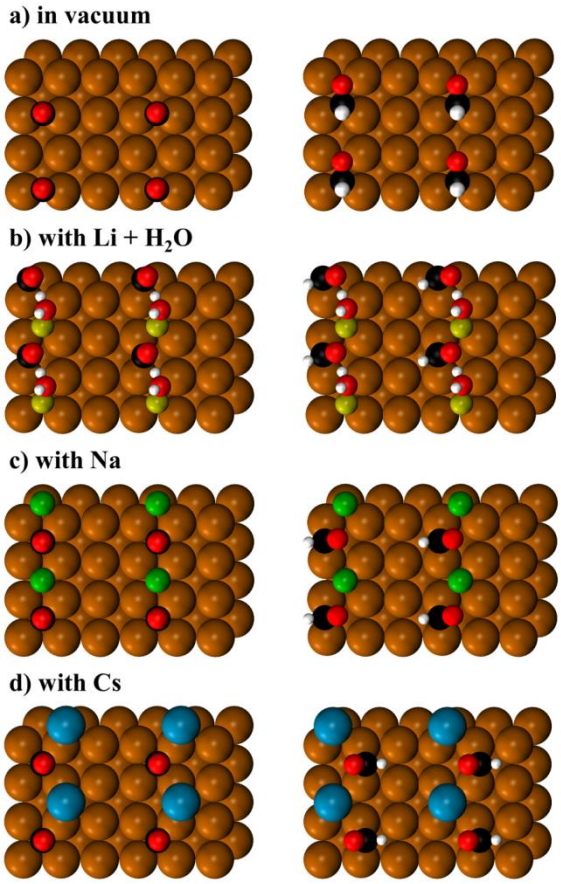

Figure AIV.10: Adsorption configurations on Cu(100) of *CO (left) and *CHO (right) in: a) vacuum, and with b) Li, c) Na, and d) Cs. Color code: C: black, Cs: blue, Cu: orange, H: white, Li: yellow, Na: green, oxygen: red

Finally, in Figures AIV.11 (C_1 pathway) and AIV.12 (C_2 pathway) we use the results in Tables AIV.2 and AIV.3 to calculate the energetics of CO adsorption, dimerization and protonation in vacuum and in presence of the cations. Note that the average values of Figures AIV.10 and AIV.11 were used to build Figure 5.3 in chapter 5.

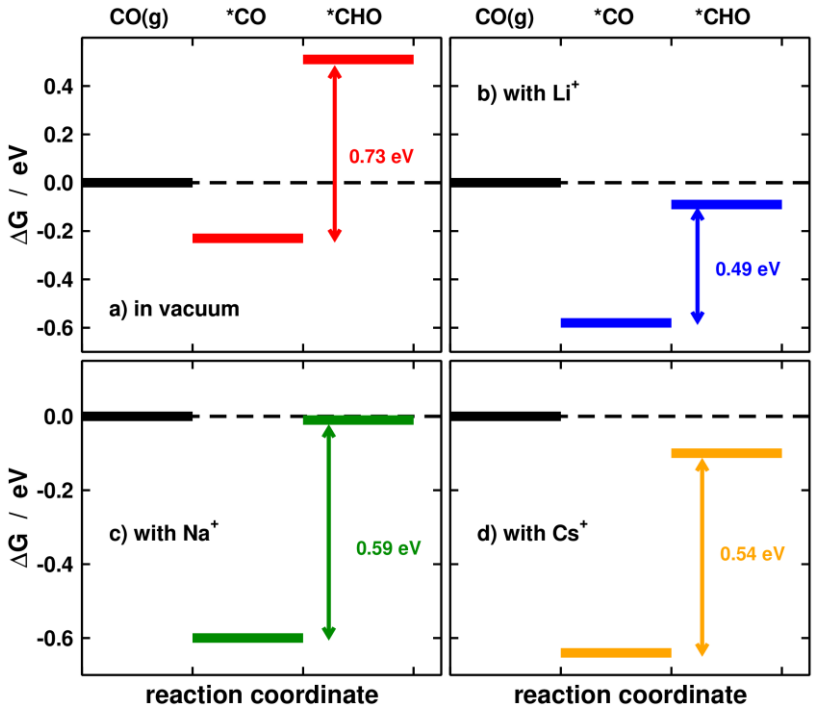

Figure AIV.11: Energetics of the first electrochemical step of CO reduction for the C_1 pathway on Cu(100) at 0 V vs RHE. a) In vacuum, and with b) Li, c) Na and d) Cs.

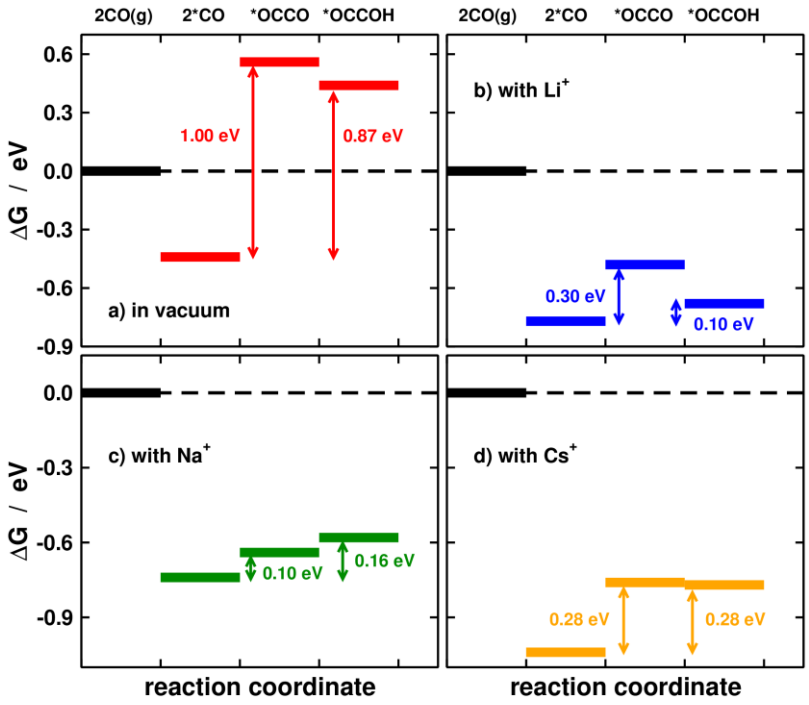

Figure AIV.12: Energetics of the first electrochemical step of CO reduction for the C_2 pathway on Cu(100) at 0 V vs RHE. a) In vacuum, and with b) Li, c) Na and d) Cs.

IV.7 Exclusion of the formation of oxalates

We have collected the solubility of some alkaline oxalates in Table AIV.4. Lithium oxalate has a solubility in water at 20 ºC of 80 g/l. On the other hand, the concentration of our hydroxides was 0.1 M. If all of the Li ions reacted to form $Li_2C_2O_4$, then 5.1 g/l would be formed. This means that all lithium oxalate that might be formed would be readily dissolved in water. Therefore, we do not expect any salt deposition during our experiments, which is corroborated by the identical cyclic voltammograms before and after electrolysis experiments.

Furthermore, we had a look at the spectra of hydrogen oxalate compounds[175] and noticed that it present a band at 1195 cm^{-1}. However, these compounds also present a prominent band at 1440 cm^{-1} corresponding to C-O stretching and a band at 1737 cm^{-1} that corresponds to C=O stretching[175]. The absence of the latter two bands in the spectra recorded during CO reduction makes it possible to rule out the formation of lithium salts of hydrogen oxalate.

We would also like to annotate that (i) we did not detect any carbonate (CO_3^{2-}) in our experiments, and (ii) oxalate ($C_2O_4^{2-}$) is a negatively charged dimer of CO_2. Taking into account that all our experiments focused on CO reduction and that carbonate was not observed, any CO-associated dimer should only have 1 or maximum 2 oxygen atoms in its structure. Therefore, if oxalate were detected from CO reduction experiments, it would counterintuitively imply that CO is first oxidized and then subsequently reduced to ethylene. Note as well that if oxalate formed from dimerization of hydrolyzed *CO, its formation rate would be slow[171] and would not account for the significant amounts of ethylene observed.

For all those reasons, we believe that oxalate is not responsible for the two bands that we attribute to the hydrogenated dimer.

Table AIV.4: Solubility in g/100 ml of several alkali oxalates

Alkali oxalate	Solubility in g/100 ml
Li	8
Na	3.7
K	36.4
Cs	313

Appendix V

Supporting information to chapter 6

V.1 Results

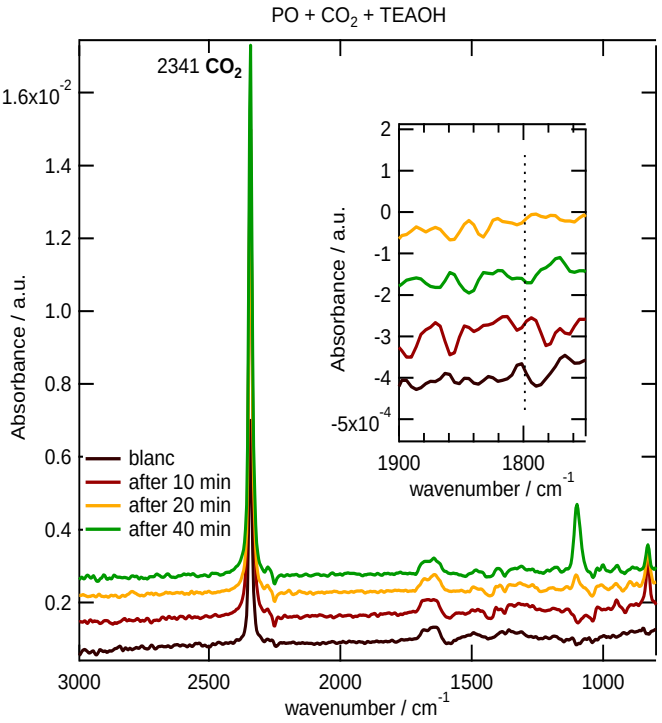

Figure AV.1: Time dependent absorbance spectra of a solution containing 0.1 M of propylene oxide, saturated carbon dioxide atmosphere in a 0.1M $TEAClO_4$ in acetonitrile solution in the absence of TEAOH (black) and in the presence of 1M TEAOH after 10 minutes (red), 20 minutes (yellow) and 40 minutes (green). The insert displays the zoom-in of the region between 1900 - 1750 cm^{-1}

Figure AV.1 shows the time dependent absorbance spectra of propylene oxide and CO_2 in the presence of a strong base (TEAOH) in a 0.1 M $TEAClO_4$ in acetonitrile solution. The spectra were recorded in order to ensure that the formation of propylene carbonate from propylene oxide and CO2 is an electrochemical process and not a chemical synthesis catalyzed by the presence of OH- which can be formed during water reduction. The spectra show an intense band at 2341 cm^{-1} corresponding to C=O stretching from CO_2 in solution. Less intense bands at 1670 cm^{-1} corresponding to decomposition products from the acetonitrile are also observed. However, the absence of a band at 1800 cm^{-1} that would correspond to propylene carbonate, supports the electrochemical nature of the synthesis of propylene carbonate instead of a chemical reaction catalyzed by OH^-, in accordance with the results observed by Yang et al.[78]

Samenvatting

Heterogene katalyse is van groots belang in industriële processen zoals de productie van ammonia, de formatie van syngas, de formatie van zwavelzuur en salpeterzuur, het katalytisch kraken van olie en in vele andere processen. Deze processen vereisen veelal hoge temperaturen en hoge druk om een effectieve conversie te bereiken. Daarnaast leiden sommige van deze processen tot ongewenste bijproducten die schadelijk kunnen zijn voor het milieu of de katalysator zelf kunnen aantasten en dus snel kunnen leiden tot een verlies in reactiviteit.

Een alternatief voor industriële processen die gebruik maken van hoge temperaturen zou het gebruik van elektrokatalyse zijn, dat een aantal voordelen herbergt ten opzichte van conventionele katalyse. Ten eerste dragen elektronen als reductie- /oxidatiemiddel bij aan schonere processen. Ten tweede leidt het gebruik van milde omstandigheden in het katalytische proces, zoals lagere temperaturen en drukken, mogelijk tot een hogere stabiliteit van het oorspronkelijke materiaal of het te vormen product. De opbrengst van de verschillende producten hangt af van de toegepaste potentiaal, en door deze te controleren kan er, in principe, selectief gericht worden op het gewenste product en kan de productie van schadelijke en/of ongewenste bijproducten vermeden worden. Ondanks deze voordelen, is elektrochemische synthese geen gemeengoed in de chemische industrie. Het achtergebleven gebruik van elektrochemische technieken kan toegeschreven worden aan een gebrek aan onderwijs in elektrochemie en katalyse, de gelimiteerde beschikbaarheid van componenten voor het bouwen van een elektrochemische cel en met name door de hoge kosten van elektriciteit en elektrochemische cellen. Het nadeel van de grote benodigde hoeveelheid energie kan verholpen worden door het gebruik van katalysatoren die gemaakt zijn van goedkope en veel voorkomende materialen en door het gebruik van elektriciteit uit duurzame bronnen. Voordat elektrochemische processen wijds toegepast kunnen worden in

de industrie, zal er echter eerst op kleinere schaal een efficiënt proces ontwikkeld moeten worden. Met dit doel voor ogen is er eerst een grondige studie van de elektrochemische katalyse nodig, zodat we het effect verschillende parameters op de product distributie en de selectiviteit en efficiëntie van de katalytische reactie kunnen begrijpen én beheersen.

In deze thesis hebben we gekeken naar aantal parameters die de elektrochemische conversie van milieuschadelijke moleculen, zoals nitraten en koolstofdioxide naar bruikbare en minder schadelijke verbindingen beïnvloeden. Hiermee proberen we de reactiemechanismes van deze processen op te helderen, met als doel om een efficiënt en selectief proces te ontwikkelen.

Deze thesis is verdeeld in twee delen; de reductie van nitraten (hoofdstuk 2) en de mechanistische studie van CO_2 conversie naar verschillende producten, zoals ethanol (hoofdstuk 3), ethyleen (hoofdstuk 4 en 5) en propyleencarbonaat (hoofdstuk 6).

Vele auteurs hebben de invloed van het materiaal van de elektrode en de zuurgraad van het elektrolyt op de verdeling van producten van de reductie van nitraten bestudeerd. In hoofdstuk 2 van deze thesis hebben we de elektrokatalytische reductie van nitraat op koperen electroden bestudeerd. De invloed van de oppervlaktestructuur van de electrode hebben we bestudeerd door middel van het gebruik van twee verschillende eenkristallijne koperelectroden, namelijk Cu(100) en Cu(111). De experimenten zijn uitgevoerd in zure en alkalische media, zodat ook de invloed van de zuurgraad in de reactie bestudeerd kon worden. De experimenten wezen uit dat de gevormde hoeveelheid van de verschillende producten afhankelijk is van de zuurgraad van het elektrolyt. In zure media wordt NO en ammonia gevormd, in alkalische media is het hoofdproduct hydroxylamine. De reductie van nitraat is alleen afhankelijk van de oppervlaktestructuur van de electrode in alkalische media, waarbij de vorming van hydroxylamine het gunstigst is op Cu(100).

Elektrochemische reductie van koolstofdioxide heeft in de laatste decennia aanzienlijke aandacht gekregen, vanwege de capaciteit van koper om CO_2 te converteren in brandstoffen zoals methaan, ethyleen en ethanol. Ondanks dat dit proces al in de jaren '80 ontdekt is, is het mechanisme van de reactie nog steeds voer voor discussie.

Bij de reductie van koolstofdioxide op koper worden producten met 2 koolstofatomen per productmolecuul (C2 producten) gevormd. Het belangrijkste C2 product is ethyleen, maar er zijn ook sporen van ethanol en aceetaldehyde aangetroffen. Aceetaldehyde is waargenomen als tussenproduct voor de formatie van ethanol tijdens de reductie van koolstofmonoxide. In hoofdstuk 3 bespreken we de invloed van de reductie van aceetaldehyde naar ethanol tijdens de reductie van CO_2 op de totale reactie. Men gelooft dat deze drie verbindingen gevormd worden via een gezamenlijk tussenproduct in de vroege stadia van de reductie van CO_2. Dit betekent dat de splitsing richting ethyleen of ethanol in een later stadium van de reactie plaats moet vinden. Onze resultaten hebben aangetoond dat het tussenproduct dat de selectiviteit richting ethyleen of ethanol bepaalt, het product is van de vijfde protonatie (CH_2CHO^*). De protonatie van dit tussenproduct is gunstig voor de vorming van ethanol op ondergecoördineerde adsorptieplekken (atomaire stapranden) op de koperelektrode. Daartegenover staat dat adsorptieplekken met een vierkante symmetrie (Cu(100)) gunstiger zijn voor de formatie van ethyleen. Ondanks de in verhouding hogere energetische barrière voor de vorming ethanol ten opzichte van ethyleen, kan de selectiviteit richting ethanol verhoogd worden door gebruik te maken van de afhankelijkheid van de oppervlaktestructuur van de reactie.

Een andere interessante stap in het mechanisme van de reductie van CO_2 is gerelateerd aan de vorming van ethyleen. De enige tussenvorm die empirisch bevestigd is tijdens de reductie van CO_2 naar ethyleen is CO. Theoretische studies hebben gesteld dat de C-C binding tijdens de reductie van CO_2 naar ethyleen vormt via reductieve dimerisatie, gevolgd door verdere hydrogenering. In hoofdstuk 4 laten we

spectroscopisch bewijs zien voor de formatie van een CO gehydrogeneerd tussenproduct (OCCOH) tijdens de reductie van CO_2 naar ethyleen. De formatie van dit tussenproduct blijkt gevoelig te zijn voor de oppervlaktestructuur, waarbij de adsorptieplekken met een vierkante symmetrie het gunstigst zijn.

Een aantal factoren, zoals de zuurgraad van het elektrolyt, de chemische eigenschappen van kationen of anionen en de oppervlaktestructuur van de electrode, zijn voorafgaand bestudeerd voor hun effecten op de reductie van CO_2. Al deze parameters leiden tot significante veranderingen in de verdeling van producten, selectiviteit en het conversiepercentage. In hoofdstuk 5 analyseren wij het samengestelde effect van de morfologie van de electrode, de grootte van de alkalische kation en de toegepaste potentiaal tijdens de reductie van CO. Over het algemeen kan gesteld worden dat grotere kationen de vorming van ethyleen verhogen bij potentialen positiever dan -0.45V. Bij potentialen negatiever dan -0.45V kan er echter gesteld worden dat grotere kationen de vorming van methaan verhogen. Wij suggereerden dat de competitie tussen deze twee reacties ervoor zorgt dat de reductie van CO_2 naar ethyleen afneemt op het moment dat de vorming van methaan toeneemt. Deze correlatie is ook afhankelijk van de grootte van een kation. We stelden dat de kationen, door een gunstige elektrostatische interactie, de tussenproducten stabiliseren en zo de katalytische reactie bevorderen. Daarnaast is ook de vorming van de gehydrogeneerde CO-dimeer die we bespraken in hoofdstuk vier (OCCOH), afhankelijk van de grootte van een kation. De gehydrogeneerde dimeer kan waargenomen worden met behulp van infrarood spectroscopie (FTIR) wanneer Li^+, Na^+ en K^+ aanwezig zijn, maar is niet zichtbaar in de aanwezigheid van Rb^+ of Cs^+. Berekeningen aan de hand van dichtheidsfunctionaaltheorie (DFT) beschrijven de vorming van *OCCOH dan ook als minder gunstig in de aanwezigheid van grotere kationen ten opzichte van kleinere kationen.

Tot slot bestudeerden we in hoofdstuk 6 de conversie van koolstofdioxide in grotere organische moleculen, specifiek in cyclische

carbonaten. We analyseerden het mechanisme van de vorming van propyleencarbonaat uit koolstofdioxide en propyleenoxide op koperen electroden. Zo konden we koolstofmonoxide en koolstof(bi)carbonaat uitsluiten als reagens tijdens de carboxylering. Ook de activatie van propyleenoxide middels 'ring opening' bleek geen rol te spelen in deze reactie. Onze experimenten suggereerden dat de elektrochemische reactie gestart wordt door de activatie van CO_2 naar CO_2^-, wat vervolgens reageert met propyleenoxide tot propyleencarbonaat.

Deze thesis heeft het belang van grondig mechanistisch onderzoek aangetoond in de zoektocht naar kennis over alle stappen die aan bod komen in een elektrochemische reactie. Het begrip van hoe verschillende factoren de selectiviteit en conversie richting een bepaald product beïnvloeden, kan helpen in het ontwerpen van een efficiënter proces. Met deze kennis kan een elektrochemische reactie, door het aanpassen van verschillende parameters in de reactie, gestuurd worden om de vorming van het gewenste product te optimaliseren.

Resumen

La catálisis heterogénea es de suma importancia en procesos industriales tales como la formación de amoníaco, la formación de gas de síntesis, el fraccionamiento o "cracking" del petróleo, la formación de ácido sulfúrico, o la formación de ácido nítrico entre muchos otros. Sin embargo, estos procesos tienen como requisito altas temperaturas y presiones, con el fin de conseguir conversiones eficientes. Además, algunos de estos procesos producen subproductos indeseados los cuales pueden ser nocivos para el medio ambiente o pueden afectar al catalizador deteriorándolo, lo cual genera una rápida pérdida de actividad.

Una alternativa razonable a procesos industriales que emplean altas temperaturas y presiones podría ser el uso de electrocatálisis, la cual presenta varias ventajas sobre la catálisis convencional. Ante todo, el uso de electrones como agentes reductores u oxidantes contribuye a un proceso más limpio. Además, el uso de condiciones moderadas tales como temperaturas y presiones bajas, puede potencialmente conducir a una mayor estabilidad de los reactivos de partida o de los productos formados. Por otra parte, ya que la distribución de los productos depende del potencial aplicado, el control de dicho potencial permitiría, en principio, formar de una manera selectiva el producto deseado, evitando así la formación de subproductos dañinos y/o indeseados. Sin embargo, la síntesis electroquímica no está mundialmente extendida en la industria. Las razones del uso limitado de técnicas electroquímicas ha sido tradicionalmente atribuida a la falta de educación en electroquímica, a la falta de medios para la construcción de células electroquímicas y, especialmente, a los altos costes de la electricidad y de las células electroquímicas. La necesidad de un alto aporte energético puede ser superado con el uso de catalizadores algunos de los cuales son abundantes y baratos, y especialmente con el uso de energías renovables. No obstante, un proceso eficiente debe de ser desarrollado en el laboratorio antes de que tenga una aplicación industrial. Para este

propósito, debe ser llevado a cabo primero, un estudio exhaustivo de la reacción electroquímica, para entender y controlar todos los diferentes parámetros que afectan a la reacción, a la distribución de los productos, a la selectividad y a la eficiencia de la misma.

En esta tesis, se discuten varios parámetros que afectan a la conversión electroquímica de sustancias nocivas para el medio ambiente tales como nitratos y dióxido de carbono a compuestos más valiosos, para elucidar el mecanismo de la reacción con el fin de obtener un sistema eficiente y selectivo.

Esta tesis está dividida en dos partes; Primero, la reducción de nitrato (capítulo 2) y segundo en un estudio del mecanismo de reacción de la conversión de dióxido de carbono a diferentes productos tales como etanol (capítulo 3), etileno (capítulos 4 y 5) y carbonato de propileno (capítulo 6).

Un gran número de trabajos previos, ha estudiado las diferencias en distribución de productos durante la reducción de nitrato utilizando varios metales y en diferentes pH. En el capítulo 2 de esta tesis se estudia la reducción electrocatalítica de nitrato en electrodos de cobre. La influencia de la morfología de la superficie del electrodo fue evaluada con el uso de dos monocristales de cobre diferentes, Cu(100) y Cu(111). Además, los experimentos fueron llevados a cabo en medio ácido y en medio alcalino, proporcionando así un estudio sobre la influencia del pH en esta reacción. Los experimentos han mostrado que la distribución de los productos varía dependiendo del pH del electrolito. Así, mientras que en medio acido los productos formados son NO y amoniaco, en medio alcalino el producto principal es la hidroxilamina. Además, la reducción de nitrato es sensible a la estructura del electrodo sólo en medio básico, con la formación de hidroxilamina favorecida en Cu(100).

La reducción electroquímica de dióxido de carbono ha recibido mucho interés en las últimas décadas debido a la capacidad del cobre de convertir CO_2 en combustibles tales como metano, etileno y etanol. Este

proceso fue descubierto en 1980, sin embargo, el mecanismo de la reacción aún está en debate.

La reducción de dióxido de carbono en electrodos de cobre forma etileno como el principal producto C2. No obstante, también han sido detectadas trazas de etanol y acetaldehído. Debido a que acetaldehído ha sido confirmado como intermediario en la formación de etanol durante la reducción de monóxido de carbono, en el capítulo 3 discutimos las implicaciones mecanísticas de la reducción de acetaldehído a etanol durante la reducción de CO_2. Se cree que estos tres compuestos comparten un intermediario común en las primeras etapas de la reducción de CO_2, sin embargo, la ruta química para la formación de etanol y de etileno debe bifurcarse en etapas posteriores de la reacción. Nuestros resultados muestran que el intermediario que determina la selectividad es el producto de la quinta protonación (CH_2CHO*). La protonación de este intermediario favorece la formación de etanol en sitios de baja coordinación. Por otra parte, los sitios de simetría cuadrada favorecen la formación de etileno. A pesar de las altas barreras energéticas encontradas en la formación de etanol en comparación con etileno, la selectividad para etanol puede incrementarse haciendo uso de la sensibilidad estructural de la reacción.

Otros pasos interesantes en el mecanismo de la reducción de CO_2 están relacionados con la formación de etileno. El único intermediario confirmado experimentalmente durante la reducción de CO_2 ha sido CO. Estudios computacionales han hipotetizado que la formación de enlaces C-C en la ruta del etileno ocurre a través de una dimerización reductiva con posterior hidrogenación. En el capítulo 4 de esta tesis proporcionamos evidencias espectroscópicas de la formación de un intermediario hidrogenado de CO (OCCOH) en la ruta del etileno. La sensibilidad estructural de la formación de este intermediario ha sido confirmada, siendo la formación del intermediario favorable en sitios con simetría cuadrada.

Varios factores tales como el pH del electrolito, la naturaleza química de los cationes o aniones y la morfología de la superficie del electrodo han sido previamente estudiados durante la reducción de CO_2. Todos estos parámetros producen cambios significantes en los productos formados, en la selectividad y en la velocidad de conversión. En el capítulo 5 analizamos el efecto de la morfología de la superficie del electrodo en combinación con el tamaño del catión y el potencial aplicado durante la reducción de CO. En general, cationes grandes favorecen la formación de etileno a potenciales más positivos que -0.45 V, mientras que a potenciales más negativos, los cationes grandes favorecen la formación de metano. Sugerimos que la ruta de reacción hacia etileno se cierra debido a la mejora de la ruta de reacción que genera metano. Esta correlación también depende del tamaño del catión. Cationes grades favorecen la selectividad del etileno en un mayor rango de potencial. Sugerimos que los cationes actúan como promotores catalíticos los cuales estabilizan los intermediarios de reacción que tienen una interacción electrostática favorable con el catión. Además, la formación del dímero de CO hidrogenado explicado en el capítulo 4 (OCCOH) también depende del tamaño del catión. Mientras que el dímero hidrogenado se puede observar con IR-TF cuando Li^+, Na^+ y K^+ están presentes en solución, el dímero no es observable en presencia de Rb^+ o Cs^+. Los cálculos basados en la teoría del funcional de la densidad describen la formación de *OCCOH en presencia de cationes grandes menos favorable que en presencia de cationes pequeños.

Finalmente, en el capítulo 6 estudiamos la conversión de dióxido de carbono en moléculas orgánicas más grandes, específicamente en carbonatos cíclicos. Hemos estudiado el mecanismo de formación de carbonato de propileno en electrodos de cobre partiendo de dióxido de carbono y oxido de propileno. Hemos excluido monóxido de carbono, carbonatos y bicarbonatos como posibles agentes de carboxilación. También se ha excluido la activación del óxido de propileno vía apertura del anillo como el paso clave en esta reacción. Nuestros experimentos sugieren que el inicio de la reacción electroquímica es la activación del

CO_2 a $CO_2^{\cdot-}$, el cual ataca al oxido de propileno para finalmente formar carbonato de propileno.

En términos generales, esta tesis enfatiza la importancia de estudios mecanísticos exhaustivos para entender todos los pasos involucrados en una reacción electroquímica. La comprensión de cómo diferentes factores afectan la selectividad y la conversión hacia un determinado producto puede ayudar a lograr procesos más eficientes mediante el ajuste de estos parámetros.

List of publications

This thesis is based on the following publications

Chapter 2

E Pérez-Gallent, MC Figueiredo, I Katsounaros, MTM Koper
Electrocatalytic reduction of Nitrate on Copper single crystals in acidic and alkaline solutions.
Electrochimica Acta, **2017**, 227, 77-84

Chapter 3

I Ledezma-Yanez, E Pérez-Gallent, MTM Koper, F Calle-Vallejo
Structure-sensitive electroreduction of acetaldehyde to ethanol on copper and its mechanistic implications for CO and CO_2 reduction
Catalysis Today, **2016**, 262, 90-94

Chapter 4

E Pérez-Gallent, MC Figueiredo, F Calle-Vallejo, MTM Koper
Spectroscopic Observation of a Hydrogenated CO Dimer Intermediate During CO Reduction on Cu (100) Electrodes
Angewandte Chemie, **2017**, 129, 3675-3678

Chapter 5

E Pérez-Gallent, G Marcandalli, MC Figueiredo, F Calle-Vallejo, MTM Koper
Structure and potential dependent cation effects on CO reduction at copper single-crystal electrodes
Journal of the American Chemical Society, **2017**, 139, 16412–16419

Chapter 6

E Pérez-Gallent, MC Figueiredo, MTM Koper
Mechanistic study of the electrosynthesis of propylene carbonate from propylene oxide and CO_2 on copper electrodes.
Submitted

Curriculum vitae

Elena Pérez Gallent was born in Valenica (Spain) on 26th August 1988. In 2006, she graduated from the Pureza de Maria high school. In that year, she started her BSc studies in Chemistry at the Universitat de València. During her studies, she visited Leiden University within the Erasmus Exchange Program for her Master thesis, which was performed under the supervision of Prof. Dr. Marc T. M Koper with the title "Electrocatalytic carbon dioxide reduction on copper single crystal electrodes". In 2013, she received the Licenciatura degree (equivalent to Master of Science) in Chemistry at Universitat de València.

After a short experience in the industry (Catexel B.V.), she started her PhD studies under the supervision of Prof. Dr. Marc T. M. Koper in the research group 'Catalysis and surface chemistry' (CASC) of the Leiden Institute of Chemistry, leiden University. During her PhD she supervised one HBO student, nine BSc students, two MSc students and the organic chemistry practical course for first-year student three times. Furthemore, she took several post-graduate courses including "Reactivity of nanoparticles for more efficient and sustainable energy conversion"; "CO2 conversion: From fundamentals towards applications"; "Catalysis, an integrated approach" and "Characterization in Catalysis Research". Parts of the results reported in this thesis were presented at several (inter)national conferences.